The Genetics and Evolution of Intraspecific Variation in Meiotic Recombination Rate

By

Richard J. Wang

A dissertation submitted in partial fulfillment of

the requirements for the degree of

Doctor of Philosophy

(Genetics)

at the

UNIVERSITY OF WISCONSIN-MADISON

2017

Date of final oral examination: 1/25/2017

The dissertation is approved by the following members of the Final Oral Committee:

Bret A. Payseur, Professor, Genetics and Medical Genetics
Cécile Ané, Professor, Statistics and Botany
Karl W. Broman, Professor, Biostatistics and Medical Informatics
John F. Doebley, Professor, Genetics
Laurence Loewe, Assistant Professor, Genetics

Table of Contents

		Page
Abstract		ii
Acknowledgements		iii
Chapter 1	Introduction	1
Chapter 2	Recombination rate evolution in mice from an isolated island	7
Chapter 3	Genetics of genome-wide recombination rate evolution in mice from an isolated island	33
Chapter 4	Genetics of synaptonemal complex length evolution in mice	59
Chapter 5	Conclusions	81
References		86

Abstract

Recombination is a fundamental evolutionary force. It introduces genetic diversity into populations by joining alleles in novel haplotypic combinations. Variation in rates of recombination pervades despite its conserved role in meiosis. The propensity for recombination differs across stretches of the genome within individuals, and differs between the genomes of individuals. Genetic investigation has successfully uncovered some of the patterns, loci, and architecture underlying differences in recombination rate. This dissertation examines recombination rate evolution within the house mouse species (*Mus musculus*). By focusing within species, the earliest forms of divergence and the connections between genomic scales are most easily explored. The ability to isolate genetic effects through experimental crosses in this model system is repeatedly leveraged. Mice derived from the Gough Island (GI) population, an isolated mouse population of recent colonists, are used throughout as closely-diverged wild representatives of the *M. m. domesticus* subspecies. Comparison of genetic maps from crosses with GI mice revealed pervasive polymorphism in recombination across the genome. Immunofluorescent cytology, a technique to visualize individual meiotic cells, was applied in two chapters to characterize recombination phenotypes in individual mice. This individual characterization enabled the detection of multiple quantitative trait loci (QTL) responsible for the evolution of genome-wide recombination rate within mouse subspecies. Cytological images were also processed by an innovative computational technique that calculated synaptonemal complex (SC) length, a meiotic phenotype closely associated with recombination rates. The high-throughput characterization of SC length enabled its genetic mapping, leading to the detection of the first QTL discovered for this trait. These results uncover new aspects of the genetics of recombination rate differences and provide a closely diverged, within species context for its evolution.

Acknowledgements

I feel very fortunate to have had Dr. Bret Payseur as my thesis advisor. I am deeply indebted for his guidance, inspiration, and scientific alacrity during my time as his graduate student. The mentorship I received under his tutelage not only made this work possible, they have fundamentally shaped how I think about science, biology, and evolution. I am grateful for his open discussions about how to navigate a career path in the scientific establishment. I would also like to thank each of the members of my dissertation committee for their enduring support and critical questioning. I would especially like to thank Dr. Cécile Ané and Dr. Karl Broman for their meticulous comments and mentorship in statistics.

The work presented here would not have been possible without funding from a variety of sources, including: the National Institutes of Health (NIH) Genetics training grant to the University of Wisconsin – Madison, the National Library of Medicine (NLM) Computation and Informatics in Biology and Medicine training grant to the UW-Madison, the Science and Medicine Graduate Research Scholars program at UW-Madison, and NIH funding for the Gough Island mouse project, R01GM100426A.

I want to thank my labmates, and lab alumni for providing a fun and creative environment to do scientific research. I am especially indebted to Beth Dumont for her assistance with the immunostaining protocol and for allowing me to use images she generated in the *musculus* x *castaneus* cross.

I am grateful for my supportive parents who did not force me to go into business school. Their love and encouragement have propelled me throughout my academic career. I thank my sister for her unwavering support of my pursuit of a PhD. Finally, I am grateful to have had the many friends in Madison to share interests, frustrations, and achievements.

Chapter 1
Introduction

For cells destined to become a sperm or egg, one of the first steps in the meiotic process of division is a program of massive self-inflicted DNA damage. Hundreds of double-strand breaks shatter the genome, initiating an extraordinary choreography of repair. In any other context, double-strand breaks are detrimental to cellular survival – the kind of molecular damage induced by ionizing radiation. In this context, meiosis cannot successfully proceed without it. A small fraction of these double-strand breaks are reassembled such that the original DNA molecules no longer have the same ends. They will have been recombined with their homolog, a copy of the chromosome inherited from the other parent. The outcome of recombination can hardly be characterized as a shortcoming of the repair process. This Rube Goldberg-esque program for germ cells and their chromosomes is pervasive among complex organisms. Recombination during meiosis is one of the defining features of sexual reproduction, a fundamental mechanic of genetic transmission in most eukaryotes. This mechanic has enormous consequences for evolution.

The reassembly of chromosomes from recombination creates new haplotypes, allelic combinations that did not previously exist on the same chromosome. Recombination is blind to the effects these alleles may have on an organism's fitness, producing permutations of both selectively advantageous and deleterious alleles. Some early theoretical investigations of recombination rate evolution predicted the decline of loci that would positively modify recombination rate, a result coined "the reduction principle" (Nei 1967; Lewontin 1971; Feldman

1972; reviewed in Feldman et al. 1996). This can be explained by the potential for recombination to break down selectively advantageous parental haplotypes. However, the production of haplotypic variation is also theorized to improve the efficacy of selection, explaining the persistence and pervasiveness of recombination (Weismann 1889; Kondrashov 1993; Burt 2000). At the crux of most models explaining this advantage is recombination's ability to break down deleterious allelic combinations in a population, known as "negative linkage disequilibrium" (Hill and Robertson 1966; Felsenstein 1974; Feldman et al. 1980; Otto and Barton 1997).

In contrast to theoretical models focusing on the indirect effects of recombination, that is by its consequences to allelic combinations in a population, the proper execution of recombination has direct and immediate consequences for cells undergoing meiosis. The formation of chromosomal crossovers from meiotic recombination creates physical tension between homolog pairs. This force stabilizes the interactions between microtubules and the centromere, promoting the proper disjunction of chromosomes (Roeder 1997; Hassold and Hunt 2001; Watanabe 2012). The failure of proper disjunction leads to aneuploidy, the presence of abnormal chromosome number and the leading genetic cause of miscarriage and congenital birth defects (Hassold et al. 2007). A minimum rate of recombination may be enforced by this requirement (Mather 1936; Villena and Sapienza 2001; Fledel-Alon et al. 2009). Though it has also been suggested that too many recombination events can be a risk factor for chromosomal rearrangements (Inoue and Lupski 2002; Coop and Przeworski 2007).

Continued discussion on recombination rates would be served by clarifying the dimensions of this metric. As a biological phenomenon, the characterization of recombination predates proof of DNA as the heritable material. The theory that crossovers, recognized as chiasmata through cytology (Janssens 1909), broke down linkage between alleles (Sturtevant

1913; Morgan 1916) led to the first metric, the centiMorgan (Haldane 1919). Quantities in this unit give the expected number of crossovers between two markers in 100 meioses. Without a physical atlas for positioning genes, the centiMorgan (cM) was mapped onto the ontology of distance despite its origin as a rate. With a better understanding of the underlying material of inheritance, the frequency of recombination became quantified across stretches of DNA rather than between a set of observable markers, giving rise to units such as cM per megabase. Finally, recombination characterized cytologically, by counting chiasmata or their proxies, is often quantified by mean counts. This can be given as the expected number of crossovers across a set of chromosomes, e.g. across autosomes, or the total number expected in a meiocyte. To be clear, all of these metrics for recombination rate quantify a kind of bulk property. Meiotic cells can be recombinant and have a discrete number of crossovers, but no single spermatocyte or oocyte has a recombination rate. Recombination rates measure the tendency to recombine from sampling a population.

Recombination rates vary between individuals, populations, and species (True et al. 1996; Kong et al. 2004; Coop et al. 2008; Smukowski and Noor 2011; Comeron et al. 2012). It is important to point out that variation in recombination rate can refer to two distinct phenomena. Firstly, it can refer to variation in the propensity for recombination in different segments of the genome, e.g. proximal versus distal regions of a chromosome. Characterization of this variation in recombination rate within genomes often implicitly assumes the absence of important genetic or environmental differences between samples. The study of this variation has revealed a number of correlated genomic parameters, including GC content, nucleotide diversity, repetitive elements, and chromosome position (Begun and Aquadro 1992; Eyre-Walker 1993; Fullerton et al. 2001; Rizzon et al. 2002; Jensen-Seamen et al. 2004). Secondly, variation in recombination

rate can refer to different propensities for recombining in the same segments of the genome. These comparisons are between samples that have known genetic or environmental differences. Further, differences in patterns of within-genome variation can exist between samples from different genetic or environmental backgrounds. Experiments focusing on variation between individuals can be useful for uncovering the genetic basis of recombination rate evolution.

Understanding the evolution of recombination rate is further complicated by the different genomic scales on which recombination rates are measured. Patterns of variation depend on the resolution at which recombination is characterized; different resolutions are also a product of the sundry collection of techniques in the geneticist's toolbox for quantifying recombination rate. At the genome-wide scale, patterns of variation between species appear dominated by karyotype, with a lower limit seemingly set by the number of chromosomes and the meiotic requirements for proper disjunction (Villena and Sapienza 2001; Fledel-Alon et al. 2009; Segura et al. 2013). Across chromosomes, megabase-sized intervals vary in different genetic backgrounds (Broman et al. 1998; Thomsen et al. 2001; Kong et al. 2002; Dumont et al. 2011; Comeron et al. 2012). And on the finest scales, "recombination hotspots" in kilobase regions are thought to evolve rapidly in some species (McVean et al. 2004; Winckler et al. 2005; Brunshcwig et al. 2012).

Evidence from these many scales paints a rough portrait of recombination rate evolution. It is clear that variation in recombination rate within and between species has a genetic basis and the ability to respond to evolutionary forces (Chinnici 1971; Kidwell and Kidwell 1976; Charlesworth and Charlesworth 1985). How evolution of recombination rate at one genomic scale contributes to evolution is less clear. Patterns of variation at different scales suggest that different factors may be controlling evolution at different scales (Paigen et al. 2008).

The identity of the evolutionary forces on recombination rate, and their contributions to its patterns of variation remain elusive. Furthermore, much of our understanding of the genetic basis of recombination rate evolution comes from studies of humans or laboratory strains. The genetic basis of natural variation in recombination rate has not been thoroughly described. The identity of loci responsible for recombination rate variation, and the architecture of their action, may be completely different between wild populations.

This dissertation uses the powerful techniques developed in the mouse model system (*Mus musculus*) to describe natural variation in recombination rate and investigate the genetics of its evolution. Using crosses in wild-derived mouse strains, this dissertation extends and compares existing knowledge from studies on laboratory strains. Experimental crosses have the advantage of separating out genetic effects by raising individuals in a common environment. One of the strains of mice used in the experimental crosses comes from Gough Island (GI). This unusual population of wild house mouse has an exceptionally large body size and is thought to have diverged from mainland populations by less than 200 years (Gray et al. 2014). The short divergence times between strains in these crosses contrasts with existing studies, providing a view of recombination rate evolution within subspecies of mice. The distinction between understanding the genetics and variation from laboratory strains and wild-derived populations should be highlighted here. Wild house mice are a species complex that diverged less than 500,000 years ago (Geraldes et al. 2011) with three main subspecies, *M. m. musculus*, *M. m. domesticus*, and *M. m. castaneus*. While laboratory strains are mostly derived from *M. m. domesticus*, they contain large nonrandomly distributed regions of intersubspecific origin (Yang et al. 2007). These relationships with other subspecies confound evolutionary interpretations from laboratory strains.

Each of the chapters in the dissertation addresses distinct aspects of the evolution of recombination rate in the house mouse. In Chapter 2, a comparison of genetic maps constructed from over 1,200 meioses reveals pervasive variation among mice from GI. This polymorphism exists despite the absence genome-wide recombination rate differences among these mice. In Chapter 3, cytological characterization of recombination rates in mice from an intercross reveals quantitative trait loci (QTL) responsible for its evolution in GI mice. A surprising result from this chapter is the presence of antagonistic alleles for recombination rate. In Chapter 4, the synaptonemal complex, a proteinaceous structure closely linked to the recombination process, and its relationship with recombination rate is examined. This chapter combines cytological techniques with computer vision algorithms to map QTL for variation in synaptonemal complex length. Finally, some additional conclusions and future directions are presented in Chapter 5.

Chapter 2
Recombination rate evolution in mice from an isolated island[1]

Abstract

Recombination rate is a heritable trait that varies among individuals. Despite the major impact of recombination rate on patterns of genetic diversity and the efficacy of selection, natural variation in this phenotype remains poorly characterized. We present a comparison of genetic maps, sampling 1,212 meioses, from a unique population of wild house mice (*Mus musculus domesticus*) that recently colonized remote Gough Island. Crosses to a mainland reference strain (WSB/EiJ) reveal pervasive variation in recombination rate among Gough Island mice, including sub-chromosomal intervals spanning up to 28% of the genome. In spite of this high level of polymorphism, the genome-wide recombination rate does not significantly vary. In general, we find that recombination rate varies more when measured in smaller genomic intervals. Using the current standard genetic map of the laboratory mouse to polarize intervals with divergent recombination rates, we infer that the majority of evolutionary change occurred in one of the two tested lines of Gough Island mice. Our results confirm that natural populations harbor a high level of recombination rate polymorphism and highlight the disparities in recombination rate evolution across genomic scales.

[1] Chapter published as peer-reviewed article: Wang, R. J., Gray, M. M., Parmenter, M. D., Broman, K. W., &

Contributions were as follows: RJW and BAP designed the study. MMG and MDP performed crosses and collected data. RJW and KWB conducted analyses. RJW and BAP wrote the manuscript.

Introduction

Recombination ensures the fidelity of chromosome pairing and segregation during meiosis (Tsubouchi and Roeder 2003; Hassold 2007; Lao et al. 2013). Recombination also shapes evolution by shuffling alleles across genetic backgrounds, increasing the efficacy of selection and muddling a population's genealogical history (Felsenstein 1974; Otto and Lenormand 2002; Griffiths and Marjoram 1996; Schierup and Hein 2000). Despite recombination's conserved functional roles, its rate varies among individuals, within and between species (True et al. 1996; Graffelman et al. 2007; Coop et al. 2008; Dumont and Payseur 2011a; Smukowski and Noor 2011; Comeron et al. 2012). Recombination rate shows resemblance among relatives (Kong et al. 2004; Coop et al. 2008; Fledel-Alon et al. 2011), maintains strain differences in a common environment (Koehler et al. 2002; Dumont and Payseur 2011b; Baier et al. 2014), and responds to artificial selection (Chinnici 1971; Kidwell and Kidwell 1976; Charlesworth and Charlesworth 1985), revealing a genetic component to individual variation. Multiple loci, including specific genes, that confer recombination rate differences have been identified (Kong et al. 2008; Murdoch et al. 2010; Dumont and Payseur 2011b; Parvanov et al. 2010; Sandor et al. 2012; Ma et al. 2015; Johnston et al. 2016; Hunter et al. 2016).

Patterns of individual variation in recombination rate depend on the genomic scale of measurement. Cytological techniques, which visualize and enumerate crossovers in meiocytes (Anderson et al. 1999; Koehler et al. 2002; Baier et al. 2014), offer direct estimates of the genome-wide recombination rate. At this scale, individual recombination rates are constrained by the requirement that each chromosome (or chromosome arm) has at least one crossover for proper chromosome segregation (Mather 1936; Villena and Sapienza 2001; Fledel-Alon et al.

2009). The connection between recombination rate and karyotype is perhaps most visible in the elevated recombination rates of bird species with genomes that are rich in micro-chromosomes (Burt et al. 2002; Groenen et al. 2009; Backstrom et al. 2010). Beyond this karyotypic pattern, the genome-wide recombination rate shows a phylogenetic signal across mammals (Dumont and Payseur 2008; Segura et al. 2013; Froehlich et al. 2015), suggesting that evolution proceeds at a slow to moderate pace.

Genetic linkage maps reveal heterogeneity in recombination rate on the chromosomal scale. Along a chromosome, recombination is often suppressed near the centromere and elevated in distal regions (Beadle 1932; Mahtani and Willard 1998; Lynn et al. 2004; Talbert and Henikoff 2010). Sex appears to be a major determinant of these stereotypical patterns: elevated recombination near telomeres predominates in males from a variety of species (Broman et al. 1998; Kochakpour and Moens 2008; Giraut et al. 2011; Liu et al. 2014; Ma et al. 2015; Smeds et al. 2016). Several genomic parameters correlate with recombination rate across the genome, including gene density, GC content, nucleotide diversity, repetitive elements, chromosome position, and certain sequence motifs (Begun and Aquadro 1992; Eyre-Walker 1993; Fullerton et al. 2001; Rizzon et al. 2002; Kong et al. 2002; Jensen-Seaman et al. 2004; Winckler et al. 2005; de Massy 2013). A subset of megabase-sized intervals also exhibit significant differences in recombination rate among individuals (Broman et al. 1998; Kong et al. 2002; Dumont et al. 2011; Smukowski and Noor 2011; Comeron et al. 2012).

On the finer scale, recombination rates across the genome can span orders of magnitude. In humans, mice, and yeast, crossovers are concentrated in kilobase-sized regions termed “recombination hotspots” (Gerton et al. 2000; Jeffreys et al. 2001; Paigen et al. 2008). Sperm genotyping demonstrates variation in the intensity and position of recombination hotspots among

men (Cullen et al. 2002; Neumann and Jeffreys 2006; Tiemann-Boege et al. 2006; Webb et al. 2008). Comparisons of linkage disequilibrium suggest rapid evolution of hotspots among human populations (McVean et al. 2004; Evans and Cardon 2005) and other primates (Ptak et al. 2005; Winckler et al. 2005; Brunschwig et al. 2012), but evolutionary stasis among finches (Singhal et al. 2015).

The collection of techniques for quantifying recombination rate currently forms a disjointed picture of how recombination evolves. Estimating recombination rate from the transmission of markers among relatives offers key advantages for characterizing recombination rate evolution. In contrast to other approaches, genetic linkage maps measure current recombination rates across the entire genome and traverse the many genomic scales on which recombination rate varies. High-resolution genetic maps exist for a growing number of species (Kong et al. 2002; Cox et al. 2009; Rockman and Kruglyak 2009; Comeron et al. 2012; Kawakami et al. 2014). Despite this progress, statistical comparisons among genetic maps with the purpose of quantifying recombination rate evolution remain rare (Poissant et al. 2010; Dumont et al. 2011; Comeron et al. 2012; Ross et al. 2015). Genomic scans for specific intervals that show heritable variation in recombination rate among individuals from a single natural population are even less common (but see Comeron et al. 2012).

Recombination has been studied more extensively in laboratory mice (*Mus musculus*) than in any other vertebrate, combining dense genetic maps (Shifman et al. 2006; Cox et al. 2009; Liu et al. 2011) with mechanistic studies (Holloway et al. 2008; Paigen and Petkov 2010; Bolcun-Filas and Schimenti 2012; Cole et al. 2014; Hunter et al. 2015). This work provides a rich context for understanding the evolution of recombination in wild mice. At the same time, distinct histories and environments raise the prospect that recombination experiences contrasting

evolutionary dynamics in wild mice and laboratory mice. Although studies of human pedigrees have detected individual differences in recombination rate (Broman et al. 1998; Kong et al. 2002), mice provide additional advantages as a model system. First, genetic and non-genetic contributions to recombination rate can be separated – a challenging task in humans – by raising mice in a common environment. This possibility is important in light of the evidence that recombination rate is shaped by an array of environmental factors (Bomblies et al. 2015). Second, inbred mice can be used to generate large recombinant families, providing statistical power to identify recombination rate differences among strains in sub-chromosomal intervals. Here we take advantage of an unusual population of wild mice to understand how recombination rate evolves in nature. Gough Island is a remote, South Atlantic island that was colonized by house mice, probably only a few hundred generations ago (Gray et al. 2014). By comparing genetic maps, we find substantial variation in the recombination rate on multiple genomic scales between two lineages of mice from this isolated island. In contrast to most previous examinations of recombination rate variation, we identify specific genomic intervals with heritable differences in rate within a single natural population.

Materials and Methods

Mice, crosses, and genotyping

Intercrosses involved mice derived from Gough Island and the wild-derived inbred strain WSB/EiJ (Jackson Laboratory, Bar Harbor, ME), which is descended from mainland North America. Gough Island is a remote volcanic island in the South Atlantic Ocean, part of a protected wildlife refuge that has been designated a UNESCO World Heritage Site. Mice from

Gough Island (GI) were live-trapped and transported to the Charmany Instructional Facility at the University of Wisconsin – Madison. A breeding colony consisting of 25 mature females and 21 mature males was established. All mice were housed in microisolator cages separated by sex in a temperature-controlled room (68-72º) set to a 12-hour light/dark cycle. Food (Teklad 6% fat mouse/rat diet; Harlan Laboratories, Madison, WI) and water were provided ad libitum, corn cobs ground to 1/8th inch were provided for bedding (Waldschmidt and Sons, Madison, WI), and irradiated sunflower seeds (Harlan Laboratories) and nesting material were provided weekly for enrichment. For identification, pups were toe tattooed with sterile lancets and tattoo paste starting at 1 week, while ears were punched at weaning (3-4 weeks) to identify adults. Additional details on the transport, housing, and establishment of the breeding colony of GI mice can be found in Gray et al. (2015).

We began the intercrosses with a full-sib male and female chosen from each of two partially inbred lines in our breeding colony of GI mice, denoted Line A and Line B. These lines were created from four generations of full-sib mating among the laboratory-born offspring of wild GI mice. The four mice, one male and one female from each of Line A and Line B, were each crossed with WSB/EiJ to generate four independent sets of F_1s and four F_2 intercrosses (Figure 2.1). We generated 497 F_2 mice from the Line A cross and 877 F_2s mice from the Line B cross, for a total of 1374 F_2s. Among these mice, 419 from the Line A cross and 793 from the Line B cross were incorporated into subsequent analyses after removing mice that were not genotyped or contained obvious genotyping errors.

Mice were genotyped on the Mega Mouse Universal Genotyping Array (MegaMUGA; Morgan et al. 2016), an Illumina Infinium array containing 77,808 markers. The vast majority of markers on the array are single nucleotide polymorphisms (SNPs), though a few structural and

transgenic markers are also present. Markers cover the autosomes, sex chromosomes, and mitochondria with an average spacing of ~33 kb across the genome. Liver tissue from F_2 individuals, as well as controls, was sent to GeneSeek (NeoGene, Lincoln, Nebraska) for DNA extraction and genotyping. Samples were divided among 16 96-well plates and several steps were taken to identify and control for errors. WSB samples were placed on each plate to account for plate extraction effects, parental GI samples were replicated across plates, and the sample from the first well of each plate was replicated across plates. Markers with high rates of missing data were omitted, as were mice with high rates of missing genotypes. We removed a small number of individuals that showed many Mendelian inconsistencies or mismatched genotypic and phenotypic sex.

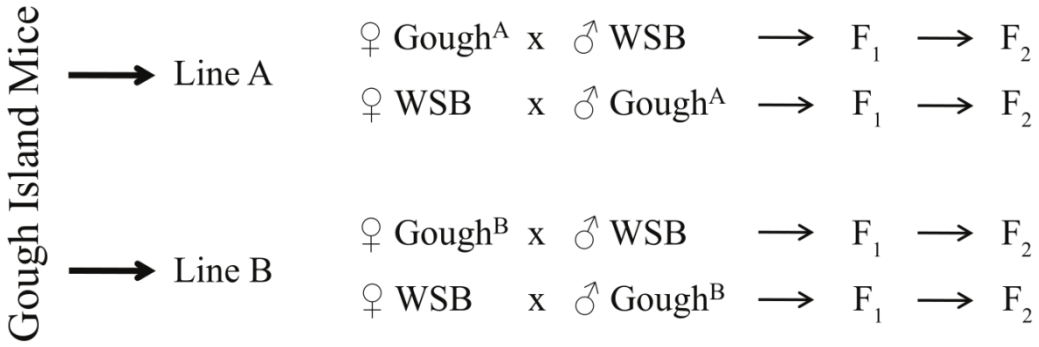

Figure 2.1. Cross Design
Partially inbred lines of Gough Island mice were crossed with the wild-derived inbred strain WSB/EiJ. Four independent F_2 intercrosses were generated from these crosses.

Construction and comparison of genetic maps

To construct and compare genetic maps, we selected a subset of 11,833 informative SNPs from our genotype data. These SNPs were invariant among the GI mice we genotyped and

displayed the segregation patterns expected for a standard F_2 intercross between inbred lines. Mapping distances for each cross were estimated from these SNPs using the Lander-Green hidden Markov model (Lander and Green 1987) implemented in the R/qtl est.map function (Broman et al. 2003). We assumed a genotyping error rate of 0.2% and converted recombination fractions to map distances with the Carter-Falconer map function (Carter and Falconer 1951). To determine thresholds for statistical significance in map length comparisons, we permuted line labels across mice and reconstructed genetic maps. We performed 2000 permutations, retaining the numbers of mice labeled as Line A or Line B in each permutation. The map length of a chromosome was determined to be significantly different between GI lines if the observed difference was at least as extreme as 5% of differences for that chromosome among permutations. We used the same approach to test for significant differences in overall map length.

To compare recombination rates among GI lines on a finer scale, we examined map lengths in sliding windows across the genome. Windows spanned 10 Mb, 25 Mb, and 50 Mb with a step size of 250 kb. We calculated a p-value for the observed difference in map length of each window as the proportion of replicates that produced a difference greater than or equal to the observed value. Each window had a respective set of 2000 permutations from which we calculated the p-value. To control for false positives arising from multiple testing in these overlapping windows, we used a false discovery rate approach (Storey and Tibshirani 2002). We calculated a q-value for each window using the full set of p-values across all windows and rejected the null hypothesis of no difference in map length at $q < 0.1$. The distributions of p-values across windows were not independent, but our use of an empirical null should be conservative (Leek and Storey 2011). We combined overlapping windows showing significant

differences to generate a final list of divergent intervals. We checked the performance of the multiple testing correction by looking for windows with significantly different map lengths in an additional set of 100 permuted maps. After controlling for false discovery using our larger set of 2000 permutations, each set of 100 permuted maps had an average of less than 10 significant windows at the $q < 0.1$ level. This is the number of significant windows we should expect in the absence of true differences in recombination rate. Finally, it is possible that the difference in sample size between the two GI line crosses could contribute to observed variation in recombination rate. To account for this effect, we repeated the search for significantly different windows with an equivalent number of mice from the two lines. Specifically, we randomly selected a subset of 419 F_2 individuals from Line B to match the number in Line A, constructed maps from this subset, and created 1,000 sets of permuted maps from this subset to calculate p-values.

To provide perspective for the differences in recombination rate between GI lines, we conducted additional comparisons with the mouse reference genetic map (downloaded from http://cgd.jax.org/mousemapconverter/). The mouse reference genetic map features data from a heterogeneous stock (HS) mouse population derived from crosses involving eight classically inbred strains (Shifman et al. 2006; Cox et al. 2009). The HS map, which sampled 3,546 meioses, was constructed from genotypes at 10,195 SNPs. For comparison to GI maps, we converted the HS map positions from the Kosambi map function to the Carter-Falconer map function, and anchored the proximal markers of the GI maps using interpolated recombination rates, following the practice in Cox et al. (2009). We re-estimated recombination rates for the HS map in sliding windows using the approach as described above. We computed correlations in recombination rate by comparing the same windows in the HS and GI maps.

Genomic features, sequencing, and motif search

To identify potential determinants of recombination rate variation, we calculated correlations between genomic features known to be associated with recombination and differences in recombination rate among GI lines. Positions of genomic features were downloaded from the UCSC annotation database for NCBI Build 37/mm9. For chromatin state, annotations by ChromHMM (Ernst and Kellis 2012) on mouse testis – the only annotated germline tissue – were downloaded from the Mouse Encode Consortium (Mouse ENCODE Consortium 2012; Yue et al. 2014). To evaluate the influence of evolutionary breakpoint regions (Farré et al. 2013; Ullastres et al. 2014), we identified 364 such regions in a synteny analysis between the mouse and human reference genomes with Cassis (Lemaitre et al 2008; Baudet et al. 2010).

To minimize autocorrelation, we estimated recombination rate in non-overlapping windows for these analyses, again sized at 10 Mb, 25 Mb, and 50 Mb. We also compared recombination rate differences among GI lines to rates estimated in corresponding non-overlapping windows for the HS map.

The PRDM9 protein is a major determinant of crossover position in the mouse genome (Baudat et al. 2010; Parvanov et al. 2010; Grey et al. 2011). We used new genome sequences to test the prediction that windows with divergent recombination rates are enriched for polymorphic binding sites for PRDM9. We sequenced the genomes of the four GI parents of our intercrosses at an average 10X coverage using 100 bp paired-end reads on an Illumina HiSeq 2500. Reads were mapped to the C57BL/6 mouse reference genome using the Burrows-Wheeler Aligner (Li and Durbin 2009) and SNPs were called with SAMtools 1.0 (Li et al. 2009). Using these sequences, we identified fixed differences between GI Lines A and B and constructed a 50 bp

window centered on each fixed difference. We used this set of windows to query against the consensus PRDM9 binding motif using its position weight matrix (Brick et al. 2012) and FIMO from the MEME Suite of bioinformatics tools (Grant et al. 2011). Additionally, we performed a signed test in intervals with divergent recombination rates to determine whether the number of variable motifs correlated with the direction of divergence. Finally, we used PCR primers fl1500U20, mZPrdm9-R1, Meis284L23, and mZPrdm9-F1 (Buard et al. 2014) to amplify the last exon of PRDM9 in the GI lines. We ran the PCR products on 1% agarose gels to determine whether their sizes matched alleles known to confer recombination rate differences within M. m. domesticus (Buard et al. 2014).

Results

We documented recombination rate variation between two lines of Gough Island (GI) mice (Lines A and B) by comparing genetic maps built from two sets of F_2 intercrosses with a common reference strain (WSB/EiJ). The genome-wide recombination rate, represented by total map length, was similar, at 1347 cM (Line A) and 1340 cM (Line B). Despite similarity in the genome-wide rate, five chromosomes (2, 5, 8, 9, and 18) showed statistically significant differences in map length (Table 2.1). Notably, chromosome 8 was 16% longer in Line B. This disparity among five chromosomes represents a significant departure from the expectation that no difference exists between the two GI Lines ($P < 0.002$; Fisher's combined p-value test).
To measure variation in recombination rate on a sub-chromosomal scale, we tiled the genome with overlapping windows of fixed physical size and compared map lengths across pairs of corresponding windows for the two lines. We repeated the analysis with three window sizes – 50

Mb, 25 Mb, and 10 Mb – to capture differences in recombination rate on multiple scales. We found 500 (50 Mb windows), 483 (25 Mb), and 165 (10 Mb) windows with significant recombination rate differences. These numbers exceed null expectations generated by analyses of permuted datasets (see Methods). On all three scales, windows that exhibited significantly different map lengths were typically adjacent to other significant windows (Figure 2.2). We combined significant windows that overlapped into discrete intervals for further analysis. Fourteen chromosomes harbored intervals with divergent recombination rate on at least one scale (Table 2.2); these intervals often displayed divergence across multiple window sizes (Figure 2.2). It is notable that no divergent intervals were identified on the X chromosome. Similar comparisons of recombination rate made between strains from different subspecies (*Mus musculus castaneus* and *Mus musculus musculus*) identified a disproportionately large number of divergent intervals on the X chromosome (Dumont et al. 2011).

The magnitude of variation in recombination rate was inversely correlated with interval size ($p < 5 \times 10^{-5}$). The greatest differences in recombination rate, as percentages of the mean (109% on chromosome 1) and as absolute differences (0.61 vs 0.96 cM/Mb on chromosome 18), were visible in the 10 Mb window analysis. In many cases, intervals discovered while scanning with smaller windows localized differences found in scans with larger windows. For example, among the differences in map length found on chromosome 15, which were identified at all three scales, the majority localized to a single 12.5 Mb interval.

Patterns of variation in recombination rate from these sub-chromosomal intervals generally matched patterns at the chromosome and genome level. Chromosomes with significantly different map lengths (Table 2.1) contained intervals with consistent differences. Total differences in map length, as a sum of the divergence in all intervals, were not statistically

significant on any window size – mirroring the absence of a significant difference in the whole genome recombination rate. These observations suggest that coarse variation in recombination rate is due to the clustering of differences at finer scales. Chromosomes 8 and 9 showed a contrasting pattern: most of the differences in recombination rate on these chromosomes were only significant when surveyed at the 50 Mb or whole chromosome level. However, differences in statistical power are a challenge when comparing rates across chromosomes. Longer chromosomes have many fewer crossovers per Mb, reducing our ability to detect differences at finer scales.

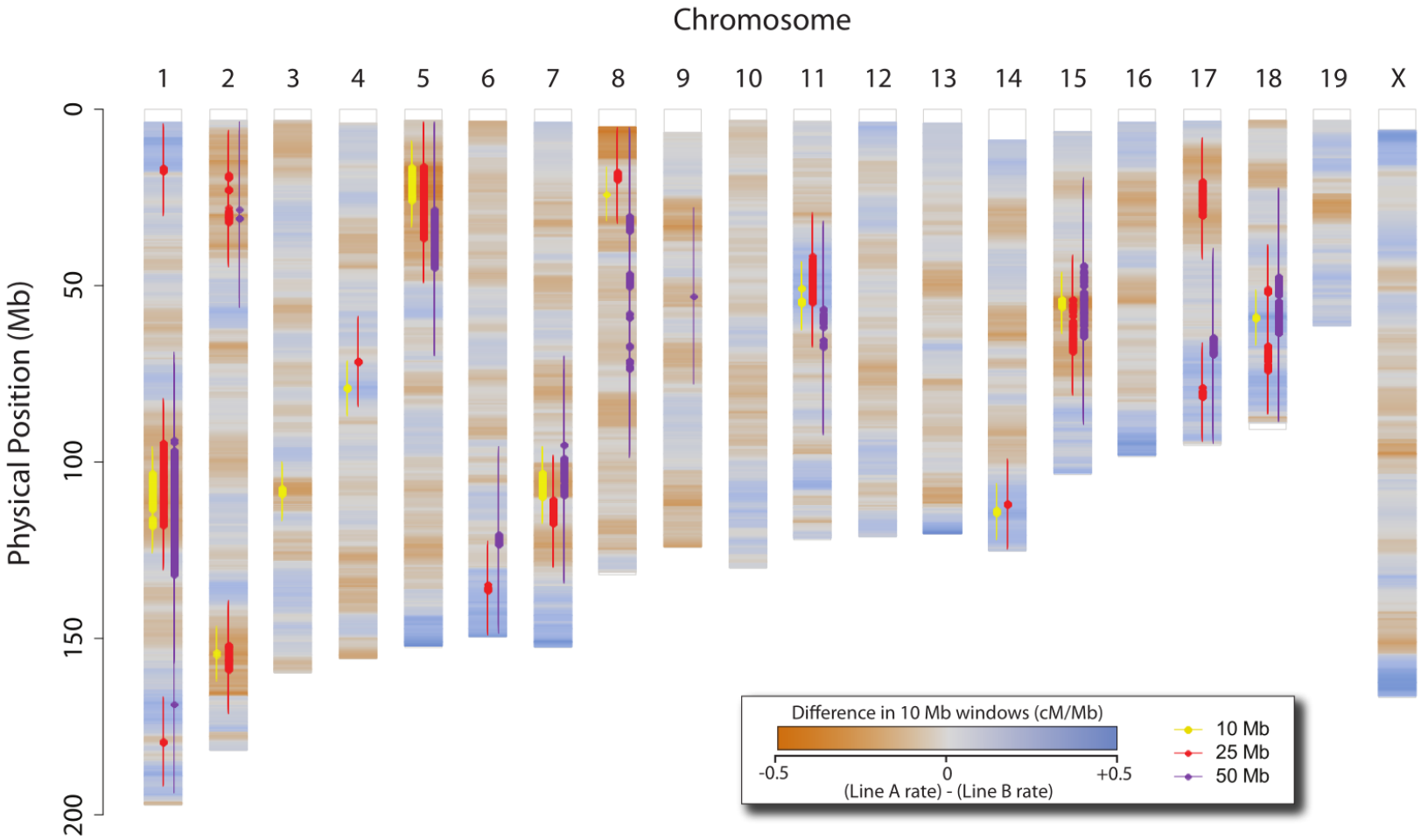

Figure 2.2. Recombination rate differences between two lines of Gough Island Mice

Differences in recombination rate between two lines of Gough Island mice visualized as a gradient along chromosomes. Intensity of gradient from yellow to purple indicates greater relative recombination rate in Line A and Line B respectively. Plot markers with whiskers show center and range of 10, 25, and 50 Mb windows where recombination rates differ significantly (10% FDR).

Table 2.1. Genetic map lengths for each chromosome in two lines of Gough Island mice. Asterisks highlight chromosomes with significantly different map lengths at the $p < 0.05$ level. P-values are calculated from two-tailed tests using 2000 permutations. Percent difference calculated as ($Length_{LineA}$ – $Length_{LineB}$) / Mean.

Chr	Line A (cM)	Line B (cM)	Diff. (cM)	% diff.	p-value
1	94.35	92.01	2.34	2.5%	0.444
2	89.18	96.15	-6.97	-7.5%	0.019 *
3	72.90	73.39	-0.49	-0.7%	0.897
4	76.83	76.40	0.43	0.6%	0.852
5	77.88	84.09	-6.21	-7.7%	0.041 *
6	70.61	69.21	1.40	2.0%	0.627
7	75.89	78.64	-2.75	-3.6%	0.338
8	60.10	70.24	-10.14	-15.6%	0.001 *
9	59.85	65.24	-5.39	-8.6%	0.032 *
10	67.17	67.73	-0.56	-0.8%	0.839
11	81.01	76.22	4.79	6.1%	0.092
12	58.00	57.27	0.73	1.3%	0.744
13	55.21	56.25	-1.04	-1.9%	0.675
14	60.29	57.96	2.33	3.9%	0.340
15	52.18	54.82	-2.64	-4.9%	0.291
16	54.22	52.83	1.39	2.6%	0.509
17	55.12	53.17	1.95	3.6%	0.427
18	56.52	50.59	5.93	11.1%	0.006 *
19	51.99	49.39	2.60	5.1%	0.231
X	70.25	65.64	4.60	6.8%	0.221
Total	1339.55	1347.24	-7.69	-0.6%	0.562

Table 2.2. Regions of divergent recombination between Gough Island lines

Recombination rate was estimated in 10 Mb, 25 Mb, and 50 Mb sliding windows across the genome. Windows with significantly divergent recombination between Gough Island lines were identified by permutation. The recombination rate in these genomic regions as measured in the heterogeneous stock (HS) is also shown for comparison.

50 Mb windows

	Physical position (Mb)			Line A rate	Line B rate		HS rate	% diff. with:	
chr	begin	end	size	(cM/Mb)	(cM/Mb)	% diff.	(cM/Mb)	Line A	Line B
1	68.7	156.9	88.25	0.291	0.354	-20%	0.365	-20%	-3%
1	143.7	193.7	50	0.717	0.617	15%	0.692	4%	-11%
2	3.3	56.1	52.75	0.500	0.582	-15%	0.563	-11%	3%
5	3.4	69.9	66.5	0.426	0.535	-23%	0.527	-19%	2%
6	95.4	148.4	53	0.692	0.587	16%	0.638	9%	-8%
7	69.9	134.4	64.5	0.408	0.502	-21%	0.542	-25%	-7%
8	5.1	98.6	93.5	0.370	0.460	-22%	0.493	-25%	-7%
9	27.8	77.8	50	0.480	0.574	-18%	0.583	-18%	-2%
11	31.5	92.3	60.75	0.620	0.527	16%	0.631	-2%	-17%
15	19.1	89.4	70.25	0.430	0.497	-14%	0.523	-18%	-5%
17	39.3	94.6	55.25	0.814	0.711	14%	0.754	8%	-6%
18	22.2	88.5	66.25	0.748	0.638	16%	0.704	6%	-9%
					Total:	0.8%	**Total:**	-2.9%	-2.0%

25 Mb windows

	Physical position (Mb)			Line A rate	Line B rate		HS rate	% diff. with:	
chr	begin	end	size	(cM/Mb)	(cM/Mb)	% diff.	(cM/Mb)	Line A	Line B
1	3.9	30.2	26.3	0.603	0.456	28%	0.370	63%	23%
1	81.9	130.4	48.5	0.179	0.291	-48%	0.294	-39%	-1%
1	166.4	191.9	25.5	0.929	0.743	22%	0.940	-1%	-21%
2	5.8	44.6	38.8	0.456	0.607	-28%	0.611	-25%	-1%
2	139.1	171.3	32.3	0.557	0.732	-27%	0.793	-30%	-8%
4	58.5	84.3	25.8	0.432	0.310	33%	0.295	47%	5%
5	3.4	49.2	45.8	0.366	0.543	-39%	0.532	-31%	2%
6	122.2	148.9	26.8	0.892	0.740	19%	0.790	13%	-6%
7	97.9	129.9	32.0	0.294	0.406	-32%	0.503	-42%	-19%
8	5.1	32.4	27.3	0.410	0.537	-27%	0.594	-31%	-10%
11	29.0	67.3	38.3	0.718	0.599	18%	0.645	11%	-7%
14	98.9	124.7	25.8	0.762	0.597	24%	0.678	12%	-12%
15	41.1	81.1	40.0	0.408	0.554	-30%	0.556	-27%	0%
17	7.8	42.6	34.8	0.251	0.365	-37%	0.429	-41%	-15%
17	66.1	94.1	28.0	1.063	0.878	19%	0.908	17%	-3%
18	38.2	64.5	26.3	0.708	0.543	26%	0.661	7%	-18%
18	54.2	86.5	32.3	1.013	0.818	21%	0.907	12%	-10%
					Total:	0.1%	**Total:**	-1.8%	-1.7%

10 Mb windows

	Physical position (Mb)			Line A rate	Line B rate		HS rate	% diff. with:	
chr	begin	end	size	(cM/Mb)	(cM/Mb)	% diff.	(cM/Mb)	Line A	Line B
1	97.9	123.2	25.3	0.064	0.218	-109%	0.203	-68%	7%
2	148.8	159.6	10.8	0.259	0.487	-61%	0.611	-58%	-20%
3	102.2	114.2	12.0	0.205	0.386	-61%	0.356	-43%	8%
4	73.5	84.3	10.8	0.502	0.272	59%	0.351	43%	-23%
5	11.2	30.9	19.8	0.336	0.606	-57%	0.652	-48%	-7%
7	97.9	114.9	17.0	0.172	0.277	-47%	0.370	-54%	-25%
8	18.9	28.9	10.0	0.203	0.395	-64%	0.588	-65%	-33%
11	45.5	60.0	14.5	0.754	0.476	45%	0.719	5%	-34%
14	108.4	119.4	11.0	0.686	0.385	56%	0.568	21%	-32%
15	48.6	61.1	12.5	0.340	0.584	-53%	0.571	-41%	2%
18	53.5	64.2	10.8	0.958	0.605	45%	0.756	27%	-20%
					Total:	0.5%	**Total:**	-1.5%	-1.0%.

Comparison to the standard mouse genetic map

Variation in the genetic maps described thus far represents an estimate of recombination rate polymorphism between two GI mice. To place this variation in a broader perspective, we compared the two genetic maps from crossing GI mice to WSB/EiJ with the standard genetic map of the laboratory mouse (the HS map). On the genome-wide level, the GI maps, at 1388 cM (averaged and converted to match the HS analysis), were shorter than the 1457 cM of the HS map. Local recombination rates in both GI lines were highly correlated with those in the HS (Table 2.3). Overall, the GI maps showed higher correlation with each other than with the HS map, with the degree of correlation decreasing as resolution increased.

We further investigated the relationship between the GI maps and HS map by focusing on windows for which recombination was significantly divergent between GI lines. Following the pattern observed in the comparison between GI lines, rate differences between the GI and HS maps were more pronounced in smaller windows (Table 2.2). By assuming that the two GI lines are more closely related to each other than either is to the collection of strains that comprise the HS (i.e. HS is the outgroup), we could polarize the changes in recombination rate in the GI lines. We observed a consistent bias: most GI-divergent intervals showed greater rate differences between Line A and the HS than between Line B and the HS (paired t-test, intervals from windows 50 Mb: $p = 0.093$, 25 Mb: $p = 0.004$, 10 Mb: $p = 0.037$) (Table 2.2). This bias was also seen in the collection of significantly different sliding windows, for which Line A rates showed substantially greater dispersion from HS rates (Levene's test, $p < 1 \times 10^{-15}$ for all three window sizes). Figure 2.3 illustrates this for 25 Mb windows; the greater squared residual deviation of rates from Line A relative to HS can be seen in the third panel. We repeated this analysis using a random subset of individuals from Line B, matching the number of individuals in Line A to

account for the possibility that the smaller sample size in Line A was responsible for its higher divergence from HS. This power-matched comparison detected 71% as many significant windows as did the analysis with the full sample, but these significant windows continued to show higher dispersion from HS in Line A vs. Line B (Levene's test, $p < 5 \times 10^{-5}$ for all three window sizes). This pattern suggests that evolution in Line A was disproportionately responsible for differences between GI lines. For example, the 109% difference between GI lines in a region of chromosome 1 mostly reflects an evolutionary reduction in recombination rate in Line A.

Table 2.3. Correlation of recombination rates between Gough Island lines and heterogeneous stock (HS)
Pearson correlation coefficients calculated for corresponding 10, 25, and 50 Mb sliding windows across the genome with respective 95% confidence intervals. Correlation coefficients were highly significant for all comparisons.

Correlation between	50 Mb		25 Mb		10 Mb	
	ρ	95% CI	ρ	95% CI	ρ	95% CI
Line A and Line B	0.909	0.905 - 0.914	0.913	0.909 - 0.916	0.882	0.877 - 0.886
Line A and HS	0.897	0.893 - 0.901	0.855	0.850 - 0.860	0.764	0.755 - 0.772
Line B and HS	0.925	0.922 - 0.927	0.891	0.887 - 0.895	0.798	0.791 - 0.805

Correlates of recombination rate polymorphism

Within-genome variation in recombination rate has been associated with a variety of genomic characteristics, including GC content, classes of repetitive elements, chromatin structure, gene density, evolutionary breakpoint regions, and distance from the centromere (Fullerton et al. 2001; Rizzon et al. 2002; Jensen-Seaman et al. 2004; Freudenberg et al. 2009; Paigen et al. 2008; Paape et al. 2012; Farré et al. 2013; Kawakami et al. 2014; Liu et al. 2014). We examined whether these genomic features were also associated with recombination rate

differences among individuals, i.e. between the two lines of GI mice. We estimated recombination rates in non-overlapping windows of 10 Mb, 25 Mb, and 50 Mb in the two GI lines and calculated the difference (RateLineA - RateLineB) between corresponding windows. Among the genomic features we evaluated, only the number of long terminal repeats (LTRs) was significantly correlated ($p < 0.05$) with the difference in recombination rate among GI lines at all three scales (Table 2.4). At the intermediate 25 Mb scale, we also detected a significant correlation between gene density and recombination rate difference. Structural rearrangements are one of the genomic features highly correlated with recombination rate variation that is absent from this analysis. The difficulty of detecting small rearrangements means that we cannot rule out the role they may be playing in recombination rate polymorphism among GI lines.

To determine whether regions of high or low recombination are enriched for recombination rate divergence, we computed correlations between the relative recombination rate differences among GI lines, $| \text{Rate}_{\text{LineA}} - \text{Rate}_{\text{LineB}} | / \text{Mean Rate}$, and recombination rate in HS mice (in non-overlapping windows). We observed a significant negative correlation ($p < 0.05$) at the 10 Mb and 50 Mb scale (Table 2.4), corresponding to higher relative variation in recombination rates in regions that experience less recombination.

PRDM9 and motifs

A portion of the kilobase-scale variation in recombination rate observed in mice is explained by specific sequence motifs (Winckler et al. 2005; Myers et al. 2008; Steiner et al. 2009). One of the best-studied motifs is the 13-bp consensus sequence bound by PRDM9, a H3K4 trimethyltransferase with a zinc finger DNA-binding domain (Hayashi et al. 2005) that regulates the location and intensity of recombination hotspots (Myers et al. 2010; Baudat et al.

2010; Parvanov et al. 2010). Variation in recombination at this fine scale depends on both allelic variation in PRDM9 – found in different subspecies and strains of mice (Baudat et al. 2010; Kono et al. 2014; Smagulova et al. 2016) – and polymorphisms in or near DNA binding sites (Baker et al. 2015). We investigated whether these determinants of hotspot variation relate to recombination rate variation between GI lines. First, we found that the two GI lines do not harbor allelic differences in PRDM9 that have been previously associated with variation in recombination rate. Next, we tested another straightforward hypothesis: the difference in the number of predicted PRDM9 binding sites among GI lines is correlated with the difference in recombination rate across genomic intervals; Stevison et al. 2016 tested a similar hypothesis across different species. Using whole-genome sequences from the parents of both crosses, we counted predicted PRDM9 binding sites in intervals of divergent recombination, and compared these values between the GI lines (see Methods). We found no evidence for an association of PRDM9 binding site number with either the direction or intensity of variation in recombination rate. While we lack the resolution to detect among-line differences in recombination rate at the kb scale, our results argue against an important contribution of PRDM9 to differences at the $\geq$ 10 Mb scale.

Table 2.4. Correlation with variation in recombination rate between Gough Island lines
Correlation of recombination rate differences between Gough Island lines in 10 Mb, 25 Mb, and 50 Mb non-overlapping windows with selected genomic features. Pearson correlation coefficient and p-value presented for GC content, CpG islands, gene density, long interspersed elements (LINE), long terminal repeats (LTR), and satellite DNA from mouse reference annotations. For chromatin state, the most prevalent state in each window was used as a categorical variable and p-values reported are from an analysis of variance. Evolutionary breakpoint regions were identified by an analysis of synteny between human and mouse reference genomes using *Cassis* (see Methods). For correlation to recombination rate itself, absolute differences in rate between the Gough lines divided by their mean rate were compared to rates from the HS map.

Genomic feature	**50 Mb**		**25 Mb**		**10 Mb**	
	ρ	**p-value**	**ρ**	**p-value**	**ρ**	**p-value**
GC content	0.019	0.82	-0.049	0.49	-0.053	0.44
CpG Islands	-0.116	0.53	-0.055	0.63	-0.100	0.14
Gene Density	-0.010	0.90	-0.168	0.02	-0.112	0.10
Chromatin State	-	0.11	-	0.99	-	0.99
LINE	0.046	0.57	0.094	0.18	0.068	0.32
LTR	-0.222	< 0.01	-0.172	0.01	-0.141	0.04
Satellite	-0.041	0.62	0.000	0.99	0.000	0.99
Breakpoint Regions	0.014	0.94	-0.046	0.68	-0.096	0.16
Distance to Centromere	0.037	0.64	0.084	0.23	0.032	0.64
Recombination Rate	-0.308	0.03	-0.142	0.15	-0.233	< 0.01

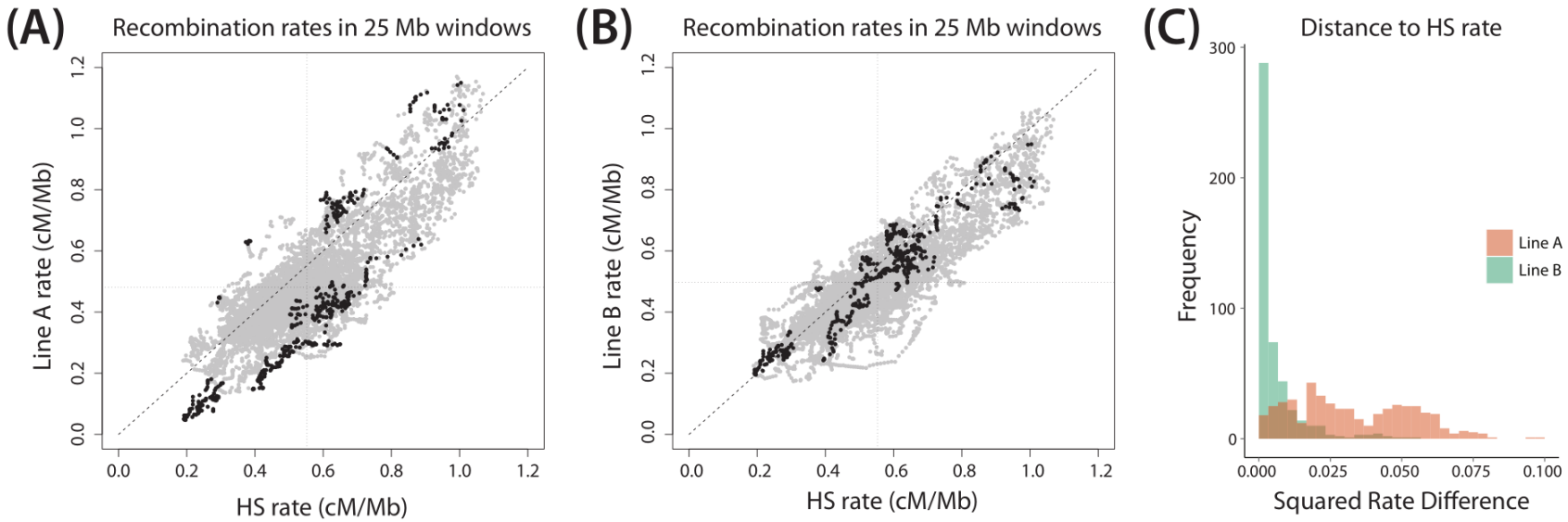

Figure 2.3. Comparisons of recombination rates in Gough Island lines and the heterogeneous stock (HS)
A comparison of recombination rates using 25 Mb sliding windows in **(A)** the HS mice and Gough Line A, and **(B)** the HS mice and Gough Line B. Each point represents a single 25 Mb window with respective recombination rates along the x and y-axis. Windows that were significantly different between Gough Island Line A and Line B are highlighted in bold on these plots. **(C)** Squared difference in recombination rate between each Gough Island line and HS for these significantly different windows, showing substantially more dispersion from HS in Line A.

Discussion

Our results reveal substantial polymorphism in the recombination rate within an isolated island population. Because the mice for this study were raised in a common environment, we interpret this polymorphism as being caused by genetic variation. Up to 28% of the genome is included within sub-chromosomal intervals that show divergent rates among Gough Island mice, and five chromosomes exhibit different map lengths. In contrast, the total genome-wide rate does not significantly vary. Two hypotheses could explain this disparity among genomic scales. First, stabilizing selection could maintain a genome-wide recombination rate even as variation accumulates at the sub-chromosomal level. This type of selection would mirror the molecular homeostasis that buffers against perturbations to the total crossover number in individual cells (Martini et al. 2006; Rosu et al. 2011; Cole et al. 2012; Lao et al. 2013). The meiotic requirement of at least one crossover per chromosome (or per chromosome arm) places a lower limit on the genome-wide recombination rate. However, our discovery of polymorphism in the chromosomal recombination rate in the absence of significant differences for total number of crossovers suggests that factors beyond proper disjunction constrain the evolution of the genome-wide rate. Indeed, experiments promoting an excess number of crossovers, with mutants that disable crossover-suppressing proteins, indicate a controlled upper bound that is independent of a biochemical maximum (Youds et al. 2010; De Muyt et al. 2012; Crismani et al. 2012). Other evidence for direct or indirect selection on overall crossover number includes the observation that mothers with higher genome-wide recombination rates are more fecund (Kong et al. 2004; Stefansson et al. 2005; Fledel-Alon et al. 2009). Perhaps recombination rate at the sub-chromosomal level has little or no effect on fitness, thereby allowing polymorphism to accumulate. An alternative explanation for the disparity in variation among genomic scales is

that selective constraints on recombination rate do not operate on the genome-wide rate. If the lower limit, set by meiotic requirements, is truly dictated by karyotype, the focus of selection should fall on recombination rates at finer (chromosomal) scales. Under this scenario, evolutionary changes to recombination rate on finer scales since the common ancestor of the two GI lines have incidentally balanced such that the overall rate remains unchanged. In this model, the genome-wide rate between these lines would presumably begin to diverge after more time passes.

We discovered that on the sub-chromosomal scale, recombination rate differences between GI lines and HS mice are asymmetric, with Line A showing more divergence. Perhaps this bias indicates a closer phylogenetic relationship between Line B and the HS mice. This seems unlikely given the history of the HS as an amalgam of classical inbred strains and the geographically singular origin of the GI mice. Alternatively, this bias might reflect the random sampling of recombination polymorphism from the GI population. Perhaps a small number of mutations modifying recombination rate are segregating in the population. Further genetic studies will be required to test this hypothesis.

Our identification of genomic correlates of recombination rate polymorphism provides additional clues into the dynamics of recombination rate evolution. Relative differences in recombination rate between GI lines were negatively correlated with the rate in the HS mice. This suggests that recombinationally cold regions are more likely to experience greater relative changes in recombination rate. We also found LTR density to be negatively correlated with differences in recombination rate between GI lines, suggesting that the evolution of recombination rate may be slower in these regions. LTR density has been strongly associated with regions of lower recombination in other organisms (Rizzon et al. 2002; Groenen et al.

2009), and LTR retrotransposons have been shown to influence double-strand break formation in meiosis (Sasaki et al. 2013).

A similar study of recombination rate variation in house mice (Dumont et al. 2011) provides an unusual opportunity to compare the evolutionary tempo of recombination rate on two timescales. Dumont et al. (2011) statistically compared genetic maps from representatives of two house mouse subspecies, *M. m. musculus* and *M. m. castaneus*. Like us, these authors constructed genetic maps from F_2 intercrosses to the WSB/EiJ reference strain, using sample sizes (580 and 554 F_2s in the two crosses) similar to ours. Thirty-one divergent windows were detected, differing on average by 4.5 cM between the *M. m. musculus* and *M. m. castaneus* maps. Divergent windows between the two GI lines are fewer and show smaller differences in recombination rate, consistent with the more recent divergence of these lines compared to *M. m. musculus* and *M. m. castaneus*. Eight of the divergent intervals we identified overlap with genomic windows that significantly differ between strains of *M. m. musculus* and *M. m. castaneus*. This is approximately consistent with the amount of overlap expected by chance given the size of the divergent intervals. However, the absence of divergent intervals on the X chromosome in the GI lines is notable given their disproportionate localization to this chromosome in the intersubspecific comparison. Our experimental design has reduced power to detect differences on the X chromosome, since the X does not recombine in F_1 males, but this is an issue shared with the previous study.

We temper our conclusions about recombination rate evolution by noting a few challenges with our experimental design. First, F_2 genetic maps reveal average recombination rates in F_1 females and F_1 males. In mice, sex is a key determinant of recombination rate on multiple genomic scales (Lynn et al. 2005; Paigen et al, 2008; Cox et al. 2009; Liu et al. 2014),

raising the prospect that females and males could differ in patterns of polymorphism. Our study is blind to this axis of variation. Second, although we detected differences among GI lines on the Mb scale, many more meioses would be required to find variation on the scale of recombination hotspots. A parallel issue is our inability to detect minor structural changes in the mouse genome. Some differences in mapping distance between GI lines could reflect inversions and other structural rearrangements segregating within the GI population. Third, the statistical power to detect differences in recombination rate depends on the total number of crossovers observed. Contrasting patterns across chromosomes, like the absence of differences at finer scales on some chromosomes, may be due to these differences in power. Finally, our interpretation of genetic map differences as polymorphism among GI lines assumes that crossing to the common reference strain (WSB/EiJ) had similar effects on recombination for both lines. Although there is no obvious reason to question this assumption, it is important to remember that the recombination we profiled occurred in F_1s and not in the GI lines. Immunocytology suggests that the genome-wide recombination rate is higher in GI mice than in WSB/EiJ (Dumont and Payseur 2011a).

The observation of substantial differences in recombination rate among a few mice drawn from an isolated population suggests that genetic variation in recombination rate is likely to be pervasive among wild house mice. The balance of evolutionary factors that govern recombination rate in nature remains unclear. A coherent model for the evolution of recombination rate will need to integrate and explain patterns of variation found on each genomic scale.

Chapter 3
Genetics of genome-wide recombination rate evolution in mice from an isolated island

Abstract

Recombination rate is a heritable quantitative trait that evolves despite the fundamentally conserved roles that recombination plays in meiosis. Differences in recombination rate can alter the landscape of the genome and the genetic diversity of populations. Yet our understanding of the genetics of recombination rate variation in natural populations remains limited. Here, we address the evolution of genome-wide recombination rate by the genetic study of its variation in Gough Island (GI) mice. GI mice are an isolated population of wild house mouse (*Mus musculus domesticus*), recently diverged from their mainland counterparts. We crossed GI-derived mice with a mainland representative and quantified genome-wide recombination rates by immunofluorescent cytology in 240 F_2s. We identified 4 QTL responsible for variation in this trait, the strongest of which had effects that opposed the direction of the parental trait differences. Candidate genes and mutations for these QTL were identified by overlapping the detected intervals with whole-genome sequencing data and publicly available transcriptomic data in spermatocytes. We also identified a QTL responsible for variance in genome-wide recombination rate among spermatocytes, suggesting a possible role for consistency in the evolution of recombination rates. Combined with existing studies, our findings suggest that genome-wide recombination rate divergence is not directional and its evolution within and between subspecies proceeds from different genetic loci.

Introduction

Meiotic recombination is a fundamental part of genetic transmission in most eukaryotes. The sets of chromosomes gametes receive have undergone an exchange of genetic material through a process known as crossing over. Crossovers, long recognized cytologically as chiasmata (Janssens 1909), fuse alleles into new haplotypic combinations. Recombination thus forms a knob that tunes the speed with which haplotypic diversity enters a population. The settings on this knob - recombination rates - are heritable, and they vary between individuals, populations and species (True et al. 1996; Kong et al. 2004; Coop et al. 2008; Smukowski and Noor 2011; Comeron et al. 2012).

The production of genetic variation among offspring by meiotic recombination is theorized to provide an advantage to organismal fitness by improving the efficacy of selection (Weismann 1889; Kondrashov 1993; Burt 2000). Many models attribute the evolutionary advantage of recombination to its ability to dispel negative, non-random allelic combinations in a population ("negative linkage disequilibrium"), produced by epistatic interactions (Feldman et al. 1980; Barton 1995) or by genetic drift (Hill and Robertson 1966; Felsenstein 1974; Otto and Barton 1997). In this theoretical framing, the advantages of eliminating negative linkage disequilibrium lead to indirect selection favoring recombination. Increased recombination rate in response to artificial selection on a variety of phenotypes (Flexon and Rodell 1982; Burt and Bell 1987; Gorlov et al. 1992; Korol and Iliadi 1994) provides corroborating evidence for this hypothesis, though some studies reveal no such increase (Bourguet et al. 2003; Fuentes et al. 2015). In nature, indirect selection on recombination rate is likely to be strongest in populations subject to directional selection, including those populations experiencing new environments (Otto and Barton 2001).

Another possibility is that recombination rate itself is targeted by selection. Human mothers with higher average rates of crossing over have more children (Kong et al. 2004; Coop et al. 2008). Chiasmata generate physical tension between homologous chromosome pairs in meiosis, a necessity for proper chromosome disjunction (Roeder 1997; Hassold and Hunt 2001). This process leads to the constraint that each chromosome, or chromosome arm, harbor at least one crossover (Villena and Sapienza 2001; Fledel-Alon et al. 2009). It has also been suggested that the number of recombination events is limited to reduce the chances of aberrant exchange, which can lead to deleterious chromosomal rearrangements (Inoue and Lupski 2002; Coop and Przeworski 2007). Furthermore, in the lab, artificial selection targeting recombination rate often generates a response (Chinnici 1971; Kidwell and Kidwell 1976; Charlesworth and Charlesworth 1985).

Understanding how recombination rate differences are inherited illuminates the evolution of this key genomic parameter. Multiple loci that shape recombination rate variation have been identified (Murdoch et al. 2010; Parvanov et al. 2010; Dumont and Payseur 2011; Hunter et al. 2016), including variants in specific genes (Kong et al. 2008; Kong et al. 2014; Sandor et al. 2012; Ma et al. 2015; Johnston et al. 2016). In addition to confirming that recombination rate is a genetically complex trait with the capacity to respond to evolutionary forces, these findings provide a window into the evolutionary history of recombination rate. Current recombination rates capture only a single moment in evolutionary time, but each allele that increases or decreases recombination rate documents a genetic change in an ancestral population.

Despite this progress, the existing picture of the genetics of recombination rate variation suffers from important biases. First, loci have either been identified through genome-wide association studies within populations (Kong et al. 2008; Kong et al. 2014; Sandor et al. 2012;

Ma et al. 2015; Hunter et al. 2016; Johnston et al. 2016) or in crosses between divergent strains (Murdoch et al. 2010; Dumont and Payseur 2011). Second, work has focused on humans and domesticated animals. As a result, the genetic basis of evolutionary differences in recombination rate between wild populations remains unprofiled.

In this study, we use an unusual population of wild house mice (*Mus musculus domesticus*) from the isolated Gough Island to address this challenge. Organisms that colonize islands often evolve extreme phenotypes in response to the substantial environmental changes they experience (Foster 1964; Case 1978; Grant and Grant 2002; Lomolino et al. 2005). Gough Island mice are exceptionally large – at approximately twice the weight of their mainland counterparts, they are the largest wild house mouse in the world (Rowe-Rowe and Crafford 1992; Jones et al. 2003). This remarkable phenotypic change likely occurred over the short time span of 130 to 200 years (Gray et al. 2014), and directional selection was probably responsible for this case of rapid evolution (Gray et al. 2015). This context provides a special opportunity to examine the indirect effects of selection on the genetic architecture of recombination rate evolution in a natural population.

Extensive knowledge about recombination also positions the house mouse as an especially powerful system for understanding its evolution. Genome-wide recombination rates are known to vary among inbred mouse strains (Koehler et al. 2002; Dumont and Payseur 2011), and dense genetic maps are available (Cox et al. 2009; Liu et al. 2014). Molecular and genetic mechanisms of recombination, including the regulation of crossover hotspots (Baudat et al. 2010; Parvanov et al. 2010; Grey et al. 2011), have been elucidated in the mouse (Paigen and Petkov 2010; Bolcun-Filas and Schimenti 2012; Cole et al. 2014; Hunter 2015). Finally, an immunofluorescent cytology technique developed in the mouse enables the total number of

crossovers during meiosis to be measured in individuals. Collectively, these resources and tools make it possible to characterize the genetic architecture of recombination rate evolution in nature.

Materials and Methods

Mice and crosses

Gough Island is an uninhabited volcanic island in the South Atlantic Ocean, more than 2500 km away from the nearest continental landmass. Mice were live-trapped from Gough Island (GI) and brought to the Charmany Instructional Facility at the University of Wisconsin – Madison. A breeding colony was established from 25 mature females and 21 mature males. Details on the transportation, housing, and establishment of this colony can be found in Gray et al. (2015). Mice derived from Gough Island were crossed with WSB/EiJ, a North American wild-derived inbred strain purchased from the Jackson Laboratory (Bar Harbor, ME). All mice were housed in micro-isolator cages, separated by sex, and kept in a temperature-controlled room (68-72º F) with a 12-hour light/dark cycle. Food and water were provided ad libitum. Animals were cared for according to protocols approved by the University of Wisconsin School of Veterinary Medicine Animal Care and Use Committee.

Several partially inbred lines were created by brother-sister mating in our breeding colony. We selected a pair of full siblings from one of these lines (Line B; Chapter 2) to cross with WSB/EiJ. This brother-sister pair was separated from wild GI mice by four generations of full-sib mating in the laboratory. From this pair, we produced two independent sets of F_1s and two independent F_2 intercrosses. We generated 877 F_2 mice, 494 with the GI grandmother and

383 with the WSB grandmother. We omitted mice with no genotype data or with obvious genotyping errors, leaving 793 F_2 individuals (♀GI x ♂WSB: 341 and ♀WSB x ♂GI: 452) for subsequent analyses.

Chromosome spreads and immunostaining

Spermatocyte spreads were prepared from a subset of F_2 males to characterize individual recombination rates (following Peters et al. 1997; Dumont and Payseur 2011). Mice were euthanized at approximately 16 weeks of age and the left testis from each individual was collected and processed as follows. The collected testis was rinsed with sterile 1x Phosphate-buffered saline (PBS) and the tunica was punctured to obtain a small fraction of the seminiferous tubules. Extracted tubules were incubated in 1.5 mL of hypotonic buffer (50 mM sucrose, 30 mM Tris, 17 mM citric acid, 5 mM EDTA, 2.5 mM dithiothreitol, 0.5 mM phenylmethane sulfonyl fluoride) at room temperature for approximately 45 minutes. The tubules were then removed from the buffer and finely shredded in 20 μL of 100 mM sucrose solution with fine-gauge forceps. Any remaining tissue was removed from the cellular mixture and another 20 μL of sucrose solution was mixed in by pipetting. The macerated cellular slurry was then mixed into 100 μL of 1% paraformaldehyde solution, with 0.15% TritonX-100. Approximately 15 μL of this suspension was added to each of 4 standard glass slides (25 mm x 75 mm), and spread evenly by gentle tilting. Slides were allowed to dry overnight in a humid chamber at room temperature. After drying, slides were rinsed in 0.4% solution of Kodak PhotoFlo and allowed to air dry. Prepared spreads were either immediately stained or stored at -20 ºC.

We adapted the immunostaining protocol from Anderson et al. (1999), De Boer et al. (2009), and Dumont and Payseur (2011). Antibody dilutions and the blocking of slides were all

performed with 1x antibody dilution buffer (ADB), prepared by diluting a 10x solution (22.5 mL 1x sterile PBS; 2.5 mL normal donkey serum, Jackson ImmunoResearch; 0.75 g bovine serum albumin, Fraction V, Fisher Scientific; 12.5 μL TritonX-100) with 1x sterile PBS. Primary antibodies against MLH1 (rabbit polyclonal; Calbiochem) and SYCP3 (goat polyclonal; Santa Cruz Biotechnology) were diluted 1:50. The primary antibody against centromeres (purified from CREST patient serum; Antibodies Incorporated) was diluted 1:200. For secondary antibodies, Alexa 488 donkey anti-rabbit (Molecular Probes) and Alexa 568 donkey anti-goat (Molecular Probes) were diluted 1:100, and A350/A280 donkey anti-human (Jackson ImmunoResearch) was diluted 1:200. All incubations were carried out at 37 ºC in an enclosed humid chamber.

Slides to be stained were first blocked in a Coplin jar with 1x ADB for 30 minutes. Once removed from the jar, excess buffer was drained from the slide by placing the long edge perpendicular to a dry paper towel. Slides received 60μL of diluted primary antibodies before being sealed with a coverslip and rubber cement. Sealed slides were incubated for 48 hours. The rubber cement was then gently removed and the slides were allowed to soak in 1x ADB until the coverslip was freed. Slides were then washed twice for 30 minutes each by being placed on a rocker with fresh 1x ADB. As before, excess buffer was drained and 60μL of diluted secondary antibodies (donkey anti-rabbit and donkey anti-human) was applied to each slide. After sealing with coverslips and rubber cement, the slides were incubated overnight. The rubber cement and coverslips were removed as before and 60μL of diluted secondary antibody (donkey anti-goat) was applied to each slide. Parafilm cut to size was used to seal the slides for this incubation step, which lasted only 2 hours. The stained slides were then washed three times, for one hour each, in

1x PBS with 0.05% TritonX-100 and allowed to air dry. Finally, slides were fixed using Prolong Gold antifade reagent (Invitrogen).

Microscopy and scoring

All slides were imaged on a Zeiss Axioplan 2 microscope with an AxioCam HR3 camera and AxioVision 4.8.2 software. Images were captured with a 100x objective and stored as 1030x1300 or 1388x1040 tiff files at 150 pixels per inch.

Cells were selected for scoring based on the morphology of the synaptonemal complex and the robustness of the MLH1 signal. We included cells for which the full set of 20 chromosomes were clearly condensed and indicative of the pachytene stage. Cells were omitted if defects in synapsis or damage from handling were obvious. We counted only MLH1 foci that appeared on autosomes, as recombination on the XY chromosome pair is not synchronous with the autosomes (Kauppi et al. 2012). We also omitted cells for which an MLH1 focus could not be detected on each autosome. The absence of a crossover from an autosome is rare and this omission ensures that staining artifacts do not influence the count. For each cell counted, we also recorded an image quality value based on the robustness of the MLH1 signal and the difficulty of scoring. This quality value ranged from 1 (weak MLH1 signal and difficult to score) to 6 (strong MLH1 signal and easy to score). For subsequent analyses, we included only cells with quality values of 2 or higher.

Genotyping and recombination in F_1s

All mice were genotyped with the Mega Mouse Universal Genotyping Array (MegaMUGA; Morgan et al. 2016). This Illumina Infinium array contains 77,808 markers

covering the autosomes, sex chromosomes, and mitochondria. Liver tissue from euthanized mice was extracted and sent to GeneSeek (Neogene, Lincoln, Nebraska) for genotyping. Several steps were taken to control for errors and ensure data quality. This included the replication of parental WSB and GI samples as well as the omission of markers and mice with either missing genotypes or Mendelian inconsistencies. We retained 11,833 informative single nucleotide polymorphisms (SNPs) that were invariant among GI mice, and whose segregation patterns were consistent with a standard F_2 intercross.

Genetic distances were estimated from this marker information using the Lander-Green hidden Markov model (Lander and Green 1987) as implemented in the R/qtl est.map() function (Broman et al. 2003). We assumed a genotyping error rate of 0.2% and converted recombination fractions to map distances with the Carter-Falconer function (Carter and Falconer 1951). We also estimated the number of crossovers in F_1 individuals by fitting this marker data to a hidden Markov model. This model removes implausibly close crossovers by including the probability of genotyping errors. Crossovers were counted on the underlying genotype, imputed with the Viterbi algorithm and assuming a genotyping error rate of 0.2%.

QTL analysis

We calculated the mean number of MLH1 foci among spermatocytes for each individual. The average individual was represented by more than 20 counts and we omitted individuals with fewer than 5 counts. We performed Haley-Knott regression to identify QTL for mean MLH1 foci using 240 F_2 individuals. Thresholds for significance were derived via permutation (Churchill and Doerge 1994), permuting phenotype data relative to genotype data. Thresholds for genome-wide significance, $\alpha = 0.05$, were established from 1000 permutation replicates.

We investigated the effects of cross direction by adding it as an interactive covariate and by performing separate analyses on each cross direction. The addition of cross direction as an interactive covariate is similar to performing the QTL analysis separately in each direction, but with constraints on residual variation based on the combined data (Broman and Sen 2009). We established significance thresholds for the former by performing two sets of permutations. Using the same random seed, we performed 1000 permutations treating cross direction as an additive covariate and 1000 permutations treating cross direction as an interactive covariate. When the analysis was split by cross direction, (♀GI x ♂WSB: 86 and ♀WSB x ♂GI: 154), we performed two separate sets of 1000 permutation replicates.

We fit several multiple QTL models to look for additional QTL and to test for interactions between them. We tested for pointwise interactions between detected QTL, calculating a p-value under the null hypothesis that LOD scores follow a χ^2 distribution. We also applied a forward/backward stepwise search algorithm with penalized LOD scores (Manichaikul et al. 2009). Penalties for additional QTL and interactions in this search were derived from 1000 permutations of a two-dimensional, two-QTL scan over the genome. Because of the computational costs of two-dimensional scans, the stepwise search and the permutation replicates were performed on a fixed 0.5 cM grid of pseudomarkers.

In addition to the analysis on mean number of crossovers, we estimated and mapped QTL for variance in the number of MLH1 foci among spermatocytes from the same individual. The identification of QTL affecting phenotypic variation, or vQTL, in multicellular organisms typically requires a comparison of variance between different genotypic groupings of individuals. This is often achieved by measuring the variance among individuals from different inbred lines (Mackay and Lyman 2005; Shen et al. 2012; Ayroles et al. 2015). Unlike most

quantitative traits, biological replicates for the number of crossovers per spermatocyte can be collected from the same individual. This unique aspect of our study allowed us to estimate variance in crossover number from single individuals. Because of the greater difficulty in estimating variance, we omitted individuals with fewer than 15 counts for this analysis, leaving 214 F_2 individuals. As with the mean, we performed Haley-Knott regression and established thresholds from 1000 permutation replicates. However, mapping the estimated variance is likely insufficient to characterize variance QTL because of confounding between the mean and variance (Rönnegård and Valdar 2011; Geiler-Samerotte et al. 2013). For example, if crossover number were Poisson-like, variance in crossover number would be linearly proportional to its mean. An analysis that tries to identify QTL from raw values of variance will capture this mean-variance relationship. To decouple this relationship, we transformed the raw counts with a generalized linear model (GLM), fitting an appropriate power variance function. This transformation preserves the mean for each individual, but removes the mean-variance relationship by explicitly parameterizing it. We sought a variance function of the form,

$$V(Y_i) = \phi\,[E(Y_i)]^{\theta}$$

where $E(Y_i)$ and $V(Y_i)$ are the mean and variance for individual Y_i, ϕ is a constant dispersion parameter, and θ is the power parameter that characterizes the mean-variance relationship. We employed the eql() function from the R/EQL package to numerically fit a power-variance function with a θ value that maximized the extended quasi-likelihood (Nelder and Pregibon 1987). The error variance from this model, estimated by the mean square residuals, represents each individual's departure from the modeled mean-dependent variance. We performed Haley-Knott regression to map error variance and established genome-wide significance thresholds with 1000 permutation replicates.

Candidate genes and parental sequences

We narrowed down candidate genes under QTL for recombination rate variation from a list of transcripts expressed in mouse spermatocytes. We incorporated data from RNA-seq experiments that characterized transcription temporally through meiosis. From Cruz et al. (2016), where RNA-seq was performed on spermatocytes sorted by flow cytometry, we included transcripts that were expressed in pachytene or leptotene/zygotene at a higher level than in secondary spermatocytes. From Ball et al. (2016), where RNA-seq and cytological data were integrated to stage transcripts, we included transcripts that were concordant with preleptotene, early leptotene, late leptotene/zygotene, and early pachytene. We omitted non-coding RNAs due to their poor annotation across databases. Transcription start and end sites were assigned from UCSC annotations on the GRCm38/mm10 build.

Variants in the GI parents were identified by whole-genome sequencing at an average depth of 10X. Sequencing was performed on an Illumina HiSeq 2500 with 100-bp paired-end reads. These reads were mapped with the Burrows-Wheeler Aligner (Li and Durbin 2009) to the C57BL/6 mouse reference genome. Variants were called with SAMtools 1.0 (Li et al. 2009) and compared to those found in the WSB/EiJ whole-genome sequence (Keane et al. 2011). For each candidate gene, we included variants that were 1kb upstream and downstream of the transcription start and end sites. To prioritize candidates, we employed the Ensembl Variant Effect Predictor (McLaren et al. 2016) and examined the predicted consequence of each variant. We also prioritized candidate mutations in genes that were associated with any Gene Ontology (GO) terms containing “recombination” (MouseMine; Motenko et al. 2015).

Results

Genome-wide recombination rates

We used fluorescent immunocytology to measure recombination rates in individual mice from GI, WSB, and our F_2 intercross. We focused on spermatocytes in pachytene, the third stage of meiotic prophase during which crossovers become apparent and antibodies against the MLH1 protein localize to sites of crossover, forming punctate foci against the condensed chromosomes (Figure 3.1). By counting the number of MLH1 foci in multiple spermatocytes from each individual, we estimated the mean autosomal recombination rate in each of 240 F_2 animals.

While outbred GI mice were previously shown to have an average of 2 more crossovers per spermatocyte than WSB/EiJ (Dumont and Payseur 2011), the derived GI line featured in our intercross exhibits only a modest elevation in recombination rate (GI mean = 22.63 foci, SE = 0.14; WSB/EiJ mean = 22.29, SE = 0.16; t-test p = 0.11). Notably, the distribution of F_2 crossover numbers contains a large number of individuals with recombination rates that lie outside the range of both parental means (Figure 3.2). This pattern of transgressive segregation is consistent with the presence of QTL alleles that have opposing effects within lines (Lynch and Walsh 1998; Rieseberg et al. 1999). We also detected a significant difference in F_2 recombination rates between cross directions. F_2s with a GI grandmother produce spermatocytes with more crossovers (mean = 22.76, SE = 0.09) than F_2s with a WSB/EiJ grandmother (mean = 22.47, SE: 0.06) (t-test p = 0.01).

In addition to cytological characterization of recombination rates in the gametes of F_2s, we tracked recombination events by analyzing F_2 genotypes at diagnostic SNPs. The resulting estimates of recombination rate differ in two important ways from our cytological estimates. First, F_2 genotypes track crossovers that occurred during gametogenesis in F_1s. Since crossovers

were realized in the cellular and genetic environment of F_1s, these estimated rates are sex-averaged, including contributions from females as well as males. Second, interference-independent crossovers, a small proportion of crossovers that do not rely on the MLH1 pathway (Hollingsworth and Brill 2004; Holloway et al. 2008), are detected in the genotypic analysis. We estimated a mean of 25.79 (SE: 0.15) crossovers per F_1 individual from the genotypes of 793 F_2s. We again noticed a significant difference in crossover number between cross directions. F_1s with GI mothers produce spermatocytes with more crossovers (mean = 26.24; SE = 0.23) than F_1s with WSB/EiJ mothers (mean = 25.46; SE = 0.19) (t-test $p < 0.01$).

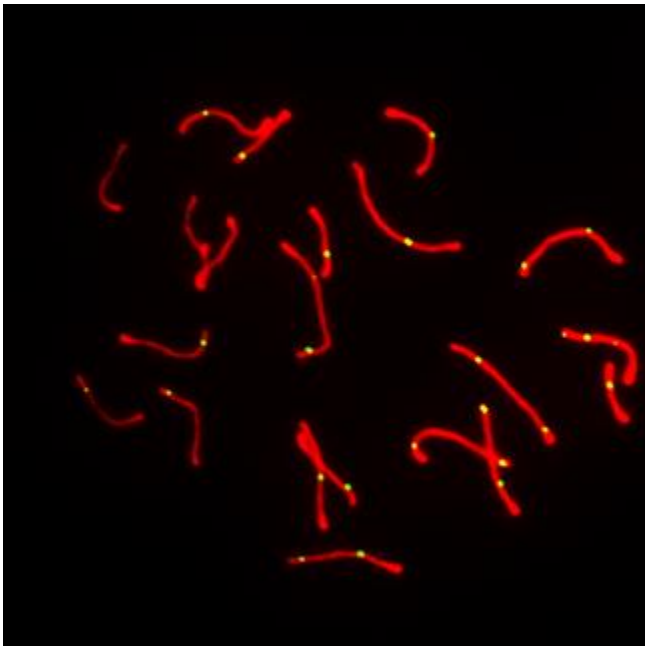

Figure 3.1 Representative image of pachytene spermatocyte. In red, the synaptonemal complex is visualized by anti-SYCP3. In green, MLH1 foci show sites of meiotic crossover.

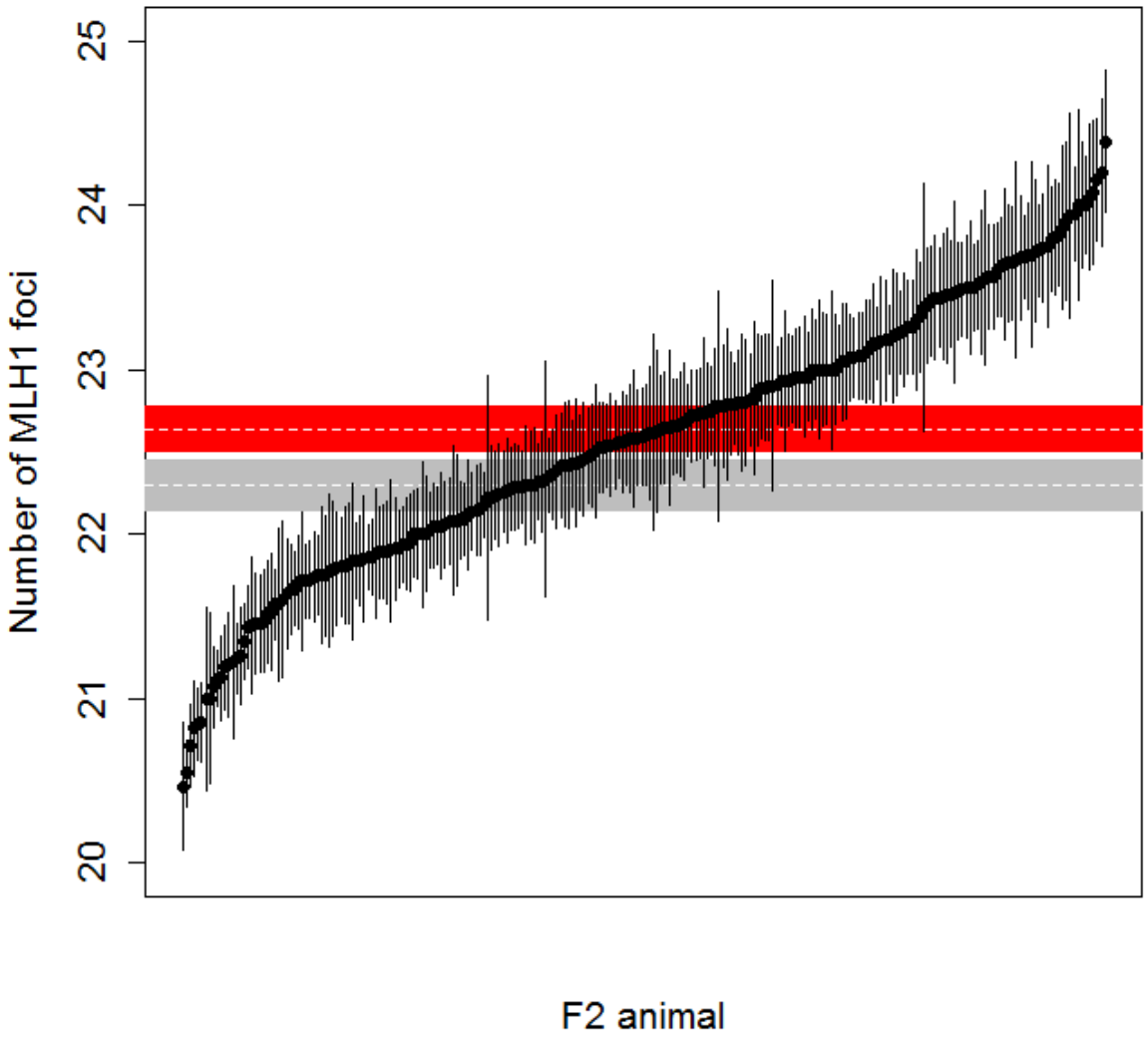

Figure 3.2 Distribution of crossovers in F_2 animals characterized by MLH1 foci. Error bars show +/- 1 S.E. Parental means with +/- 1 SE also shown in red, for GI mice, and gray, for WSB/EiJ.

QTL for genome-wide recombination rate evolution

We detected three genomic regions linked to variation in mean MLH1 count (Figure 3.3). The strongest of these QTL, in terms of effect size and LOD score, localizes to the proximal end of chromosome 14. Genomic regions on chromosomes 5 and 6 also contribute to mean MLH1 count (Table 3.1). We repeated the scan for QTL with image quality (see Methods) and cross direction as additive covariates, but did not find a substantial difference in the results.
Given the elevated crossover number detected in F_1 individuals with GI mothers from the genotypic analysis, we added cross direction as an interactive covariate in our QTL mapping analysis. We found evidence for an additional QTL on chromosome 10, whose effects significantly differ between the two cross directions. These results suggest a QTL on chromosome 10 for mean crossover number that is either segregating within the GI line, interacting with loci segregating within the GI line, or interacting with a maternal effect. Model-based multiple QTL mapping (Broman and Speed 2002) did not identify new QTL or interactions between QTL, though QTL positions were refined (Table 3.1).

As predicted from the transgressive distribution of mean crossover number, we found a QTL with phenotypic effects opposite of the parental trait difference. The GI allele at the QTL on chromosome 14 confers a reduction in mean crossover number. In contrast, GI alleles at the QTL on chromosomes 5, 6, and 10 are associated with increases in mean crossover number. Alleles at three QTL act additively; the QTL on chromosome 10 shows signs of overdominance (Table 3.1).

Together, detected QTL explain an estimated 33% of the variance in mean crossover number among F_2s. While this percentage is almost certainly inflated by the Beavis effect (Beavis 1994; Xu 2003), it is possible that the detected QTL explain a majority of the genetic

variance. The narrow-sense heritability of recombination rate has been estimated at 0.46 for mice (Dumont et al. 2009).

Table 3.1. QTL for the genome-wide recombination rate

Chr.	Single QTL Model		Multiple QTL Model		Pos[a] (Mb)	1.5 LOD Interval[b] (Mb)	% var[c]	Estimated phenotypic means (SE)[d]		
	Pos. (cM)	LOD	Pos. (cM)	LOD				GG	GW	WW
5	53.5	4.39	36.9	4.61	83.8	74.3 - 132.5	6.1	22.91 (0.11)	22.58 (0.07)	22.30 (0.10)
6	50.3	5.12	29.8	4.50	81.4	73.5 - 134.7	5.9	22.88 (0.10)	22.55 (0.07)	22.23 (0.11)
14	12.5	6.66	20.0	7.57	56.5	28.2 - 60.9	10.4	22.12 (0.11)	22.55 (0.07)	22.90 (0.09)
10[e]	55.1	4.54	58.0	5.12	122.8	114.5 - 123.8	6.9	22.68 (0.19)	23.06 (0.12)	22.21 (0.16)
								22.33 (0.13)	22.45 (0.09)	22.62 (0.12)

[a] Estimated from position of LOD peak in a multiple QTL model.
[b] Estimated from single QTL model (a more conservative estimate).
[c] Percentage of phenotypic variance among F_2s explained.
[d] G = Gough; W = WSB/EiJ.
[e] Single QTL model position and LOD from GxW cross alone; estimated phenotypic means for the GxW cross (first row) and WxG cross (second row).

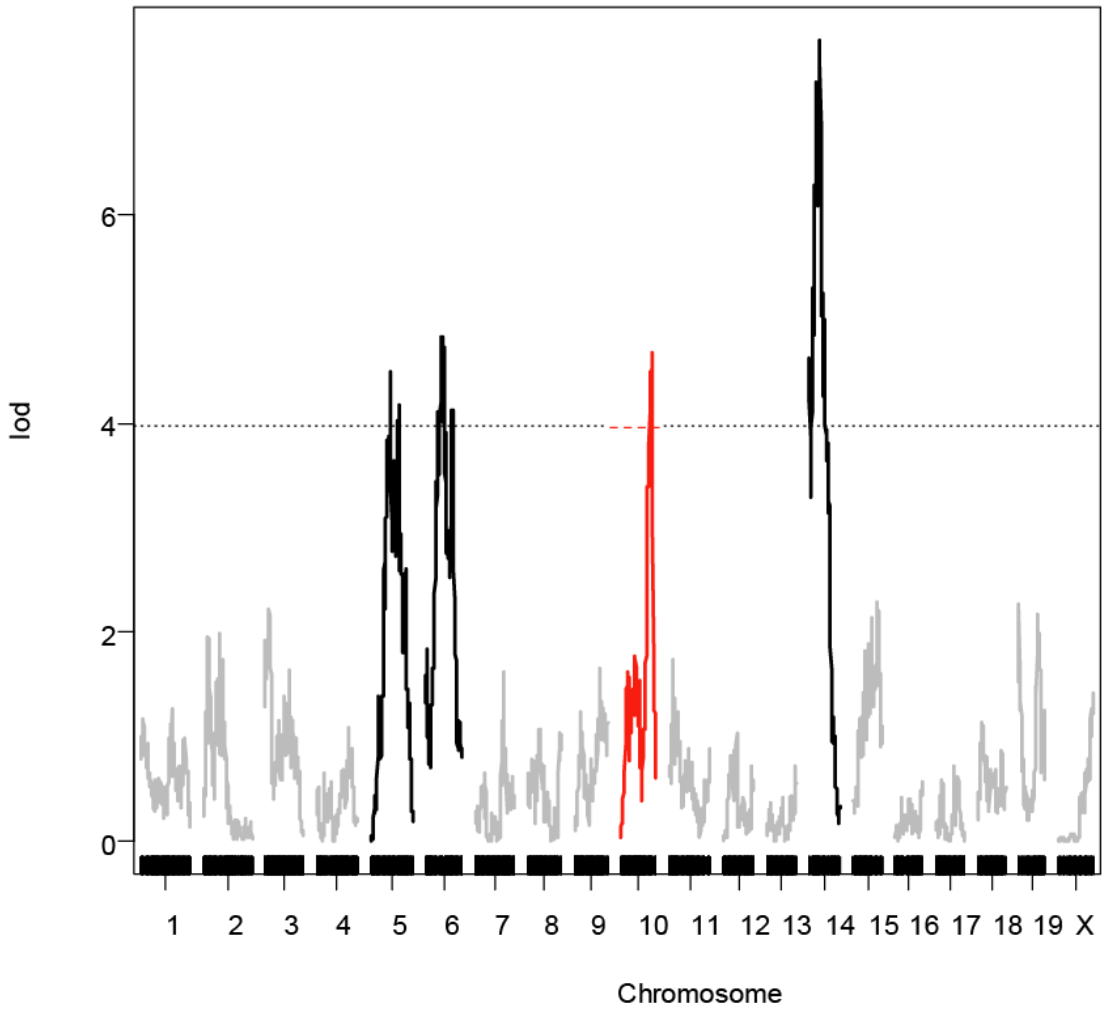

Figure 3.3. LOD plot of QTL for genome-wide recombination rate. In red, the QTL on chromosome 10 appears only after taking into account cross direction. Dashed lines show genome-wide (α = 0.05) threshold for the respective scans.

QTL for within-animal variance in the genome-wide recombination rate

The distribution of within-animal variances in crossover number is shown in Figure 3.4. GI mice display significantly lower variance in crossover number among spermatocytes than WSB/EiJ (Levene's test, $p < 0.005$), and the center of the F_2 distribution is closer to the GI value. We detected a single region on chromosome 14 that confers differences in within-animal variance (peak = 34.1 Mb, LOD = 5.83). The 1.5 LOD interval of this QTL (29.1 Mb to 69.1 Mb) overlaps substantially with the previously identified QTL on this chromosome for mean crossover number.

The distribution of crossover number among F_2 individuals is highly heteroscedastic: variance is positively correlated with the mean (Pearson's $r = 0.50$). Using two separate approaches to deconvolve the mean-variance relationship (see Methods), the LOD score for the QTL on chromosome 14 dropped but remained suggestive, reaching the $\alpha = 0.20$ level for genome-wide significance (Figure 3.5a). Coupled with the absence of other suggestive peaks, particularly from chromosomes with QTL affecting mean crossover number, we conclude that the QTL on chromosome 14 likely contributes to variance in crossover number. The GI allele at this locus dominantly reduces within-animal variance in crossover number (Figure 3.5b), an effect that could partially account for the shift in the F_2 distribution toward the GI parent. This QTL explains 4-5% of the variance in within-animal crossover number variance.

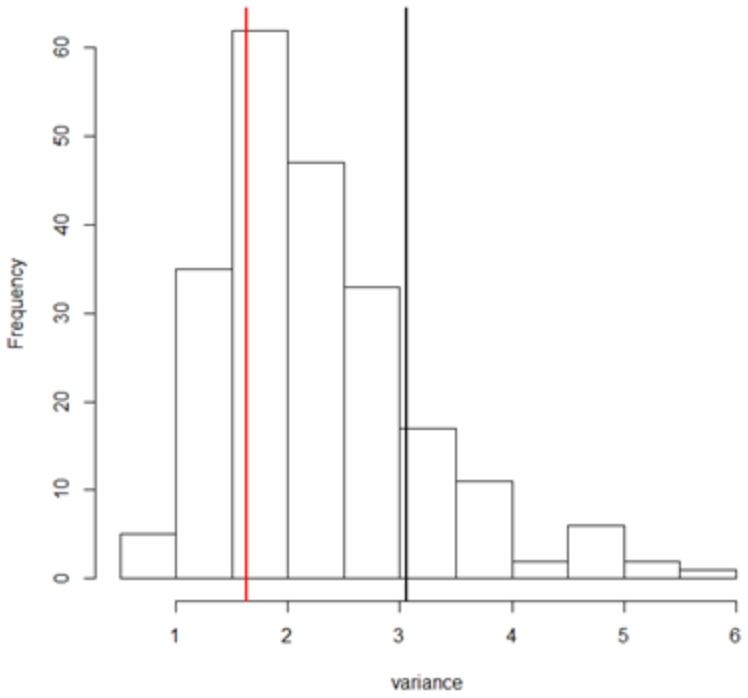

Figure 3.4. Variance in MLH1 count. Lines show variance in Gough (red) and WSB (black) parentals.

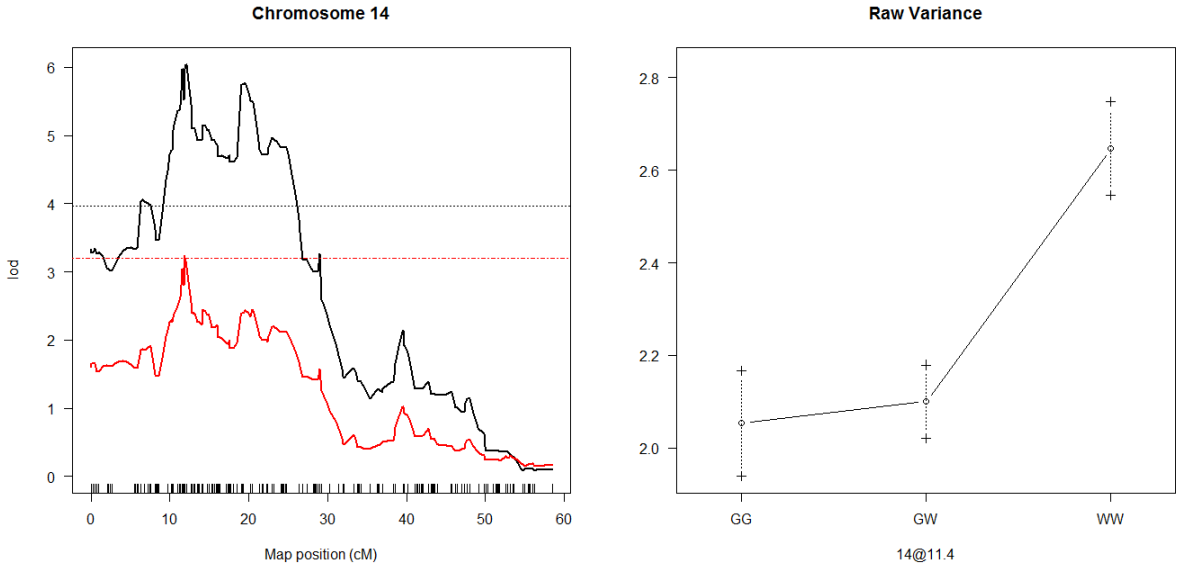

Figure 3.5. LOD plot for variance QTL (left) and estimated effects by genotype (right). LOD plot is for raw variance (black) with α = 0.05 threshold for genome-wide significance (dashed lines), and transformed variance (red) with α = 0.20 threshold.

Candidate genes for genome-wide recombination rate evolution

We overlapped multiple types of data to identify candidate genes under QTL peaks responsible for recombination rate variation. Studies of gene expression in mouse spermatocytes suggest that most transcripts involved in meiotic recombination are expressed before mid-pachytene, whereupon transcription switches to spermiogenesis-related genes (Fallahi et al. 2010; Margolin et al. 2014; Cruz et al. 2016; Ball et al. 2016). We merged two RNA-seq datasets that characterized temporal patterns of gene expression in mouse spermatocytes (Cruz et al. 2016; Ball et al. 2016). Our initial set of candidate genes was established by taking transcripts expressed in early meiotic prophase. After including genes with GO terms associated with meiotic recombination, our list included 8501 genes. From this list, we selected candidates that were within the 1.5 LOD intervals of our QTL peaks.

Using knowledge of temporal expression patterns and gene ontology terms (see Methods), we identified a total of 590 candidate genes under the detected QTL peaks on chromosomes 5, 6, 10, and 14. To prioritize this list, we examined the SNP and short indel differences between the GI and WSB/EiJ lines for the candidate genes. Here, we focus on the most compelling candidates: those genes with a recombination-associated GO term that contain a variant conferring a change to either a nonsynonymous site or a transcription factor binding site. We identify strong candidate genes for QTL on chromosomes 5, 6, and 14 (Table 3.2), including DNA helicases that mediate homologous recombination (Bugreev et al. 2007; De Muyt et al. 2012) and E3 ligases thought to regulate the crossover/non-crossover decision (Reynolds et al. 2013; Qiao et al. 2014).

Table 3.2. Candidate genes and mutations for QTL.

Gene Name	Chr.	Position[a]	Base Change	AA change	Zygosity in GI parents	Variant Effect[b]
Rnf212	5	108770595	C -> T	V -> I	Homo; Het	SIFT: 0.05
Rnf212	5	108729476	T -> C	I -> V	Homo; Homo	SIFT: 0.49
Rnf212	5	108744012	T -> C	--	Homo; Het	Low Info TF site
Helq	5	100794483	Indel	--	Homo; Homo	Low Info TF site
Hfm1	5	106871789	G -> T	S -> Y	Homo; Homo	SIFT: 0.04
Hfm1	5	106904814	C -> T	A -> T	Homo; Homo	SIFT: 0.74
Hfm1	5	106911653	A -> G	C -> R	Homo; Homo	SIFT: 0.08
Hfm1	5	106853422	C -> T	--	Homo; Homo	Low Info TF site
Rad18	6	112649678	G -> A	S -> L	Homo; Homo	SIFT: 0.02-0.1
Rad18	6	112649714	G -> A	S -> L	Homo; Homo	SIFT: 0.07-0.11
Rad18	6	112664108	A -> G	W -> R	Homo; Homo	SIFT: 0.01-0.03
Rad51ap1	6	126928176	T -> C	H -> R	Homo; Homo	SIFT: 0.79-0.84
Rad51ap1	6	126928188	C -> T	G -> D	Homo; Homo	SIFT: 0.6-0.62
Rad51ap1	6	126928206	T -> C	E -> G	Homo; Homo	SIFT: 0.22
Rad51ap1	6	126939497	A -> G	I -> T	Homo; Homo	SIFT: 0.17-0.22
Apex1	14	50925294	G -> A	A -> T	Het; Het	SIFT: 0.14-0.6
Ccnb1ip1	14	50791413	T -> C	--	Het; Het	Low Info TF site
Rec8	14	55625075	C -> T	A -> V	Het; Het	SIFT: 0.31
Tep1	14	50824758	T -> G	N -> H	Het; Het	SIFT: 0.2
Tep1	14	50837421	G -> A	R -> C	Het; Het	SIFT: 0.16
Tep1	14	50839000	T -> C	D -> G	Homo; Het	SIFT: 0.4
Tep1	14	50853017	C -> T	G -> D	Homo; Homo	SIFT: 0.09
Tep1	14	50855613	C -> T	V -> I	Homo; Homo	SIFT: 1
Tep1	14	50860668	C -> T	G -> S	Homo; Homo	SIFT: 0.02
Tep1	14	50863639	G -> T	L -> I	Homo; Homo	SIFT: 0
Tep1	14	50868186	G -> A	P -> S	Homo; Homo	SIFT: 0.29
Tep1	14	50868261	G -> T	H -> N	Homo; Homo	SIFT: 0.05
Tep1	14	50824479	G -> A	--	Het; Het	High Info TF site
Tep1	14	50837421	G -> A	--	Het; Het	Low Info TF site

[a] Position in GRCm38/mm10

[b] Predicted variant effect for nonsynonymous changes as SIFT score 0.0 (deleterious) – 1.0 (tolerated), (Kumar et al. 2009); for variants at predicted transcription factor (TF) binding sites, variants are classified as being in high or low information regions.

Discussion

While most genetic mapping studies feature parental lines with notable differences between trait means, the absence of large differences does not obviate a history of divergence nor the potential to reconstruct it. In this study, the genome-wide recombination rate showed transgressive segregation and was linked to multiple QTL. Not only were QTL alleles with antagonistic effects harbored in the same line, but the allele with the strongest effect opposed the phenotypic pattern seen in the parents. Transgressive segregation may be a relatively common phenomenon, especially in crosses where the difference between parental trait means is small (Lynch and Walsh 1998; Rieseberg et al. 2003). What is remarkable is the observation of transgressive segregation and complementary QTL effects in all three studies that mapped QTL for genome-wide recombination rate variation in mice (Murdoch et al. 2010; Dumont and Payseur 2011). Furthermore, in both cases in which only wild-derived mice were used (this study and Dumont and Payseur 2011), the leading QTL displayed antagonistic effects. This finding suggests that an antagonistic genetic architecture may be a common feature of genome-wide recombination rate evolution.

The distribution of QTL effects can be used to draw inferences about the role of natural selection (True et al. 1997; Orr 1998). When the direction of QTL effects consistently matches the direction of parental phenotypic differences, a history of directional selection may be hypothesized. The repeated finding of antagonistic loci therefore argues against scenarios that invoke consistent directional selection on the genome-wide recombination rate.

The proposal that recombination rate may evolve in response to rapid shifts in the selective optima of multiple traits, as in the case of domestication (Burt and Bell 1987; Ross-Ibarra 2004), has previously been challenged by examples from mammals and insects (Wilfert et al. 2007;

Munoz-Fuentes et al. 2015). Alternative explanations include genetic drift, stabilizing selection, or fluctuating selection. From a molecular genetics standpoint, the case for stabilizing selection on genome-wide recombination rate seems strongest. Meiotic requirements appear to set boundaries based on the increased risk of aneuploidy in crossover-deficient meiotic cells (Roeder 1997; Hassold and Hunt 2001) and the presumed risks to genome integrity from an excess of crossovers (Inoue and Lupski 2002; Coop and Przeworski 2007). Another possibility is that the evolution of recombination rate is governed by drift (with no optimum value) within these boundaries (Dumont and Payseur 2008). The possibility that the direction of selection on recombination rate has shifted over time is intriguing and less explored. Meiotic constraints may evolve as chromosome structure changes, shifting the bounds imposed on genome-wide recombination rate (Borodin et al. 2008; Dumont 2017). Whether episodic shifts in selection could explain the preponderance of antagonistic loci for recombination rate in mice would depend on their timing and frequency.

Our sample size was similar to those in other genetic mapping studies of genome-wide recombination rate variation in mice (Murdoch et al. 2010; Dumont and Payseur 2011), enabling straightforward comparisons between the results. We detected fewer QTL, an outcome potentially explained by the much higher phenotypic divergence between the lines used in the other studies (both of which involved inter-subspecific crosses). The absence of X-linked QTL in GI x WSB/EiJ is notable because the X chromosome has been repeatedly linked to genome-wide recombination rate divergence between lines from different mouse subspecies (Murdoch et al. 2010; Dumont and Payseur 2011; Balcova et al. 2016). The QTL we discovered on chromosome 14 lies near a QTL found in the C57BL/6J x CAST/EiJ cross (Murdoch et al. 2010). Intriguingly, this QTL showed antagonistic effects in both crosses. This coincidence raises the tantalizing

possibility that a shared variant, in GI and C57BL/6J, reduces recombination rates. A dearth of overlapping QTL with the wild-derived *M. m. musculus* x *M. m. castaneus* cross in Dumont and Payseur (2011) suggests that different loci are responsible for recombination rate evolution within and between subspecies. Nevertheless, our list of candidate genes supports the notion that the number of loci contributing to natural variation in recombination rate is limited. Our most promising candidates include Rnf212, Rec8, and Ccnb1ip1 (HEI10), genes that have been linked to variation in recombination rate within multiple mammalian species (Sandor et al. 2012; Kong et al. 2014; Qiao et al. 2014; Johnston et al. 2016).

Our observation of significantly more crossovers among F_2 mice from the cross direction with GI mothers can mostly be explained by the QTL on chromosome 10. Since the GI parents were not completely inbred, our observation that this QTL confers direction-specific effects suggests it segregates within the GI line. The antagonistic allele on chromosome 14 may actually be polymorphic within GI mice as well, since higher genome-wide recombination rates were observed in outbred mice from the island (Dumont and Payseur 2011).

Our experimental design provided a rare opportunity to characterize the genetics of differences in within-animal recombination rate variance. Genetically controlled reduction of phenotypic variability may increase developmental consistency and robustness to environmental fluctuations (Waddington 1942; Rutherford and Lindquist 1998; Mackay and Lyman 2005; Levy and Siegal 2008). Alternatively, increased phenotypic variability can be advantageous and may contribute to adaptation (Losick and Desplan 2008; Beaumont et al. 2009; Eldar and Elowitz 2010). Not only did we find significantly lower variation in genome-wide recombination rate in GI compared to WSB/EiJ, but we discovered a GI QTL allele (on chromosome 14) that reduces both the variance and the mean crossover number. Although QTL that control variance have

been previously identified for several traits (Shen et al. 2012; Hulse and Cai 2013; Mulder et al. 2016), ours is the first report of such a QTL for recombination rate. The causative variant(s) underlying this QTL might act by modulating the stringency of meiotic checkpoints, which ensure consistency among gametes (Hochwagen and Amon 2006; Li and Schimenti 2007; Jaramillo-Lambert 2010; Kauppi et al. 2013). However, patterns of natural variation in the consistency of recombination rate among gametes are poorly understood. Our results, along with the abundance of meiotic surveillance mechanisms, raise the intriguing prospect that gamete consistency plays an important role in the evolution of recombination rate.

Chapter 4
Genetics of synaptonemal complex length evolution in mice[2]

Abstract

During meiosis, chromosomes pair for genetic exchange in the process of recombination. Recombination is crucial for the proper segregation of chromosomes during meiosis and also has the evolutionary effect of introducing haplotypic variation into a population. To study the genetic mechanisms underlying variation in recombination rate, we examined the synaptonemal complex. The synaptonemal complex (SC) is a proteinaceous scaffold essential to the process of chromosome synapsis and subsequent recombination. The length of the SC axis is strongly correlated with rates of genome-wide recombination. Using the house mouse as a model system, we quantified SC length in single spermatocytes by immunofluorescent cytology. We developed a high-throughput method to accurately measure SC lengths from cytological images. This method was applied to images of spermatocytes from two F_2 intercrosses to genetically map loci responsible for SC length variation. These two intercrosses, (1) between strains representative of *M. m. musculus* and *M. m. castaneus* and (2) between two representatives of *M. m. domesticus*, exhibit different levels of both trait and phylogenetic divergence. We identified 3 QTL in the first cross and 2 QTL in the second cross for SC length variation. The absence of overlapping QTL between these crosses suggests different loci are responsible for the evolution of SC length within and between mouse subspecies. Using covariate analysis, we discovered many of the QTL for SC length were pleiotropic, also controlling variation in the genome-wide recombination rate.

[2] Immunofluorescent images from the *muculuss* x *castaneus* cross were collected by Beth L. Dumont.

Our results help elucidate the genetic architecture behind genome-wide recombination rate evolution.

Introduction

Homologous chromosomes are paired early in meiosis in a process known as synapsis. In most sexually reproducing organisms, synapsis is essential to the formation of meiotic crossovers and the proper segregation of chromosomes in gametogenesis (Page and Hawley 2004; Yang and Wang 2008; Nagaoka et al. 2012; Cahoon and Hawley 2016). The synaptonemal complex (SC) is a meiosis-specific protein structure that holds together the four chromatids of a chromosome to achieve synapsis. This supramolecular structure, whose assembly is completed by the pachytene stage, keeps homologs tightly aligned along their entire length. As a canonical structure of meiosis, the structure and function of the SC are conserved across eukaryotes, though its constituent proteins show substantial variation (Grishaeva and Bogdanov 2014; Hemmer and Blumenstiel 2016).

The process of synapsis is intimately linked with the formation of crossovers. The formation of the SC begins at sites of meiotically programmed DNA double-strand breaks (Zickler et al. 1992; Hunter 2003; Henderson and Keeney 2005). These sites of DSBs mediate the homology search that precedes chromosome pairing, and a small subset of these DSBs become the sites of reciprocal exchange. At synapsis, chromatin is organized into an array of loops along a central proteinaceous axis. The size of these loops and the length of this axis, but not the spacing between loops, have been shown to vary based on the genomic contents in different organisms (Novak et al. 2008; Kleckner 2006; Zickler and Kleckner 2015). Variation in the length of this axis thus reflects both differences in the degree of compaction and interaction between homologs.

The length of this central axis of the SC can be observed by microscopy, and a positive correlation between this length and the number of meiotic crossovers has long been observed. An

early finding from electron microscopy on human meiocytes was the presence of approximately twice as many crossovers as well as twice the SC length in oocytes relative to spermatocytes (Rasmussen and Holm 1978; Bojko 1985). More recent techniques involving immunofluorescent cytology have found the total length of the autosomal SC to be correlated with the number of crossovers in individual meiotic cells from humans and mice (Lynn et al. 2002; Tease and Hulten 2004; Pan et al. 2012; Baier et al. 2014). However, the ratio of crossovers to SC length appears to vary substantially among individual humans. Among different strains of mice, this ratio appears relatively consistent, at ~7 μm of SC/crossover (Lynn et al. 2002). The tight relationship between these two traits appears to extend across species of mice, with evidence suggesting that crossover number and SC length may have co-evolved (Dumont and Payseur 2011). However, this relationship may not be universal among mammals; in cattle, sheep, and goats, no correlation was found between the number of crossovers and total SC length within or between species, despite significant correlation within individual cells (Froehlich et al. 2015).

The evolution of recombination rate has received substantial consideration and study, partly due to the many consequences that recombination has on molecular evolution (Begun and Aquadro 1992; Charlesworth et al. 1993; Duret and Ardnt 2008). Structural changes in the genome, including rearrangements and altered chromosome number, have been implicated in the evolution of recombination rate (Fledel-Alon et al. 2009; Smukowski and Noor 2011; Segura et al. 2013; Tiley and Burleigh 2015). Evolution of the SC represents direct change to the physical structure of the genome exactly when recombination occurs. Despite its prominence in the meiotic program, and this link to recombination rate, variation in the SC has not garnered as much attention as recombination rate. While the SC has been studied extensively from a molecular and mechanistic perspective (Page and Hawley 2004; Fraune et al. 2012; Zickler and

Kleckner 2015), the genetic basis of its variation has not been established (but see Vranis et al. 2010). In contrast, variation in recombination rate has been shown to have a genetic basis, and significant progress has been made in identifying specific loci that control this variation (Kong et al. 2008; Murdoch et al. 2010; Dumont and Payseur 2011; Parvanov et al. 2010; Johnston et al. 2016).

Genetic analysis of variation in SC length will improve our understanding of its evolution along with recombination rate. The covariation of SC length and recombination frequency suggests a shared genetic basis. In this study, we genetically map variation in SC length from two intercrosses between wild-derived strains of house mice (*Mus musculus*). Mice are an ideal system for studying SC length, informed by a rich context of molecular and genetic studies on meiosis and recombination rate (Hunt and Hassold 2002; Koehler et al. 2002; Paigen and Petkov 2010; Handel and Schimenti 2010; Cole et al. 2012; Keeney et al. 2014). More importantly, the ability to perform immunofluorescent cytology in mouse spermatocytes allows SC length to be characterized in a large number of samples. Existing studies of SC length have focused mostly on humans and laboratory strains of mice. Variation in SC length, and the extent to which recombination rate is connected to this variation, have not been characterized in natural populations.

Manual measurement of SC lengths in thousands of spermatocytes, needed for genetic mapping, is a laborious task. We developed a computer vision technique to automate this process. This technique was applied to images from immunofluorescent cytology originally collected to characterize variation in crossover frequency in two separate intercrosses. Loci responsible for recombination frequency were detected in these two crosses, enabling a powerful comparison between the genetics of SC length and recombination frequency in the same set of

animals. Further, these two crosses represent two different levels of divergence within house mice – between subspecies and within subspecies. Comparison between these two levels of divergence provides a model for how SC length may evolve.

Materials and Methods

Crosses

Data presented in this study was gathered using images of spermatocytes from F_2 males from two separate intercrosses. The first of these was a cross between PWD/PhJ, a representative of the *Mus musculus musculus* subspecies (herein referred to as *mus*), and CAST/EiJ, a representative of *Mus musculus castaneus* (herein referred to as *cast*). A total of 315 F_2 males were sacrificed from this cross at approximately 10 weeks of age, of which 289 were included in the final analysis. The second of these crosses was between Gough Island (GI) mice and WSB/EiJ, both from the *Mus musculus domesticus* subspecies. A total of 618 F_2 males were sacrificed from this cross at approximately 16 weeks of age, of which 229 were included in the final analysis. Additional details on cross design and animal husbandry can be found in Dumont and Payseur (2011) and Gray et al. (2015) respectively. In all cases, animal care and experimental protocols were approved by the University of Wisconsin Animal Care and Use Committee.

Tissue collection, immunostaining, and microscopy

Details on the preparation of spermatocyte spreads and immunostaining can be found in Chapter 3 and Dumont and Payseur (2011). Here, we very briefly summarize the shared steps taken to arrive at stained spermatocyte images.

Seminiferous tubules were extracted from the testis of sacrificed males and incubated in hypotonic buffer. The macerated tubules were then ripped apart to liberate spermatocytes. The cellular slurry was fixed onto a glass slide with a paraformaldehyde solution and allowed to dry. These prepared slides were incubated with primary antibodies against MLH1, a mismatch repair protein that localizes to sites of meiotic crossover, and SYCP3, an essential structural element spanning the synaptonemal complex. After several wash steps, the slides were then incubated with a set of secondary antibodies tagged with fluorophores, at 488 nm and 568 nm for MLH1 and SYCP3 respectively, and then mounted for visualization.

Slides from the *mus* x *cast* cross were imaged on a Zeiss Axioskop microscope with an AxioCam HRc camera. Images from this cross were stored as .tiff files with a resolution of 1030x1300 pixels and 150 pixels per inch. Slides from the GI x WSB cross were imaged on a Zeiss Axioplan 2 microscope with an AxioCam HR3 camera. Images from this cross were stored as .tiff files at either 1030x1300 or 1388x1040 at 150 pixels per inch. In both cases, images were captured with a 100x objective lens.

Measuring SC length

All images were manually curated and only cells with a clearly condensed, full set of 20 chromosomes were included. Images of cells with obvious defects or damage from handling were omitted.

We utilized techniques from computer vision to determine the total length of the SC in each spermatocyte from captured immunofluorescent images. We applied algorithms for image processing and analysis as implemented in the scikit-image package for Python 3 (van der Walt et al. 2014; scikit-image.org). For each image, we first isolated the red channel, which contains information from the fluorescence of secondary antibodies against anti-SYCP3 at 568 nm. The image gradient on the isolated channel was then taken with a 3 pixel-wide disk structuring element. This creates an image where regions of contrast, or edges, are enhanced. Otsu's method was applied to the image gradient (Otsu 1979), a clustering technique on pixels that reduces the grayscale gradient image to a binary image. Spurious pixels were removed by applying a morphological opening operator, followed by a morphological closing, with a 4 pixel-wide square structuring element (Serra 1983). Finally, the cleaned binary image was reduced to a single-pixel wide representation with the skeletonize algorithm as implemented in scikit-image. The total number of pixels in this single-pixel wide representation was taken as the total SC length for a spermatocyte.

The reliability of this technique was assessed by comparison to measurements made by manual tracing. Performance was evaluated in a test set of 217 spermatocyte images, from 5 *mus* x *cast* F_2s and 5 GI x WSB F_2s.

Genotyping and QTL analysis

Mice from the *mus* x *cast* cross were genotyped at 295 SNPs using the Sequenom iPLEX MassARRAY system (Gabriel et al. 2009). Of these, 222 SNPs with Mendelian segregation patterns were retained for the QTL analysis. Mice from the GI x WSB cross were genotyped at 77,808 markers on the Mega Mouse Universal Genotyping Array (MegaMUGA; Morgan et al.

2016). Of these, 11,833 SNPs with Mendelian segregation patterns were retained for the QTL analysis.

Representative total SC length for spermatocytes from an individual was calculated by taking the mean SC length among its imaged spermatocytes. Individuals represented by fewer than 5 spermatocytes were omitted from the analysis. Haley-Knott regression (Haley and Knott 1992) was performed on data from both crosses to identify QTL for variation in mean SC length. Individuals were weighted by the number of spermatocyte observations, and we included cross direction as an additive covariate. Thresholds for significance were determined by permutation (Churchill and Doerge 1994), with genome-wide $\alpha = 0.05$, and established from 1000 replicates for each cross. We tested multiple QTL models by applying a forward/backwards stepwise search algorithm with penalized LOD scores (Manichaikul et al. 2009), as implemented as stepwise() in R/qtl (Broman et al. 2003). Conditional analyses were performed with MLH1 count and SC length as additive covariates. Separate sets of permutations, 1000 replicates each, were performed for each of the conditional scans to establish genome-wide significance levels.

Results

SC lengths were collected from images of spermatocytes subject to immunofluorescent cytology. We included only spermatocytes that were in pachytene, the stage at which the SC is fully mature. Computer vision techniques were applied to collect total SC length, including the XY pair, from images of individual spermatocytes. Figure 4.1 illustrates a typical spermatocyte and intermediates in the image processing steps that yield the SC length. These techniques reliably reproduced lengths obtained in a test set of manually traced images from spermatocytes

of both intercrosses (R^2 = 0.74, *mus* x *cast* cross; R^2 = 0.81, GI x WSB cross). When the total SC lengths of multiple spermatocytes from the same individuals in this test set were averaged, the goodness of fit was even higher (R^2 = 0.94, *mus* x *cast* cross; R^2 = 0.90 GI x WSB cross).

From the *mus* x *cast* cross, we analyzed total SC lengths from 5893 spermatocytes, representing 289 F_2 individuals. Total SC length in spermatocytes from the *musculus* parent was significantly greater than from the *castaneus* parent (*mus* mean = 174.2 μm, SE: 0.7 μm; *cast* mean = 150.4 μm, SE: 0.4 μm; t-test $p < 0.05$). The distribution of SC lengths from F_2 individuals and their relation to the parental values is shown in Figure 4.2a. The difference in SC length between the parental strains and the distribution of their F_2s closely matches patterns observed in mean crossover number among spermatocytes (Dumont and Payseur 2011): a continuous distribution of the trait among F_2s, with a mean value that is close to the mid-parent value.

From the GI x WSB cross, we analyzed total SC lengths from 3639 spermatocytes, representing 229 F_2 individuals. SC lengths were modestly, but significantly, greater in spermatocytes from the GI parent compared to WSB (GI mean = 139.6 μm, SE: 1.6 μm; WSB mean = 131.8 μm, SE: 1.4 μm; t-test $p < 0.05$). Approximately half of the F_2 individuals from this cross have mean SC length outside the parental means, Figure 4.2b. This type of distribution was also observed for mean crossover number among spermatocytes, wherein a large number of individuals had trait values that fell outside the range of the parental means (Chapter 3). However, the level of transgressive segregation for SC length is not as severe as observed for crossover number, with a smaller fraction of F_2 individuals falling outside the range of the parental means. Nevertheless, it may indicate the presence of QTL alleles with opposing effects within the lines (Lynch and Walsh 1998; Rieseberg et al. 1999).

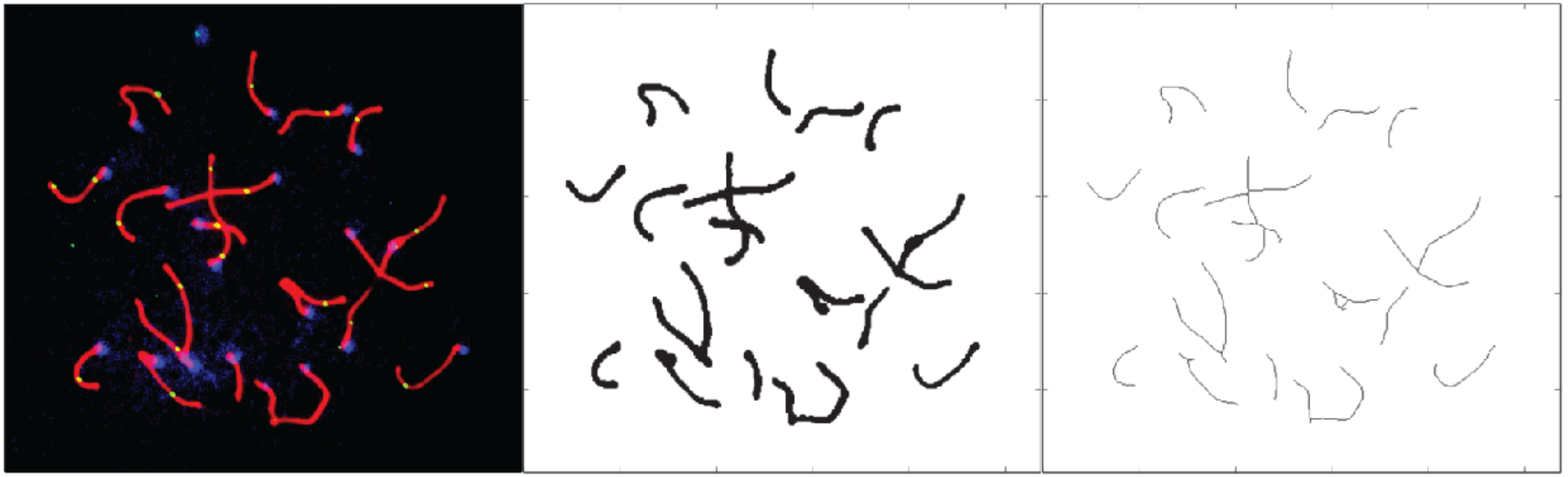

Figure 4.1. Typical immunofluorescent image from spermatocyte and its progression through image analysis.
The original image (left), isolated red channel (middle), and single pixel-wide skeletonized representation (right).

Correlation with recombination frequency

The total length of the SC and the number of crossovers in a meiocyte are known to strongly covary. We examined this relationship in spermatocytes from F_2 individuals of both intercrosses, comparing total SC length to the number of MLH1 foci per spermatocyte. While the correlation between these two traits was significant among spermatocytes from both intercrosses, the correlation was substantially stronger in the *mus* x *cast* cross (*mus* x *cast*: Pearson's r = 0.38, 95% CI [0.36, 0.40]; GI x WSB: Pearson's r = 0.15, 95% CI [0.12, 0.18]). Further, we examined the covariation between these two traits among individuals, i.e. the correlation between mean SC length and mean number of MLH1 foci in spermatocytes from each F_2 individual. Figure 4.3 shows the relationship between these two traits in the two intercrosses. In both cases, the correlation coefficient was higher for trait values representative of individuals rather than individual spermatocytes (*mus* x *cast*: Pearson's r = 0.52, 95% CI [0.42, 0.60]; GI x WSB: Pearson's r = 0.16, 95% CI [0.04, 0.28]). Previous studies note variation in the ratio of SC length to total crossover number among spermatocytes from different individuals, particularly in humans (Lynn et al. 2002; Pan et al. 2012). We performed a linear regression to examine the ratio between SC length and total crossover number among individuals of both intercrosses (regression line pictured in Figure 4.3). We found similar coefficients for this relationship in both cases (*mus* x *cast* $\beta = 2.03$, SE = 0.21; GI x WSB $\beta = 1.58$, SE = 0.55).

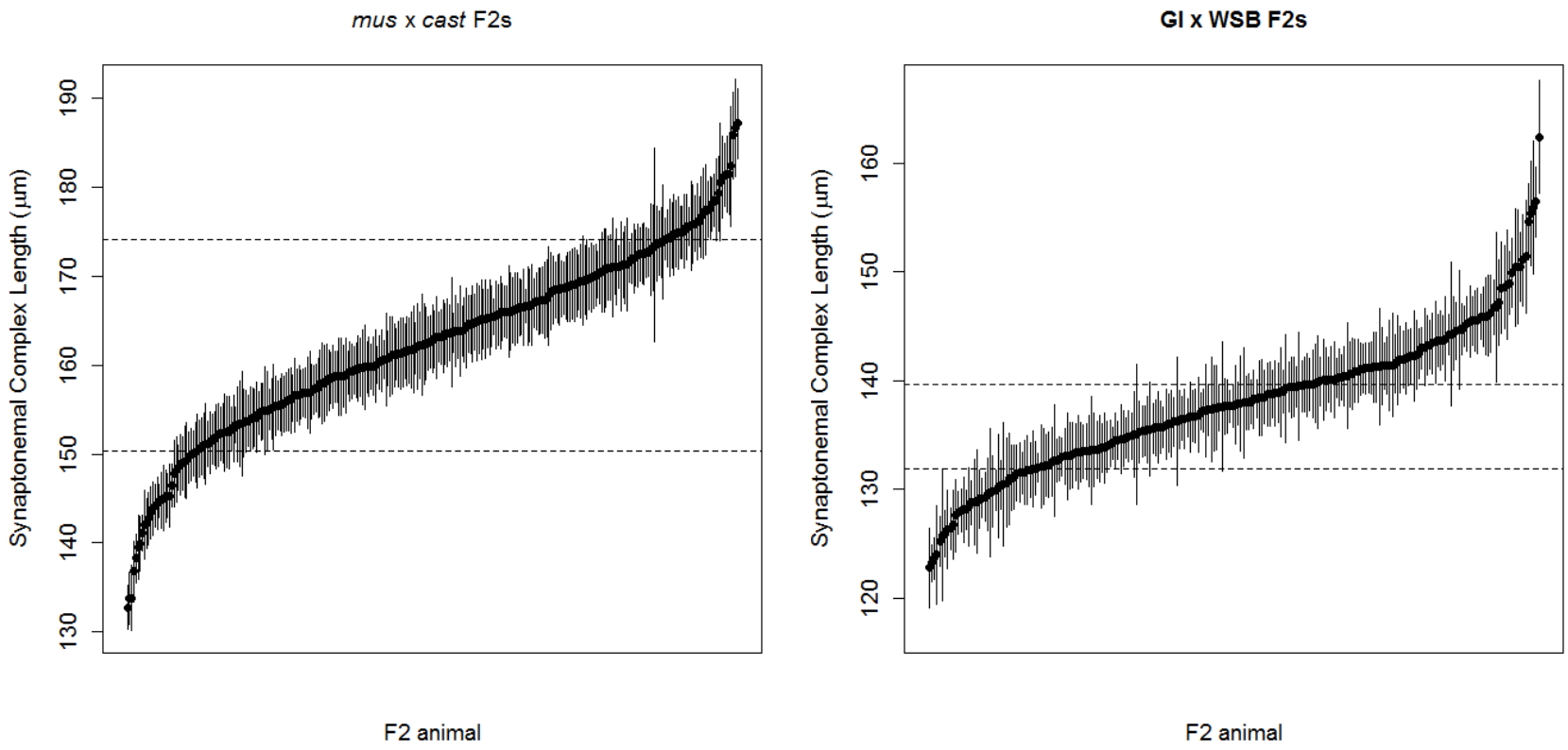

Figure 4.2. Distribution of mean SC length in spermatocytes from F_2 individuals.
Parental means shown as dashed lines. Error bars show +/- 1 S.E. in F_2 individuals.

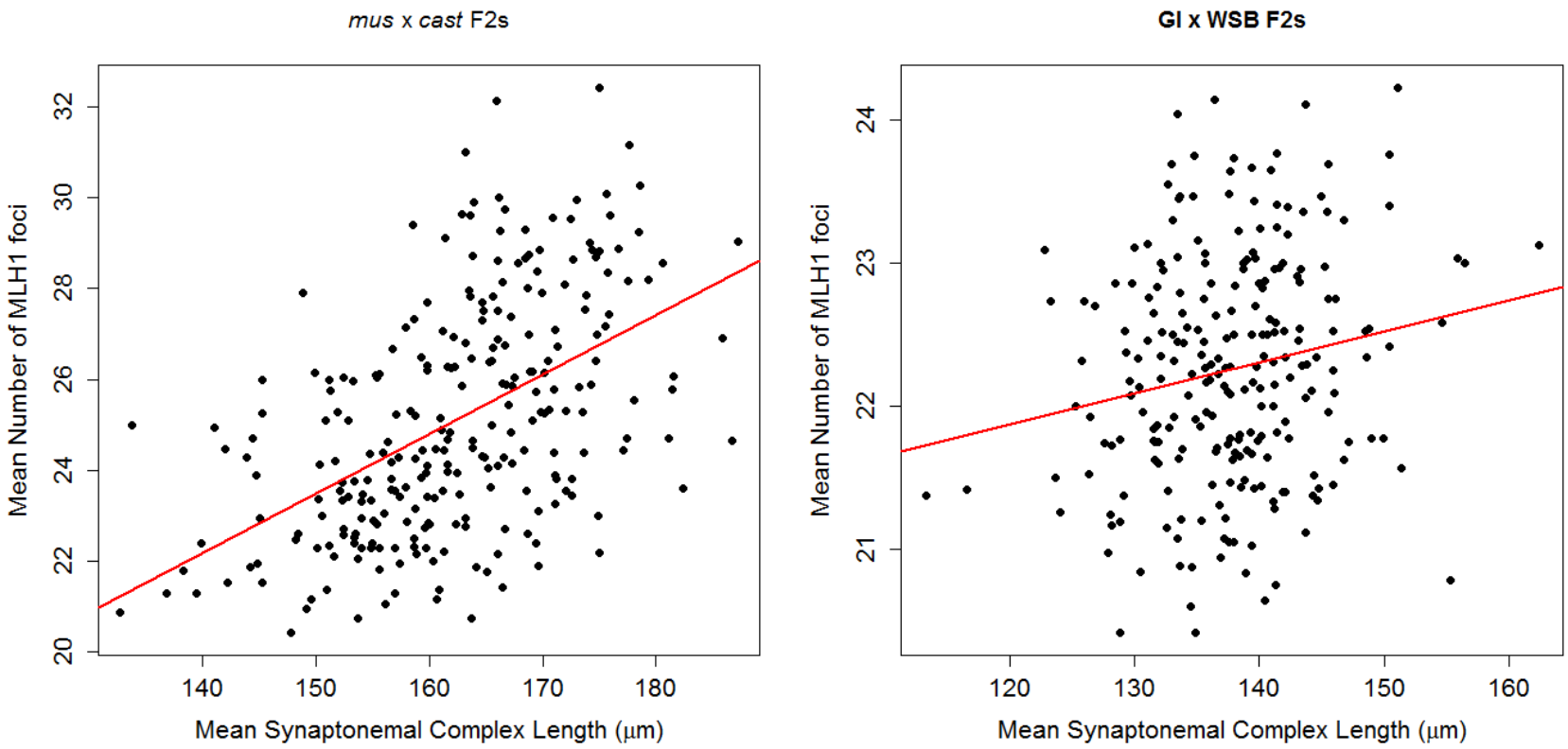

Figure 4.3. Relationship between mean SC length and mean number of MLH1 foci in spermatocytes from F_2 individuals. Regression lines in red.

QTL for total synaptonemal complex length

In the intersubspecific cross between representatives of *M. m. musculus* and *M. m. castaneus*, we identified three QTL responsible for variation in mean SC length among spermatocytes from an individual. The QTL with the greatest effect localized to the X chromosome (Figure 4.4a). Intriguingly, the X chromosome also harbors the QTL with the greatest effect on mean MLH1 count in this cross (Dumont and Payseur 2011). In addition to this QTL, genomic regions on chromosomes 3 and 4 were found to contribute to mean SC length (Table 4.1). Both of these chromosomes also harbor QTL for mean MLH1 counts in this cross.

These QTL explain an estimated 28.5% of the variance in mean SC length among the *mus* x *cast* F_2s. The effects of the alleles at QTL on chromosomes 3 and 4 were additive, with the *musculus* allele conferring greater mean SC length. The QTL on the X chromosome, however, had phenotypic effects that opposed the parental trait differences. The *musculus* allele at this locus confers a reduction to mean SC length. This pattern of effects, including the antagonistic effect of the *musculus* allele on the X, is consistent with the effects of QTL found on the same chromosomes for mean MLH1 counts, raising the prospect that the same loci are responsible for variation in both SC lengths and MLH1 counts.

In the intrasubspecific cross between GI mice and WSB, we identified two QTL responsible for variation in mean SC length, on chromosomes 5 and X (Figure 4.4b; Table 4.1). Together, they explain 12.8% of the variance in mean SC length among the GI x WSB F_2s. Chromosome 5 also harbors a QTL affecting mean MLH1 count in this cross, but the QTL on the X appears to be unique for SC length. The effect of alleles at the QTL on the X chromosome matches the direction of the parental differences, with the GI allele conferring greater mean SC

length. In contrast, the QTL on chromosome 5 appears to be underdominant, with a reduction in SC length specifically among heterozygotes.

We applied model-based multiple QTL mapping and evaluated the potential for epistasis between detected QTL in both intercrosses (Broman and Speed 2002; Manichaikul et al. 2009), but did not find any evidence for additional QTL or interactions between detected QTL.

Table 4.1. QTL for synaptonemal complex length

Chr.	Pos. (cM)	LOD	Pos. (Mb)	1.5 LOD Interval (Mb)	% var.[a]	Estimated phenotypic means (SE)[b]		
						MM / MY	MC	CC / CY
mus x *cast* cross								
3	38.0	4.12	103.5	68.0 - 128.6	6.4	165.7 (1.3)	162.7 (0.9)	157.8 (1.4)
4	44.0	5.10	112.3	65.8 - 146.5	6.7	167.6 (1.7)	162.0 (0.9)	158.5 (1.3)
X	31.9	9.51	71.7	52.9 - 90.7	14.6	158.3 (0.8)	--	166.1 (0.8)
GI x WSB cross						GG / GY	GW	WW / WY
5	44.8	4.97	106.3	102.9 - 115.4	6.8	139.2 (0.9)	136.5 (0.6)	140.8 (0.8)
X	54.0	3.78	138.1	123.0 - 153.8	4.9	140.1 (0.6)	--	136.8 (0.6)

[a] Percentage of phenotypic variance among F_2s explained
[b] M – *Musculus*, C – *Castaneus*; MY and CY genotypes for QTL on X

Causality and pleiotropy

The known relationship between total SC length and crossover frequency motivated us to examine evidence for causal relationships between the two traits and the detected QTL. We performed conditioned genomic scans for QTL, using one trait as a covariate in the analysis of the other trait. Differences in the LOD score at detected QTL, between conditioned and unconditioned scans, provide evidence for a causal relationship between the locus and the

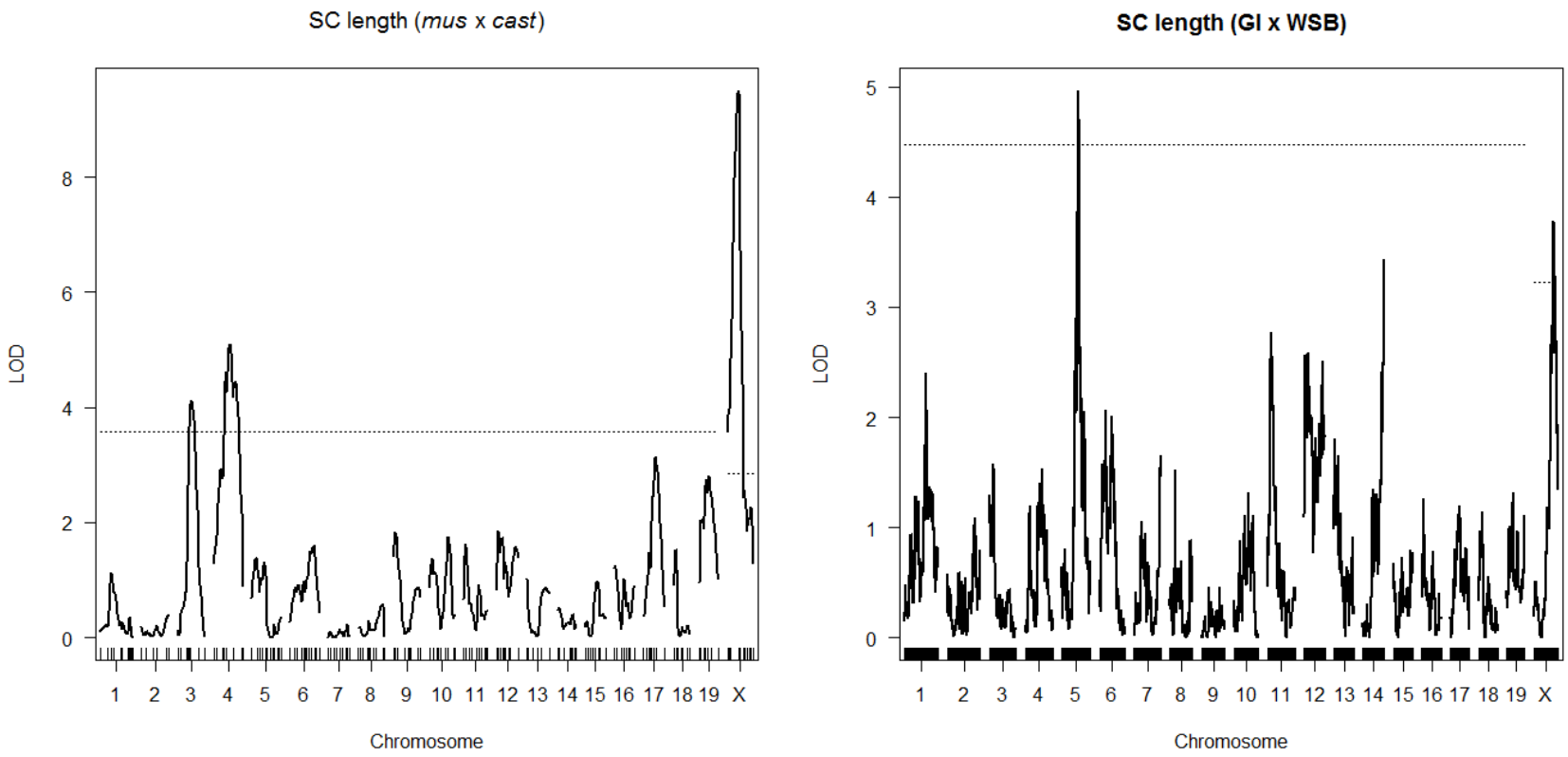

Figure 4.4. LOD plots of single QTL scans for SC length.
Dashed lines show α = 0.05 genome-wide significance threshold.

conditioning trait (Li et al. 2006; Rosa et al. 2011). A decrease in the LOD score at the locus upon conditioning suggests pleiotropy, as variation in the conditioning variable explains the effects of the locus. An increase in the LOD score upon conditioning suggests the locus is upstream or downstream of the causal relationship between the traits, as effects of the locus are masked in the unconditioned scan.

We performed conditioned genomic scans in both intercrosses, looking for changes in LOD score at QTL detected for mean SC length and mean MLH1 count (Dumont and Payseur 2011; Chapter 3). We identified three QTL with significant differences in LOD score upon conditioning in the *mus* x *cast* cross (Table 4.2). This included a dramatic reduction in the LOD score for the QTL on the X chromosome, strongly suggesting its pleiotropic effect on both SC length and recombination frequency. A significant decrease in LOD score was similarly detected for the QTL on chromosome 4. In contrast, the LOD score for the MLH1 count QTL on chromosome 7 significantly increased upon conditioning.

For the GI x WSB cross, none of the QTL had significant changes to their LOD score upon conditioning. The only QTL for both traits that co-localized to the same chromosome, on chromosome 5, had an increase in LOD score upon conditioning. The absence of a reduction in LOD score, combined with the underdominance effects of this locus on SC lengths, which contrasts with the additive effects of alleles at this locus for the number of MLH1 foci, suggests two causative loci may underlie this QTL.

Table 4.2. Changes to LOD scores of QTL when correlated traits are used as covariates

QTL for mean MLH1 foci (SC length as covariate)			QTL for mean SC length (MLH1 foci as covariate)		
mus x *cast* cross					
Chr.	Pos. (cM)	ΔLOD	Chr.	Pos. (cM)	ΔLOD
3	30.0	0.96	3	30.0	0.97
4	32.0	-2.22 *	4	32.0	-2.44 *
7	6.0	2.65 *		--	
11	5.5	-0.70		--	
15	36.8	-0.74		--	
17	32.0	-1.84		--	
X	31.9	-8.95 *	X	31.9	-9.27 *
GI x WSB cross					
Chr.	Pos. (cM)	ΔLOD	Chr.	Pos. (cM)	ΔLOD
5	47.8	1.15	5	46.7	1.35
6	31.1	-0.37		--	
10	29.1	0.26		--	
14	58.5	-0.30		--	
	--		X	55.6	-0.61

Discussion

In this study, we developed a novel computational approach to characterize SC length from immunofluorescent images in a large number of spermatocytes. This enabled mapping of the trait in two separate intercrosses, linking variation in SC length to multiple QTL. To our knowledge, these are the first QTL to be reported for SC length. Our results establish a strong genetic basis for natural variation in total SC length, within and between subspecies of house mice. The absence of overlapping QTL within and between subspecies for SC length suggests different loci are responsible for its evolution within and between subspecies. Different loci within and between subspecies are also suggested to be responsible for the evolution of genome-wide recombination rate in these crosses (Chapter 3).

Previous genetic mapping studies on recombination frequency in the same two crosses (Dumont and Payseur 2011; Chapter 3) provided a unique opportunity to examine its genetic relationship with SC length. As we may have expected, a greater number of QTL were detected in the *mus* x *cast* cross, where greater divergence exists between the parents. This mirrors the greater number of QTL found for mean MLH1 count in this intersubspecific cross. Surprisingly, the QTL with the greatest effect in the GI x WSB cross for crossover frequency had no effect on SC length. Transgressive segregation of MLH1 count in the GI x WSB cross was explained by the presence of such a QTL on chromosome 14 (Chapter 3). Based on the distribution of SC lengths and the parental trait values in GI and WSB, we may have expected to identify just such an antagonistic QTL. Nevertheless, antagonistic architecture for SC length persists in the *mus* x *cast* cross, paralleling patterns found for MLH1 count.

Our conditional mapping analyses provide evidence for a causal genetic relationship between SC length and crossover frequency in the *mus* x *cast* cross. The greater correlation

between the two traits when values from spermatocytes are averaged by individual is consistent with such a relationship. The strongest evidence for pleiotropy is from the reduction in LOD score for the QTL on the X chromosome in the conditional analysis. Similar patterns of allelic effects further argue for pleiotropy at this locus. Evidence for genetic control of crossover frequency independent of control on SC length comes from the significantly increased LOD score of the QTL on chromosome 7 in the conditional analysis, and its absence from explaining variation in SC length. Similarly, the presence of a unique QTL on the X in the GI x WSB cross for SC length suggests that its genetic control can be independent of loci influencing crossover frequency. If this complex genetic relationship between SC length and crossover frequency also exists in humans, segregation of loci responsible for independent variation of the two traits may explain differences in the ratio of SC length and MLH1 counts among different individuals (Lynn et al. 2002; Pan et al. 2012).

Conditional analyses in the GI x WSB cross indicated no significant differences in LOD score at any of the QTL. The absence of causally linked QTL in this cross is consistent with lower levels of correlation between SC length and crossover frequency among its F_2s, relative to the *mus* x *cast* cross. This suggests a different architecture linking the two traits may exist in the two crosses. Perhaps the evolution of the two traits is constrained by the meiotic pathway such that QTL with large effect on one trait must affect the other, e.g. the QTL on the X in the *mus* x *cast* cross. However, the absence of significant changes to the LOD score of QTL in conditional analyses from the GI x WSB cross is not evidence for the absence of a causal relationship. Differences in measurement error between traits frustrates conclusions about causality in QTL studies (Broman and Sen 2009). There is reduced power to detect QTL for traits measured with greater error, and conditioning on such traits may not produce significant differences in LOD

score despite a causal relationship. Between the two traits in our analysis, SC length likely suffers from more technical as well as biological noise. While more QTL were detected for mean MLH1 foci than mean SC length, greater measurement error for the latter also undermines inferences this may provide about the relative complexity of the traits.

Chapter 5
Conclusions

This dissertation examined patterns of variation and the genetics underlying this variation to better understand the evolution of recombination rate. By examining differences in recombination rate within subspecies, we sought to find the origins of divergence and perhaps the environment in which divergence arises. This work demonstrated the indispensability of the mouse model system, which armed us with the powerful genetic and cytological techniques needed to answer evolutionary questions. Using classical genetic techniques, we examined intrasubspecific variation of recombination rate in Chapter 2. With the short divergence times between strains, the variation we observed here may be more aptly classified as polymorphism within a population. Chapters 3 and 4 focus more heavily on understanding the genetics of recombination rate evolution. Additional context from genetic studies of recombination rate evolution between subspecies of the mouse particularly enriches the conclusions of these chapters. A repeated theme from these two chapters is the treatment of genome-wide recombination rate, and its surrogates, as quantitative traits. This treatment made ready the tools of quantitative genetics, providing tremendous genetic insight into how recombination rates evolve.

From comparisons of genetic maps, pervasive variation in recombination rate between two lines of GI mice was discovered. If this level of variation is representative of natural variation in mice, only the broadest patterns of recombination documented by genetic maps of laboratory mice are applicable to wild populations. This finding is similar to the pattern

described by Comeron et al. (2012), where wild-derived lines of fruit flies, *Drosophila melanogaster*, were found to have distinct landscapes of recombination. That regions of recombination rate divergence within the GI population, as described in Chapter 2, would not be shared with regions of divergence found in comparisons between mouse subspecies (Dumont et al. 2011) may not be surprising. If differences are pervasive from samples within a population, we may not expect the same patterns to persist over the time of subspecies divergence. While some genomic regions may be more prone to recombination rate divergence, enough of the genome shows variation that these regions are not predictive of broader patterns. The absence of a significant difference in the genome-wide rate in the face of pervasive variation across the genome argues that different evolutionary forces may be acting at different genomic scales. Whether this supports the view that genome-wide rates are under some form of stabilizing selection is debatable.

One of the goals of Chapter 2 was to connect different scales of recombination rate evolution. Discovering polymorphism within the genome in the absence of genome-wide rate differences highlights the importance of this goal. Currently, no model of recombination rate evolution truly connects patterns of variation from the kilobase scale of hotspots, through the patterns on chromosomes, to the genome-wide rate. Though some notable attempts, e.g. Ubeda and Wilkins (2011), have been made to explicitly model connections between some of these scales. This problem may be exacerbated by empirical data that focuses on divergence between species. If the dynamics between the different genomic scales are themselves evolving between species, observed patterns of divergence across genomic scales may be confounded by a changing relationship between them. If so, continued efforts probing intraspecific variation may be more illuminating than trying to connect the many findings across disparate taxa.

The genetic mapping of genome-wide recombination rate between GI and WSB mice uncovered multiple QTL responsible for a small amount of divergence in the trait. This was explained by the large transgressive effects of alleles at one of the loci. While antagonistic alleles may not be that rare, they are present with strong effects in all three crosses mapping genome-wide recombination rates in mice. There are many evolutionary modes by which this pattern could have emerged, but this finding strongly argues against directional selection on recombination rate. While this form of selection seems unlikely to exist on genome-wide rates across taxa, evidence for selection on recombination rate in artificial selection experiments and the rapid evolution of body size in GI mice raised its possibility in this study.

Fine mapping of detected loci is one possibility to further characterize the genetics of recombination rate evolution. While useful for understanding the mechanism of action, the understanding of recombination rate evolution would likely be better served by sampling from more wild populations. This includes characterizing genome-wide as well as fine-scale rates from a variety of wild populations. Genetic dissection in a variety of populations may be prohibitive, but crosses with a common strain to sample the distribution of effects among offspring may be illuminating even without genetic mapping. The suggestion of variance QTL for genome-wide recombination rate provides another avenue for further research. The introduction of automated techniques, like the ones in Chapter 4, may allow for increases to sample size so that variance can be better characterized in future studies. An important pattern in genome-wide recombination rates that Chapters 3 and 4 do not address is the difference in recombination rates between the sexes. In mice, and many other species, oocytes have a greater number of crossovers as well as longer synaptonemal complex lengths. Large differences in the meiotic program exist between spermatocytes and oocytes, providing many opportunities for

genetic and evolutionary divergence to arise. However, the technical challenges of immunofluorescent cytology on oocytes prevented us from characterizing genome-wide recombination rates in females. The findings presented in this dissertation would be substantially enhanced by similar experiments in oocytes.

Genetic mapping for synaptonemal complex length revealed the first such QTL for this phenotype. As a trait strongly correlated with genome-wide recombination rate, we may have expected many of the QTL for SC length to appear shared with QTL for MLH1 count. However, the existence of QTL that are unique to each trait, suggests genetic control of each independent of the other. This need not have been the case; imperfect correlation with crossover number could have been due to non-genetic differences. These differences in genetic control call into question the focus on recombination rates when discussing meiotic requirements. It may be possible that evolutionary forces are acting on other meiotic phenotypes to ensure proper chromosome segregation, and the evolution of recombination rate is a side effect rather than the underlying target.

To put our results on SC length into perspective, a phylogenetic comparison of this trait across populations and species of mice would be very useful. One of the unstated motivations for examining the synaptonemal complex was the idea that counting only MLH1 foci from immunofluorescent images was squandering the rich image data. Measurement of SC lengths extracts additional data from these images. However, immunofluorescent cytology techniques can offer further views into variation along the meiotic pathway. Variation in recombination associated proteins, such as *Dmc1* and *Rad51*, can be observed by cytology and QTL mapped in a similar way. Guided by an understanding of the mechanisms in meiosis, genetic analysis of variation in selected meiotic phenotypes can partition variation in recombination rate to variation

in elements of the pathway. Computer vision techniques may be able to mitigate the amount of labor needed to process these additional phenotypes.

References

Anderson, L. K., Reeves, A., Webb, L. M., & Ashley, T. (1999). Distribution of crossing over on mouse synaptonemal complexes using immunofluorescent localization of MLH1 protein. *Genetics*, *151*(4), 1569–1579.

Ayroles, J. F., Buchanan, S. M., O'Leary, C., Skutt-Kakaria, K., Grenier, J. K., Clark, A. G., … de Bivort, B. L. (2015). Behavioral idiosyncrasy reveals genetic control of phenotypic variability. *Proceedings of the National Academy of Sciences*, *112*(21), 6706–6711.

Backstrom, N., Forstmeier, W., Schielzeth, H., Mellenius, H., Nam, K., Bolund, E., … Ellegren, H. (2010). The recombination landscape of the zebra finch Taeniopygia guttata genome. *Genome Research*, *20*(4), 485–495. https://doi.org/10.1101/gr.101410.109

Baier, B., Hunt, P., Broman, K. W., & Hassold, T. (2014). Variation in Genome-Wide Levels of Meiotic Recombination Is Established at the Onset of Prophase in Mammalian Males. *Plos Genetics*, *10*(1), e1004125. https://doi.org/10.1371/journal.pgen.1004125

Baker, C. L., Kajita, S., Walker, M., Saxl, R. L., Raghupathy, N., Choi, K., … Paigen, K. (2015). PRDM9 Drives Evolutionary Erosion of Hotspots in Mus musculus through Haplotype-Specific Initiation of Meiotic Recombination. *Plos Genetics*, *11*(1), e1004916. https://doi.org/10.1371/journal.pgen.1004916

Balcova, M., Faltusova, B., Gergelits, V., Bhattacharyya, T., Mihola, O., Trachtulec, Z., … Gregorova, S. (2016). Hybrid sterility locus on chromosome X controls meiotic recombination rate in mouse. *PLoS Genet*, *12*(4), e1005906.

Ball, R. L., Fujiwara, Y., Sun, F., Hu, J., Hibbs, M. A., Handel, M. A., & Carter, G. W. (2016).

Regulatory complexity revealed by integrated cytological and RNA-seq analyses of meiotic substages in mouse spermatocytes. *BMC Genomics*, *17*(1), 628.

Barton, N. H. (1995). A general model for the evolution of recombination. *Genetical Research*, *65*(02), 123–144.

Baudat, F., Buard, J., Grey, C., Fledel-Alon, A., Ober, C., Przeworski, M., … de Massy, B. (2010). PRDM9 Is a Major Determinant of Meiotic Recombination Hotspots in Humans and Mice. *Science*, *327*(5967), 836–840. https://doi.org/10.1126/science.1183439

Baudet, C., Lemaitre, C., Dias, Z., Gautier, C., Tannier, E., & Sagot, M.-F. (2010). Cassis: detection of genomic rearrangement breakpoints. *Bioinformatics*, *26*(15), 1897–1898. https://doi.org/10.1093/bioinformatics/btq301

Beadle, G. W. (1932). A Possible Influence of the Spindle Fibre on Crossing-Over in Drosophila. *Proceedings of the National Academy of Sciences of the United States of America*, *18*(2), 160–165.

Beaumont, H. J., Gallie, J., Kost, C., Ferguson, G. C., & Rainey, P. B. (2009). Experimental evolution of bet hedging. *Nature*, *462*(7269), 90–93.

Beavis, W. D. (1994). The power and deceit of QTL experiments: lessons from comparative QTL studies. In *Proceedings of the forty-ninth annual corn and sorghum industry research conference* (pp. 250–266). Chicago, IL.

Begun, D., & Aquadro, C. (1992). Levels of Naturally-Occurring Dna Polymorphism Correlate with Recombination Rates in Drosophila-Melanogaster. *Nature*, *356*(6369), 519–520. https://doi.org/10.1038/356519a0

Bojko, M. (1985). Human meiosis IX. Crossing over and chiasma formation in oocytes. *Carlsberg Research Communications*, *50*(2), 43–72.

Bolcun-Filas, E., & Schimenti, J. C. (2012). Genetics of Meiosis and Recombination in Mice. In K. W. Jeon (Ed.), *International Review of Cell and Molecular Biology, Vol 298* (Vol. 298, pp. 179–227). San Diego: Elsevier Academic Press Inc.

Bomblies, K., Higgins, J. D., & Yant, L. (2015). Meiosis evolves: adaptation to external and internal environments. *New Phytologist*, *208*(2), 306–323. https://doi.org/10.1111/nph.13499

Borodin, P. M., Karamysheva, T. V., Belonogova, N. M., Torgasheva, A. A., Rubtsov, N. B., & Searle, J. B. (2008). Recombination map of the common shrew, Sorex araneus (Eulipotyphla, Mammalia). *Genetics*, *178*(2), 621–632.

Boulton, A., Myers, R. S., & Redfield, R. J. (1997). The hotspot conversion paradox and the evolution of meiotic recombination. *Proceedings of the National Academy of Sciences of the United States of America*, *94*(15), 8058–8063. https://doi.org/10.1073/pnas.94.15.8058

Bourguet, D., Gair, J., Mattice, M., & Whitlock, M. C. (2003). Genetic recombination and adaptation to fluctuating environments: selection for geotaxis in Drosophila melanogaster. *Heredity*, *91*(1), 78–84.

Brick, K., Smagulova, F., Khil, P., Camerini-Otero, R. D., & Petukhova, G. V. (2012). Genetic recombination is directed away from functional genomic elements in mice. *Nature*, *485*(7400), 642–645. https://doi.org/10.1038/nature11089

Broman, K. W., Murray, J. C., Sheffield, V. C., White, R. L., & Weber, J. L. (1998). Comprehensive human genetic maps: Individual and sex-specific variation in recombination. *American Journal of Human Genetics*, *63*(3), 861–869. https://doi.org/10.1086/302011

Broman, K. W., & Sen, S. (2009). Guide to QTL Mapping with R/qtl. In *Guide to QTL Mapping with R/qtl*.

Broman, K. W., & Speed, T. P. (2002). A model selection approach for the identification of quantitative trait loci in experimental crosses. *Journal of the Royal Statistical Society: Series B (Statistical Methodology)*, *64*(4), 641–656.

Broman, K. W., Wu, H., Sen, Ś., & Churchill, G. A. (2003). R/qtl: QTL mapping in experimental crosses. *Bioinformatics*, *19*(7), 889-890.

Browning, S. R., & Browning, B. L. (2007). Rapid and accurate haplotype phasing and missing-data inference for whole-genome association studies by use of localized haplotype clustering. *American Journal of Human Genetics*, *81*(5), 1084–1097. https://doi.org/10.1086/521987

Brunschwig, H., Levi, L., Ben-David, E., Williams, R. W., Yakir, B., & Shifman, S. (2012). Fine-scale maps of recombination rates and hotspots in the mouse genome. *Genetics*, *191*(3), 757–764.

Buard, J., Rivals, E., de Segonzac, D. D., Garres, C., Caminade, P., de Massy, B., & Boursot, P. (2014). Diversity of Prdm9 Zinc Finger Array in Wild Mice Unravels New Facets of the Evolutionary Turnover of this Coding Minisatellite. *Plos One*, *9*(1), e85021. https://doi.org/10.1371/journal.pone.0085021

Bugreev, D. V., Yu, X., Egelman, E. H., & Mazin, A. V. (2007). Novel pro-and anti-recombination activities of the Bloom's syndrome helicase. *Genes & Development*, *21*(23), 3085–3094.

Burt, A. (2000). Perspective: sex, recombination, and the efficacy of selection—was Weismann right? *Evolution*, *54*(2), 337–351.

Burt, A., & Bell, G. (1987). Mammalian chiasma frequencies as a test of two theories of recombination. *Nature*, *326*(6115), 803–805.

Burt, D. W. (2002). Origin and evolution of avian microchromosomes. *Cytogenetic and Genome Research*, *96*(1–4), 97–112. https://doi.org/10.1159/000063018

Cahoon, C. K., & Hawley, R. S. (2016). Regulating the construction and demolition of the synaptonemal complex. *Nature Structural & Molecular Biology*, *23*(5), 369–377.

Carter, T. C., & Falconer, D. S. (1951). Stocks for detecting linkage in the mouse, and the theory of their design. *Jour Genetics*, *50*((2)), 307–323. https://doi.org/10.1007/BF02996226

Case, T. J. (1978). A general explanation for insular body size trends in terrestrial vertebrates. *Ecology*, *59*(1), 1–18.

Charlesworth, B., & Charlesworth, D. (1985). Genetic variation in recombination in Drosophila. I. Responses to selection and preliminary genetic analysis. *Heredity*, *54*(1), 71–84.

Chinnici, J. P. (1971). Modification of recombination frequency in Drosophila. I. Selection for increased and decreased crossing over. *Genetics*, *69*(1), 71.

Churchill, G. A., & Doerge, R. W. (1994). Empirical threshold values for quantitative trait mapping. *Genetics*, *138*(3), 963–971.

Cole, F., Baudat, F., Grey, C., Keeney, S., de Massy, B., & Jasin, M. (2014). Mouse tetrad analysis provides insights into recombination mechanisms and hotspot evolutionary dynamics. *Nature Genetics*, *46*(10), 1072–1080. https://doi.org/10.1038/ng.3068

Cole, F., Kauppi, L., Lange, J., Roig, I., Wang, R., Keeney, S., & Jasin, M. (2012). Homeostatic control of recombination is implemented progressively in mouse meiosis. *Nature Cell Biology*, *14*(4), 424–+. https://doi.org/10.1038/ncb2451

Comeron, J. M., Ratnappan, R., & Bailin, S. (2012). The Many Landscapes of Recombination in

Drosophila melanogaster. *Plos Genetics*, *8*(10), e1002905. https://doi.org/10.1371/journal.pgen.1002905

Coop, G., & Myers, S. R. (2007). Live hot, die young: Transmission distortion in recombination hotspots. *Plos Genetics*, *3*(3), 377–386. https://doi.org/10.1371/journal.pgen.0030035

Coop, G., & Przeworski, M. (2007). An evolutionary view of human recombination. *Nature Reviews Genetics*, *8*(1), 23–34.

Coop, G., Wen, X., Ober, C., Pritchard, J. K., & Przeworski, M. (2008). High-resolution mapping of crossovers reveals extensive variation in fine-scale recombination patterns among humans. *Science, 319*(5868), 1395–1398. https://doi.org/10.1126/science.1151851

Cox, A., Ackert-Bicknell, C. L., Dumont, B. L., Ding, Y., Bell, J. T., Brockmann, G. A., … Broman, K. W. (2009). A New Standard Genetic Map for the Laboratory Mouse. *Genetics, 182*(4), 1335–1344. https://doi.org/10.1534/genetics.108.105486

Crismani, W., Girard, C., Froger, N., Pradillo, M., Luis Santos, J., Chelysheva, L., … Mercier, R. (2012). FANCM Limits Meiotic Crossovers. *Science, 336*(6088), 1588–1590. https://doi.org/10.1126/science.1220381

Cullen, M., Perfetto, S. P., Klitz, W., Nelson, G., & Carrington, M. (2002). High-resolution patterns of meiotic recombination across the human major histocompatibility complex. *American Journal of Human Genetics, 71*(4), 759–776. https://doi.org/10.1086/342973

da Cruz, I., Rodríguez-Casuriaga, R., Santiñaque, F. F., Farías, J., Curti, G., Capoano, C. A., … Geisinger, A. (2016). Transcriptome analysis of highly purified mouse spermatogenic cell populations: gene expression signatures switch from meiotic-to postmeiotic-related processes at pachytene stage. *BMC Genomics, 17*(1), 1.

de Boer, E., Lhuissier, F. G., & Heyting, C. (2009). Cytological analysis of interference in mouse

meiosis. *Meiosis: Volume 2, Cytological Methods*, 355–382.

de Massy, B. (2013). Initiation of Meiotic Recombination: How and Where? Conservation and Specificities Among Eukaryotes. In B. L. Bassler, M. Lichten, & G. Schupbach (Eds.), *Annual Review of Genetics, Vol 47* (Vol. 47, pp. 563–599). Palo Alto: Annual Reviews.

De Muyt, A., Jessop, L., Kolar, E., Sourirajan, A., Chen, J., Dayani, Y., & Lichten, M. (2012a). BLM helicase ortholog Sgs1 is a central regulator of meiotic recombination intermediate metabolism. *Molecular Cell*, *46*(1), 43–53.

De Muyt, A., Jessop, L., Kolar, E., Sourirajan, A., Chen, J., Dayani, Y., & Lichten, M. (2012b). BLM Helicase Ortholog Sgs1 Is a Central Regulator of Meiotic Recombination Intermediate Metabolism. *Molecular Cell*, *46*(1), 43–53. https://doi.org/10.1016/j.molcel.2012.02.020

de Villena, F. P.-M., & Sapienza, C. (2001). Nonrandom segregation during meiosis: the unfairness of females. *Mammalian Genome*, *12*(5), 331–339.

Dumont, B. L. (2017). Variation and Evolution of the Meiotic Requirement for Crossing Over in Mammals. *Genetics*, *205*(1), 155–168.

Dumont, B. L., Broman, K. W., & Payseur, B. A. (2009). Variation in genomic recombination rates among heterogeneous stock mice. *Genetics*, *182*(4), 1345–1349.

Dumont, B. L., & Payseur, B. A. (2011a). Evolution of the Genomic Recombination Rate in Murid Rodents. *Genetics*, *187*(3), 643–657. https://doi.org/10.1534/genetics.110.123851

Dumont, B. L., & Payseur, B. A. (2011b). Genetic Analysis of Genome-Scale Recombination Rate Evolution in House Mice. *Plos Genetics*, *7*(6), e1002116. https://doi.org/10.1371/journal.pgen.1002116

Dumont, B. L., White, M. A., Steffy, B., Wiltshire, T., & Payseur, B. A. (2011). Extensive

recombination rate variation in the house mouse species complex inferred from genetic linkage maps. *Genome Research*, *21*(1), 114–125.

Duret, L., & Arndt, P. F. (2008). The impact of recombination on nucleotide substitutions in the human genome. *PLoS Genet*, *4*(5), e1000071.

Duret, L., & Galtier, N. (2009). Biased Gene Conversion and the Evolution of Mammalian Genomic Landscapes. In *Annual Review of Genomics and Human Genetics* (Vol. 10, pp. 285–311). Palo Alto: Annual Reviews.

Eldar, A., & Elowitz, M. B. (2010). Functional roles for noise in genetic circuits. *Nature*, *467*(7312), 167–173.

Ernst, J., & Kellis, M. (2012). ChromHMM: automating chromatin-state discovery and characterization. *Nature Methods*, *9*(3), 215–216. https://doi.org/10.1038/nmeth.1906

Evans, D. M., & Cardon, L. R. (2005). A comparison of linkage disequilibrium patterns and estimated population recombination rates across multiple populations. *American Journal of Human Genetics*, *76*(4), 681–687. https://doi.org/10.1086/429274

Eyre-Walker, A. (1993). Recombination and mammalian genome evolution. *Proceedings of the Royal Society of London B: Biological Sciences*, *252*(1335), 237–243.

Fallahi, M., Getun, I. V., Wu, Z. K., & Bois, P. R. (2010). A global expression switch marks pachytene initiation during mouse male meiosis. *Genes*, *1*(3), 469–483.

Farré, M., Micheletti, D., & Ruiz-Herrera, A. (2013). Recombination Rates and Genomic Shuffling in Human and Chimpanzee—A New Twist in the Chromosomal Speciation Theory. *Molecular Biology and Evolution*, *30*(4), 853–864. https://doi.org/10.1093/molbev/mss272

Feldman, M. W. (1972). Selection for linkage modification: I. Random mating populations.

Theoretical Population Biology, *3*(3), 324–346. https://doi.org/10.1016/0040-5809(72)90007-X

Feldman, M. W., Christiansen, F. B., & Brooks, L. D. (1980). Evolution of recombination in a constant environment. *Proceedings of the National Academy of Sciences*, *77*(8), 4838–4841.

Feldman, M. W., Otto, S. P., & Christiansen, F. B. (1996). Population genetic perspectives on the evolution of recombination. *Annual Review of Genetics*, *30*(1), 261–295.

Felsenstein, J. (1974). The Evolutionary Advantage of Recombination. *Genetics*, *78*(2), 737–756.

Fledel-Alon, A., Leffler, E. M., Guan, Y., Stephens, M., Coop, G., & Przeworski, M. (2011). Variation in Human Recombination Rates and Its Genetic Determinants. *Plos One*, *6*(6), e20321. https://doi.org/10.1371/journal.pone.0020321

Fledel-Alon, A., Wilson, D. J., Broman, K., Wen, X., Ober, C., Coop, G., & Przeworski, M. (2009). Broad-Scale Recombination Patterns Underlying Proper Disjunction in Humans. *Plos Genetics*, *5*(9), e1000658. https://doi.org/10.1371/journal.pgen.1000658

Flexon, P. B., & Rodell, C. F. (1982). Genetic recombination and directional selection for DDT resistance in Drosophila melanogaster.

Foster, J. B. (1964). Evolution of mammals on islands.

Fraune, J., Schramm, S., Alsheimer, M., & Benavente, R. (2012). The mammalian synaptonemal complex: protein components, assembly and role in meiotic recombination. *Experimental Cell Research*, *318*(12), 1340–1346.

Freudenberg, J., Wang, M., Yang, Y., & Li, W. (2009). Partial correlation analysis indicates causal relationships between GC-content, exon density and recombination rate in the

human genome. *Bmc Bioinformatics*, *10*, S66. https://doi.org/10.1186/1471-2105-10-S1-S66

Froehlich, J., Vozdova, M., Kubickova, S., Cernohorska, H., Sebestova, H., & Rubes, J. (2015). Variation of Meiotic Recombination Rates and MLH1 Foci Distribution in Spermatocytes of Cattle, Sheep and Goats. *Cytogenetic and Genome Research*, *146*(3), 211–221. https://doi.org/10.1159/000439452

Fullerton, S. M., Carvalho, A. B., & Clark, A. G. (2001). Local rates of recombination are positively correlated with GC content in the human genome. *Molecular Biology and Evolution*, *18*(6), 1139–1142.

Gabriel, S., Ziaugra, L., & Tabbaa, D. (2009). SNP genotyping using the Sequenom MassARRAY iPLEX platform. *Current Protocols in Human Genetics*, 2.12. 1-2.12. 16.

Geiler-Samerotte, K. A., Bauer, C. R., Li, S., Ziv, N., Gresham, D., & Siegal, M. L. (2013). The details in the distributions: why and how to study phenotypic variability. *Current Opinion in Biotechnology*, *24*(4), 752–759.

Geraldes, A., Basset, P., Smith, K. L., & Nachman, M. W. (2011). Higher differentiation among subspecies of the house mouse (Mus musculus) in genomic regions with low recombination. *Molecular Ecology*, *20*(22), 4722–4736.

Gerton, J. L., DeRisi, J., Shroff, R., Lichten, M., Brown, P. O., & Petes, T. D. (2000). Global mapping of meiotic recombination hotspots and coldspots in the yeast Saccharomyces cerevisiae. *Proceedings of the National Academy of Sciences of the United States of America*, *97*(21), 11383–11390. https://doi.org/10.1073/pnas.97.21.11383

Giraut, L., Falque, M., Drouaud, J., Pereira, L., Martin, O. C., & Mézard, C. (2011). Genome-Wide Crossover Distribution in Arabidopsis thaliana Meiosis Reveals Sex-Specific

Patterns along Chromosomes. *PLOS Genet*, *7*(11), e1002354. https://doi.org/10.1371/journal.pgen.1002354

Gorlov, I., Schuler, L., Bunger, L., & Borodin, P. (1992). Chiasma frequency in strains of mice selected for litter size and for high body weight. *Theoretical and Applied Genetics*, *84*(5–6), 640–642.

Graffelman, J., Balding, D. J., Gonzalez-Neira, A., & Bertranpetit, J. (2007). Variation in estimated recombination rates across human populations. *Human Genetics*, *122*(3–4), 301–310. https://doi.org/10.1007/s00439-007-0391-6

Grant, C. E., Bailey, T. L., & Noble, W. S. (2011). FIMO: scanning for occurrences of a given motif. *Bioinformatics*, *27*(7), 1017–1018. https://doi.org/10.1093/bioinformatics/btr064

Grant, P. R., & Grant, B. R. (2002). Unpredictable evolution in a 30-year study of Darwin's finches. *Science*, *296*(5568), 707–711.

Gray, M. M., Parmenter, M. D., Hogan, C. A., Ford, I., Cuthbert, R. J., Ryan, P. G., … Payseur, B. A. (2015). Genetics of Rapid and Extreme Size Evolution in Island Mice. *Genetics*, *201*(1), 213–+. https://doi.org/10.1534/genetics.115.177790

Gray, M. M., Wegmann, D., Haasl, R. J., White, M. A., Gabriel, S. I., Searle, J. B., … Payseur, B. A. (2014). Demographic history of a recent invasion of house mice on the isolated Island of Gough. *Molecular Ecology*, *23*(8), 1923–1939. https://doi.org/10.1111/mec.12715

Grey, C., Barthès, P., Friec, G. C.-L., Langa, F., Baudat, F., & Massy, B. de. (2011). Mouse PRDM9 DNA-Binding Specificity Determines Sites of Histone H3 Lysine 4 Trimethylation for Initiation of Meiotic Recombination. *PLOS Biology*, *9*(10), e1001176. https://doi.org/10.1371/journal.pbio.1001176

Griffiths, R. c., & Marjoram, P. (1996). Ancestral Inference from Samples of DNA Sequences with Recombination. *Journal of Computational Biology*, *3*(4), 479–502. https://doi.org/10.1089/cmb.1996.3.479

Grishaeva, T. M., & Bogdanov, Y. F. (2014). Conservation and variability of synaptonemal complex proteins in phylogenesis of eukaryotes. *International Journal of Evolutionary Biology*, *2014*.

Groenen, M. A. M., Wahlberg, P., Foglio, M., Cheng, H. H., Megens, H.-J., Crooijmans, R. P. M. A., … Andersson, L. (2009). A high-density SNP-based linkage map of the chicken genome reveals sequence features correlated with recombination rate. *Genome Research*, *19*(3), 510–519. https://doi.org/10.1101/gr.086538.108

Haldane, J. B. S. (1919). The combination of linkage values and the calculation of distances between the loci of linked factors. *J Genet*, *8*(29), 299–309.

Haley, C. S., & Knott, S. A. (1992). A simple regression method for mapping quantitative trait loci in line crosses using flanking markers. *Heredity*, *69*(4), 315–324.

Handel, M. A., & Schimenti, J. C. (2010). Genetics of mammalian meiosis: regulation, dynamics and impact on fertility. *Nature Reviews Genetics*, *11*(2), 124–136.

Hassold, T., Hall, H., & Hunt, P. (2007). The origin of human aneuploidy: where we have been, where we are going. *Human Molecular Genetics*, *16*(R2), R203–R208. https://doi.org/10.1093/hmg/ddm243

Hassold, T., & Hunt, P. (2001). To err (meiotically) is human: the genesis of human aneuploidy. *Nature Reviews Genetics*, *2*(4), 280–291.

Hayashi, K., Yoshida, K., & Matsui, Y. (2005). A histone H3 methyltransferase controls epigenetic events required for meiotic prophase. *Nature*, *438*(7066), 374–378.

https://doi.org/10.1038/nature04112

Hemmer, L. W., & Blumenstiel, J. P. (2016). Holding it together: rapid evolution and positive selection in the synaptonemal complex of Drosophila. *BMC Evolutionary Biology, 16*(1), 1.

Henderson, K. A., & Keeney, S. (2005). Synaptonemal complex formation: where does it start? *Bioessays*, *27*(10), 995–998.

Hill, W. G., & Robertson, A. (1966). The effect of linkage on limits to artificial selection. *Genetical Research*, *8*(03), 269–294.

Hochwagen, A., & Amon, A. (2006). Checking your breaks: surveillance mechanisms of meiotic recombination. *Current Biology*, *16*(6), R217–R228.

Hollingsworth, N. M., & Brill, S. J. (2004). The Mus81 solution to resolution: generating meiotic crossovers without Holliday junctions. *Genes & Development*, *18*(2), 117–125.

Holloway, J. K., Booth, J., Edelmann, W., McGowan, C. H., & Cohen, P. E. (2008). MUS81 Generates a Subset of MLH1-MLH3-Independent Crossovers in Mammalian Meiosis. *Plos Genetics*, *4*(9), e1000186. https://doi.org/10.1371/journal.pgen.1000186

Hulse, A. M., & Cai, J. J. (2013). Genetic variants contribute to gene expression variability in humans. *Genetics*, *193*(1), 95–108.

Hunter, C. M., Huang, W., Mackay, T. F. C., & Singh, N. D. (2016). The Genetic Architecture of Natural Variation in Recombination Rate in Drosophila melanogaster. *Plos Genetics*, *12*(4), e1005951. https://doi.org/10.1371/journal.pgen.1005951

Hunter, N. (2003). Synaptonemal complexities and commonalities. *Molecular Cell*, *12*(3), 533–535.

Hunter, N. (2015). Meiotic recombination: the essence of heredity. *Cold Spring Harbor*

Perspectives in Biology, *7*(12), a016618.

Inoue, K., & Lupski, J. R. (2002). Molecular mechanisms for genomic disorders. *Annual Review of Genomics and Human Genetics*, *3*(1), 199–242.

Janssens, F. A. (1909). *La Théorie de la Chiasmatypie*...

Jaramillo-Lambert, A., Harigaya, Y., Vitt, J., Villeneuve, A., & Engebrecht, J. (2010). Meiotic errors activate checkpoints that improve gamete quality without triggering apoptosis in male germ cells. *Current Biology*, *20*(23), 2078–2089.

Jeffreys, A. J., Kauppi, L., & Neumann, R. (2001). Intensely punctate meiotic recombination in the class II region of the major histocompatibility complex. *Nature Genetics*, *29*(2), 217–222. https://doi.org/10.1038/ng1001-217

Jensen-Seaman, M. I., Furey, T. S., Payseur, B. A., Lu, Y., Roskin, K. M., Chen, C.-F., … Jacob, H. J. (2004). Comparative recombination rates in the rat, mouse, and human genomes. *Genome Research*, *14*(4), 528–538.

Johnston, S. E., Berenos, C., Slate, J., & Pemberton, J. M. (2016). Conserved Genetic Architecture Underlying Individual Recombination Rate Variation in a Wild Population of Soay Sheep (Ovis aries). *Genetics*, *203*(1), 583–+. https://doi.org/10.1534/genetics.115.185553

Jones, A. G., Chown, S. L., & Gaston, K. J. (2003). Introduced house mice as a conservation concern on Gough Island. *Biodiversity & Conservation*, *12*(10), 2107–2119.

Kauppi, L., Barchi, M., Lange, J., Baudat, F., Jasin, M., & Keeney, S. (2013). Numerical constraints and feedback control of double-strand breaks in mouse meiosis. *Genes & Development*, *27*(8), 873–886.

Kauppi, L., Jasin, M., & Keeney, S. (2012). The tricky path to recombining X and Y

chromosomes in meiosis. *Annals of the New York Academy of Sciences*, *1267*(1), 18–23.

Kawakami, T., Smeds, L., Backstrom, N., Husby, A., Qvarnstrom, A., Mugal, C. F., … Ellegren, H. (2014). A high-density linkage map enables a second-generation collared flycatcher genome assembly and reveals the patterns of avian recombination rate variation and chromosomal evolution. *Molecular Ecology*, *23*(16), 4035–4058. https://doi.org/10.1111/mec.12810

Keane, T. M., Goodstadt, L., Danecek, P., White, M. A., Wong, K., Yalcin, B., … Goodson, M. (2011). Mouse genomic variation and its effect on phenotypes and gene regulation. *Nature*, *477*(7364), 289–294.

Keeney, S., Lange, J., & Mohibullah, N. (2014). Self-organization of meiotic recombination initiation: general principles and molecular pathways. *Annual Review of Genetics*, *48*, 187.

Kidwell, M., & Kidwell, J. (1976). Selection for Male Recombination in Drosophila-Melanogaster. *Genetics*, *84*(2), 333–351.

Kleckner, N. (2006). Chiasma formation: chromatin/axis interplay and the role (s) of the synaptonemal complex. *Chromosoma*, *115*(3), 175–194.

Kochakpour, N., & Moens, P. B. (2008). Sex-specific crossover patterns in Zebrafish (Danio rerio). *Heredity*, *100*(5), 489–495. https://doi.org/10.1038/sj.hdy.6801091

Koehler, K. E., Cherry, J. P., Lynn, A., Hunt, P. A., & Hassold, T. J. (2002). Genetic control of mammalian meiotic recombination. I. Variation in exchange frequencies among males from inbred mouse strains. *Genetics*, *162*(1), 297–306.

Kondrashov, A. S. (1993). Classification of hypotheses on the advantage of amphimixis. *Journal of Heredity*, *84*(5), 372–387.

Kong, A., Barnard, J., Gudbjartsson, D. F., Thorleifsson, G., Jonsdottir, G., Sigurdardottir, S., … Frigge, M. L. (2004). Recombination rate and reproductive success in humans. *Nature Genetics*, *36*(11), 1203–1206.

Kong, A., Gudbjartsson, D. F., Sainz, J., Jonsdottir, G. M., Gudjonsson, S. A., Richardsson, B., … Masson, G. (2002). A high-resolution recombination map of the human genome. *Nature Genetics*, *31*(3), 241–247.

Kong, A., Thorleifsson, G., Frigge, M. L., Masson, G., Gudbjartsson, D. F., Villemoes, R., … Stefansson, K. (2014). Common and low-frequency variants associated with genome-wide recombination rate. *Nature Genetics*, *46*(1), 11–16.

Kong, A., Thorleifsson, G., Stefansson, H., Masson, G., Helgason, A., Gudbjartsson, D. F., … Stefansson, K. (2008). Sequence variants in the RNF212 gene associate with genome-wide recombination rate. *Science*, *319*(5868), 1398–1401. https://doi.org/10.1126/science.1152422

Kono, H., Tamura, M., Osada, N., Suzuki, H., Abe, K., Moriwaki, K., … Shiroishi, T. (2014). Prdm9 Polymorphism Unveils Mouse Evolutionary Tracks. *Dna Research*, *21*(3), 315–326. https://doi.org/10.1093/dnares/dst059

Korol, A. B., & Iliadi, K. G. (1994). Increased recombination frequencies resulting from directional selection for geotaxis in Drosophila. *Heredity*, *72*(1), 64–68.

Lander, E., & Green, P. (1987). Construction of Multilocus Genetic-Linkage Maps in Humans. *Proceedings of the National Academy of Sciences of the United States of America*, *84*(8), 2363–2367. https://doi.org/10.1073/pnas.84.8.2363

Lao, J. P., Cloud, V., Huang, C.-C., Grubb, J., Thacker, D., Lee, C.-Y., … Bishop, D. K. (2013). Meiotic Crossover Control by Concerted Action of Rad51-Dmc1 in Homolog Template

Bias and Robust Homeostatic Regulation. *PLOS Genet*, *9*(12), e1003978. https://doi.org/10.1371/journal.pgen.1003978

Leek, J. T., & Storey, J. D. (2011). The Joint Null Criterion for Multiple Hypothesis Tests. *Statistical Applications in Genetics and Molecular Biology*, *10*(1), 28. https://doi.org/10.2202/1544-6115.1673

Lemaitre, C., Tannier, E., Gautier, C., & Sagot, M.-F. (2008). Precise detection of rearrangement breakpoints in mammalian chromosomes. *BMC Bioinformatics*, *9*, 286. https://doi.org/10.1186/1471-2105-9-286

Levy, S. F., & Siegal, M. L. (2008). Network hubs buffer environmental variation in Saccharomyces cerevisiae. *PLoS Biol*, *6*(11), e264.

Lewontin, R. C. (1971). The Effect of Genetic Linkage on the Mean Fitness of a Population. *Proceedings of the National Academy of Sciences of the United States of America*, *68*(5), 984–986.

Li, H., & Durbin, R. (2009). Fast and accurate short read alignment with Burrows-Wheeler transform. *Bioinformatics*, *25*(14), 1754–1760. https://doi.org/10.1093/bioinformatics/btp324

Li, H., Handsaker, B., Wysoker, A., Fennell, T., Ruan, J., Homer, N., … Durbin, R. (2009). The Sequence Alignment/Map format and SAMtools. *Bioinformatics*, *25*(16), 2078–2079. https://doi.org/10.1093/bioinformatics/btp352

Li, R., Tsaih, S.-W., Shockley, K., Stylianou, I. M., Wergedal, J., Paigen, B., & Churchill, G. A. (2006). Structural model analysis of multiple quantitative traits. *PLoS Genet*, *2*(7), e114.

Li, X., & Schimenti, J. C. (2007). Mouse pachytene checkpoint 2 (trip13) is required for completing meiotic recombination but not synapsis. *PLoS Genet*, *3*(8), e130.

Liu, E. Y., Morgan, A. P., Chesler, E. J., Wang, W., Churchill, G. A., & de Villena, F. P.-M. (2014). High-Resolution Sex-Specific Linkage Maps of the Mouse Reveal Polarized Distribution of Crossovers in Male Germline. *Genetics*, *197*(1), 91–106. https://doi.org/10.1534/genetics.114.161653

Lomolino, M. V. (2005). Body size evolution in insular vertebrates: generality of the island rule. *Journal of Biogeography*, *32*(10), 1683–1699.

Losick, R., & Desplan, C. (2008). Stochasticity and cell fate. *Science*, *320*(5872), 65–68.

Lynch, M., & Walsh, B. (1998). *Genetics and analysis of quantitative traits* (Vol. 1). Sinauer Sunderland, MA.

Lynn, A., Ashley, T., & Hassold, T. (2004). Variation in Human Meiotic Recombination. *Annual Review of Genomics and Human Genetics*, *5*(1), 317–349. https://doi.org/10.1146/annurev.genom.4.070802.110217

Lynn, A., Koehler, K. E., Judis, L., Chan, E. R., Cherry, J. P., Schwartz, S., … Hassold, T. J. (2002). Covariation of synaptonemal complex length and mammalian meiotic exchange rates. *Science*, *296*(5576), 2222–2225.

Lynn, A., Schrump, S., Cherry, J., Hassold, T., & Hunt, P. (2005). Sex, not genotype, determines recombination levels in mice. *American Journal of Human Genetics*, *77*(4), 670–675. https://doi.org/10.1086/491718

Ma, L., O'Connell, J. R., VanRaden, P. M., Shen, B., Padhi, A., Sun, C., … Wiggans, G. R. (2015). Cattle Sex-Specific Recombination and Genetic Control from a Large Pedigree Analysis. *Plos Genetics*, *11*(11), e1005387. https://doi.org/10.1371/journal.pgen.1005387

Mackay, T. F., & Lyman, R. F. (2005a). Drosophila bristles and the nature of quantitative genetic variation. *Philosophical Transactions of the Royal Society of London B:*

Biological Sciences, *360*(1459), 1513–1527.

Mackay, T. F., & Lyman, R. F. (2005b). Drosophila bristles and the nature of quantitative genetic variation. *Philosophical Transactions of the Royal Society of London B: Biological Sciences*, *360*(1459), 1513–1527.

Mahtani, M. M., & Willard, H. F. (1998). Physical and genetic mapping of the human X chromosome centromere: Repression of recombination. *Genome Research*, *8*(2), 100–110.

Manichaikul, A., Moon, J. Y., Sen, Ś., Yandell, B. S., & Broman, K. W. (2009). A model selection approach for the identification of quantitative trait loci in experimental crosses, allowing epistasis. *Genetics*, *181*(3), 1077–1086.

Margolin, G., Khil, P. P., Kim, J., Bellani, M. A., & Camerini-Otero, R. D. (2014). Integrated transcriptome analysis of mouse spermatogenesis. *BMC Genomics*, *15*(1), 1.

Martini, E., Diaz, R. L., Hunter, N., & Keeney, S. (2006). Crossover homeostasis in yeast meiosis. *Cell*, *126*(2), 285–295. https://doi.org/10.1016/j.cell.2006.05.044

Mather, K. (1936). The determination of position in crossing-over. *Journal of Genetics*, *33*(2), 207–235.

McLaren, W., Pritchard, B., Rios, D., Chen, Y., Flicek, P., & Cunningham, F. (2010). Deriving the consequences of genomic variants with the Ensembl API and SNP Effect Predictor. *Bioinformatics*, *26*(16), 2069–2070.

McVean, G. A., Myers, S. R., Hunt, S., Deloukas, P., Bentley, D. R., & Donnelly, P. (2004). The fine-scale structure of recombination rate variation in the human genome. *Science*, *304*(5670), 581–584.

Morgan, A. P., Fu, C.-P., Kao, C.-Y., Welsh, C. E., Didion, J. P., Yadgary, L., … de Villena, F.

P.-M. (2016). The Mouse Universal Genotyping Array: From Substrains to Subspecies. *G3-Genes Genomes Genetics*, *6*(2), 263–279. https://doi.org/10.1534/g3.115.022087

Morgan, T. H. (1916). *A Critique of the Theory of Evolution*. Princeton University Press.

Motenko, H., Neuhauser, S. B., O'Keefe, M., & Richardson, J. E. (2015). MouseMine: a new data warehouse for MGI. *Mammalian Genome*, *26*(7–8), 325–330.

Mouse ENCODE Consortium, Stamatoyannopoulos, J. A., Snyder, M., Hardison, R., Ren, B., Gingeras, T., … Adams, L. B. (2012). An encyclopedia of mouse DNA elements (Mouse ENCODE). *Genome Biology*, *13*(8), 418. https://doi.org/10.1186/gb-2012-13-8-418

Mulder, H. A., Gienapp, P., & Visser, M. E. (2016). Genetic variation in variability: Phenotypic variability of fledging weight and its evolution in a songbird population. *Evolution*, *70*(9), 2004–2016.

Muñoz-Fuentes, V., Marcet-Ortega, M., Alkorta-Aranburu, G., Forsberg, C. L., Morrell, J. M., Manzano-Piedras, E., … Toth, A. (2015). Strong artificial selection in domestic mammals did not result in an increased recombination rate. *Molecular Biology and Evolution*, *32*(2), 510–523.

Murdoch, B., Owen, N., Shirley, S., Crumb, S., Broman, K. W., & Hassold, T. (2010). Multiple loci contribute to genome-wide recombination levels in male mice. *Mammalian Genome*, *21*(11–12), 550–555. https://doi.org/10.1007/s00335-010-9303-5

Myers, S., Bowden, R., Tumian, A., Bontrop, R. E., Freeman, C., MacFie, T. S., … Donnelly, P. (2010). Drive Against Hotspot Motifs in Primates Implicates the PRDM9 Gene in Meiotic Recombination. *Science*, *327*(5967), 876–879. https://doi.org/10.1126/science.1182363

Myers, S., Freeman, C., Auton, A., Donnelly, P., & McVean, G. (2008). A common sequence

motif associated with recombination hot spots and genome instability in humans. *Nature Genetics*, *40*(9), 1124–1129. https://doi.org/10.1038/ng.213

Nagaoka, S. I., Hassold, T. J., & Hunt, P. A. (2012). Human aneuploidy: mechanisms and new insights into an age-old problem. *Nature Reviews Genetics*, *13*(7), 493–504.

Nei, M. (1967). Modification of Linkage Intensity by Natural Selection. *Genetics*, *57*(3), 625–641.

Nelder, J. A., & Pregibon, D. (1987). An extended quasi-likelihood function. *Biometrika*, *74*(2), 221–232.

Neumann, R., & Jeffreys, A. J. (2006). Polymorphism in the activity of human crossover hotspots independent of local DNA sequence variation. *Human Molecular Genetics*, *15*(9), 1401–1411. https://doi.org/10.1093/hmg/ddl063

Novak, I., Wang, H., Revenkova, E., Jessberger, R., Scherthan, H., & Höög, C. (2008). Cohesin Smc1β determines meiotic chromatin axis loop organization. *The Journal of Cell Biology*, *180*(1), 83–90.

Orr, H. A. (1998). Testing natural selection vs. genetic drift in phenotypic evolution using quantitative trait locus data. *Genetics*, *149*(4), 2099–2104.

Otsu, N. (1975). A threshold selection method from gray-level histograms. *Automatica*, *11*(285-296), 23-27.

Otto, S. P., & Barton, N. H. (1997). The evolution of recombination: removing the limits to natural selection. *Genetics*, *147*(2), 879–906.

Otto, S. P., & Barton, N. H. (2001). Selection for recombination in small populations. *Evolution*, *55*(10), 1921–1931.

Otto, S. P., & Lenormand, T. (2002). Resolving the paradox of sex and recombination. *Nature*

Reviews Genetics, *3*(4), 252–261. https://doi.org/10.1038/nrg761

Paape, T., Zhou, P., Branca, A., Briskine, R., Young, N., & Tiffin, P. (2012). Fine-Scale Population Recombination Rates, Hotspots, and Correlates of Recombination in the Medicago truncatula Genome. *Genome Biology and Evolution*, *4*(5), 726–737. https://doi.org/10.1093/gbe/evs046

Page, S. L., & Hawley, R. S. (2004). The genetics and molecular biology of the synaptonemal complex. *Annu. Rev. Cell Dev. Biol.*, *20*, 525–558.

Paigen, K., & Petkov, P. (2010). Mammalian recombination hot spots: properties, control and evolution. *Nature Reviews Genetics*, *11*(3), 221–233. https://doi.org/10.1038/nrg2712

Paigen, K., Szatkiewicz, J. P., Sawyer, K., Leahy, N., Parvanov, E. D., Ng, S. H. S., … Petkov, P. M. (2008). The Recombinational Anatomy of a Mouse Chromosome. *Plos Genetics*, *4*(7), e1000119. https://doi.org/10.1371/journal.pgen.1000119

Pan, Z., Yang, Q., Ye, N., Wang, L., Li, J., Yu, D., … Shi, Q. (2012). Complex relationship between meiotic recombination frequency and autosomal synaptonemal complex length per cell in normal human males. *American Journal of Medical Genetics Part A*, *158*(3), 581–587.

Parvanov, E. D., Petkov, P. M., & Paigen, K. (2010). Prdm9 Controls Activation of Mammalian Recombination Hotspots. *Science*, *327*(5967), 835–835. https://doi.org/10.1126/science.1181495

Peters, A. H., Plug, A. W., van Vugt, M. J., & de Boer, P. (1997). SHORT COMMUNICATIONS A drying-down technique for the spreading of mammalian meiocytes from the male and female germline. *Chromosome Research*, *5*(1), 66–68.

Poissant, J., Hogg, J. T., Davis, C. S., Miller, J. M., Maddox, J. F., & Coltman, D. W. (2010).

Genetic linkage map of a wild genome: genomic structure, recombination and sexual dimorphism in bighorn sheep. *Bmc Genomics*, *11*, 524. https://doi.org/10.1186/1471-2164-11-524

Ptak, S. E., Hinds, D. A., Koehler, K., Nickel, B., Patil, N., Ballinger, D. G., … Paabo, S. (2005). Fine-scale recombination patterns differ between chimpanzees and humans. *Nature Genetics*, *37*(4), 429–434. https://doi.org/10.1038/ng1529

Qiao, H., Rao, H. P., Yang, Y., Fong, J. H., Cloutier, J. M., Deacon, D. C., … Holloway, J. K. (2014). Antagonistic roles of ubiquitin ligase HEI10 and SUMO ligase RNF212 regulate meiotic recombination. *Nature Genetics*, *46*(2), 194–199.

Rasmussen, S. W., & Holm, P. B. (1978). Human meiosis II. Chromosome pairing and recombination nodules in human spermatocytes. *Carlsberg Research Communications*, *43*(5), 275–327.

Reynolds, A., Qiao, H., Yang, Y., Chen, J. K., Jackson, N., Biswas, K., … Wang, J. (2013). RNF212 is a dosage-sensitive regulator of crossing-over during mammalian meiosis. *Nature Genetics*, *45*(3), 269–278.

Rieseberg, L. H., Archer, M. A., & Wayne, R. K. (1999). Transgressive segregation, adaptation and speciation. *Heredity*, *83*(4), 363–372.

Rizzon, C., Marais, G., Gouy, M., & Biémont, C. (2002). Recombination rate and the distribution of transposable elements in the Drosophila melanogaster genome. *Genome Research*, *12*(3), 400–407.

Rockman, M. V., & Kruglyak, L. (2009). Recombinational Landscape and Population Genomics of Caenorhabditis elegans. *Plos Genetics*, *5*(3), e1000419. https://doi.org/10.1371/journal.pgen.1000419

Roeder, G. S. (1997). Meiotic chromosomes: it takes two to tango. *Genes & Development*, *11*(20), 2600–2621.

Rönnegård, L., & Valdar, W. (2011). Detecting major genetic loci controlling phenotypic variability in experimental crosses. *Genetics*, *188*(2), 435–447.

Rosa, G. J., Valente, B. D., de los Campos, G., Wu, X.-L., Gianola, D., & Silva, M. A. (2011). Inferring causal phenotype networks using structural equation models. *Genetics Selection Evolution*, *43*(1), 1.

Ross, C. R., DeFelice, D. S., Hunt, G. J., Ihle, K. E., Amdam, G. V., & Rueppell, O. (2015). Genomic correlates of recombination rate and its variability across eight recombination maps in the western honey bee (Apis mellifera L.). *Bmc Genomics*, *16*, 107. https://doi.org/10.1186/s12864-015-1281-2

Ross-Ibarra, J. (2004). The evolution of recombination under domestication: a test of two hypotheses. *The American Naturalist*, *163*(1), 105–112.

Rosu, S., Libuda, D. E., & Villeneuve, A. M. (2011). Robust Crossover Assurance and Regulated Interhomolog Access Maintain Meiotic Crossover Number. *Science*, *334*(6060), 1286–1289. https://doi.org/10.1126/science.1212424

Rowe-Rowe, D. T., & Crafford, J. E. (1992). Density, body size, and reproduction of feral house mice on Gough Island. *South African Journal of Zoology*, *27*(1), 1–5.

Rutherford, S. L., & Lindquist, S. (1998). Hsp90 as a capacitor for morphological evolution. *Nature*, *396*(6709), 336–342.

Sandor, C., Li, W., Coppieters, W., Druet, T., Charlier, C., & Georges, M. (2012). Genetic Variants in REC8, RNF212, and PRDM9 Influence Male Recombination in Cattle. *Plos Genetics*, *8*(7), e1002854. https://doi.org/10.1371/journal.pgen.1002854

Sasaki, M., Tischfield, S. E., Overbeek, M. van, & Keeney, S. (2013). Meiotic Recombination Initiation in and around Retrotransposable Elements in Saccharomyces cerevisiae. *PLOS Genet*, *9*(8), e1003732. https://doi.org/10.1371/journal.pgen.1003732

Schierup, M. H., & Hein, J. (2000). Consequences of Recombination on Traditional Phylogenetic Analysis. *Genetics*, *156*(2), 879–891.

Segura, J., Ferretti, L., Ramos-Onsins, S., Capilla, L., Farré, M., Reis, F., … Garcia-Caldés, M. (2013). Evolution of recombination in eutherian mammals: insights into mechanisms that affect recombination rates and crossover interference. *Proceedings of the Royal Society of London B: Biological Sciences*, *280*(1771), 20131945.

Serra, J. (1982). *Image analysis and mathematical morphology*. Orlando, FL: Academic press.

Shen, X., Pettersson, M., Rönnegård, L., & Carlborg, Ö. (2012). Inheritance beyond plain heritability: variance-controlling genes in Arabidopsis thaliana. *PLoS Genet*, *8*(8), e1002839.

Shifman, S., Bell, J. T., Copley, R. R., Taylor, M. S., Williams, R. W., Mott, R., & Flint, J. (2006). A high-resolution single nucleotide polymorphism genetic map of the mouse genome. *Plos Biology*, *4*(12), 2227–2237. https://doi.org/10.1371/journal.pbio.0040395

Singhal, S., Leffler, E. M., Sannareddy, K., Turner, I., Venn, O., Hooper, D. M., … Przeworski, M. (2015). Stable recombination hotspots in birds. *Science*, *350*(6263), 928–932. https://doi.org/10.1126/science.aad0843

Smagulova, F., Brick, K., Pu, Y., Camerini-Otero, R. D., & Petukhova, G. V. (2016). The evolutionary turnover of recombination hot spots contributes to speciation in mice. *Genes & Development*, *30*(3), 266–280. https://doi.org/10.1101/gad.270009.115

Smeds, L., Mugal, C. F., Qvarnström, A., & Ellegren, H. (2016). High-Resolution Mapping of

Crossover and Non-crossover Recombination Events by Whole-Genome Re-sequencing of an Avian Pedigree. *PLOS Genet*, *12*(5), e1006044. https://doi.org/10.1371/journal.pgen.1006044

Smukowski, C. S., & Noor, M. a. F. (2011). Recombination rate variation in closely related species. *Heredity*, *107*(6), 496–508. https://doi.org/10.1038/hdy.2011.44

Stefansson, H., Helgason, A., Thorleifsson, G., Steinthorsdottir, V., Masson, G., Barnard, J., … Stefansson, K. (2005). A common inversion under selection in Europeans. *Nature Genetics*, *37*(2), 129–137. https://doi.org/10.1038/ng1508

Steiner, W. W., Steiner, E. M., Girvin, A. R., & Plewik, L. E. (2009). Novel Nucleotide Sequence Motifs That Produce Hotspots of Meiotic Recombination in Schizosaccharomyces pombe. *Genetics*, *182*(2), 459–469. https://doi.org/10.1534/genetics.109.101253

Stevison, L. S., Woerner, A. E., Kidd, J. M., Kelley, J. L., Veeramah, K. R., McManus, K. F., … Wall, J. D. (2016). The Time Scale of Recombination Rate Evolution in Great Apes. *Molecular Biology and Evolution*, *33*(4), 928–945. https://doi.org/10.1093/molbev/msv331

Storey, J. D., & Tibshirani, R. (2003). Statistical significance for genomewide studies. *Proceedings of the National Academy of Sciences of the United States of America*, *100*(16), 9440–9445. https://doi.org/10.1073/pnas.1530509100

Sturtevant, A. H. (1913). The linear arrangement of six sex-linked factors in Drosophila, as shown by their mode of association. *Journal of Experimental Zoology*, *14*(1), 43–59.

Talbert, P. B., & Henikoff, S. (2010). Centromeres Convert but Don't Cross. *Plos Biology*, *8*(3), e1000326. https://doi.org/10.1371/journal.pbio.1000326

Tease, C., & Hultén, M. A. (2004). Inter-sex variation in synaptonemal complex lengths largely determine the different recombination rates in male and female germ cells. *Cytogenetic and Genome Research*, *107*(3–4), 208–215.

Thomsen, H., Reinsch, N., Xu, N., Bennewitz, J., Looft, C., Grupe, S., … Leyhe-Horn, B. (2001). A whole genome scan for differences in recombination rates among three Bos taurus breeds. *Mammalian Genome*, *12*(9), 724–728.

Tiemann-Boege, I., Calabrese, P., Cochran, D. M., Sokol, R., & Arnheim, N. (2006). High-resolution recombination patterns in a region of human chromosome. *Plos Genetics*, *2*(5), 682–692. https://doi.org/10.1371/journal.pgen.0020070

Tiley, G. P., & Burleigh, G. (2015). The relationship of recombination rate, genome structure, and patterns of molecular evolution across angiosperms. *BMC Evolutionary Biology*, *15*(1), 194.

True, J. R., Liu, J., Stam, L. F., Zeng, Z.-B., & Laurie, C. C. (1997). Quantitative genetic analysis of divergence in male secondary sexual traits between Drosophila simulans and Drosophila mauritiana. *Evolution*, 816–832.

True, J. R., Mercer, J. M., & Laurie, C. C. (1996). Differences in Crossover Frequency and Distribution among Three Sibling Species of Drosophila. *Genetics*, *142*(2), 507–523.

True, J. R., Weir, B. S., & Laurie, C. C. (1996). A genome-wide survey of hybrid incompatibility factors by the introgression of marked segments of Drosophila mauritiana chromosomes into Drosophila simulans. *Genetics*, *142*(3), 819–837.

Tsubouchi, H., & Roeder, G. S. (2003). The Importance of Genetic Recombination for Fidelity of Chromosome Pairing in Meiosis. *Developmental Cell*, *5*(6), 915–925. https://doi.org/10.1016/S1534-5807(03)00357-5

Uchimura, A., Higuchi, M., Minakuchi, Y., Ohno, M., Toyoda, A., Fujiyama, A., … Yagi, T. (2015). Germline mutation rates and the long-term phenotypic effects of mutation accumulation in wild-type laboratory mice and mutator mice. *Genome Research*, *25*(8), 1125–1134. https://doi.org/10.1101/gr.186148.114

Ullastres, A., Farré, M., Capilla, L., & Ruiz-Herrera, A. (2014). Unraveling the effect of genomic structural changes in the rhesus macaque - implications for the adaptive role of inversions. *BMC Genomics*, *15*, 530. https://doi.org/10.1186/1471-2164-15-530

Van der Walt, S., Schönberger, J. L., Nunez-Iglesias, J., Boulogne, F., Warner, J. D., Yager, N., … Yu, T. (2014). scikit-image: image processing in Python. *PeerJ*, *2*, e453.

Villena, F. P.-M. de, & Sapienza, C. (2001). Recombination is proportional to the number of chromosome arms in mammals. *Mammalian Genome*, *12*(4), 318–322. https://doi.org/10.1007/s003350020005

Vranis, N. M., Van der Heijden, G. W., Malki, S., & Bortvin, A. (2010). Synaptonemal complex length variation in wild-type male mice. *Genes*, *1*(3), 505–520.

Waddington, C. H. (1942). Canalization of development and the inheritance of acquired characters. *Nature*, *150*(3811), 563–565.

Watanabe, Y. (2012). Geometry and force behind kinetochore orientation: lessons from meiosis. *Nature Reviews Molecular Cell Biology*, *13*(6), 370–382.

Webb, A. J., Berg, I. L., & Jeffreys, A. (2008). Sperm cross-over activity in regions of the human genome showing extreme breakdown of marker association. *Proceedings of the National Academy of Sciences of the United States of America*, *105*(30), 10471–10476. https://doi.org/10.1073/pnas.0804933105

Weissman, A. (1889). *Essays on Heredity*. Clarendon Press, Oxford, England.

Wilfert, L., Gadau, J., & Schmid-Hempel, P. (2007). Variation in genomic recombination rates among animal taxa and the case of social insects. *Heredity*, *98*(4), 189–197.

Winckler, W., Myers, S. R., Richter, D. J., Onofrio, R. C., McDonald, G. J., Bontrop, R. E., … Donnelly, P. (2005). Comparison of fine-scale recombination rates in humans and chimpanzees. *Science*, *308*(5718), 107–111.

Xu, S. (2003). Theoretical basis of the Beavis effect. *Genetics*, *165*(4), 2259–2268.

Yang, F., & Wang, P. (2008). The mammalian synaptonemal complex: a scaffold and beyond. In *Meiosis* (Vol. 5, pp. 69–80). Karger Publishers.

Yang, H., Bell, T. A., Churchill, G. A., & de Villena, F. P.-M. (2007). On the subspecific origin of the laboratory mouse. *Nature Genetics*, *39*(9), 1100–1107.

Youds, J. L., Mets, D. G., McIlwraith, M. J., Martin, J. S., Ward, J. D., ONeil, N. J., … Boulton, S. J. (2010). RTEL-1 Enforces Meiotic Crossover Interference and Homeostasis. *Science*, *327*(5970), 1254–1258. https://doi.org/10.1126/science.1183112

Yue, F., Cheng, Y., Breschi, A., Vierstra, J., Wu, W., Ryba, T., … The Mouse ENCODE Consortium. (2014). A comparative encyclopedia of DNA elements in the mouse genome. *Nature*, *515*(7527), 355–364. https://doi.org/10.1038/nature13992

Zickler, D., & Kleckner, N. (2015). Recombination, pairing, and synapsis of homologs during meiosis. *Cold Spring Harbor Perspectives in Biology*, *7*(6), a016626.

Zickler, D., Moreau, P. J., Huynh, A. D., & Slezec, A.-M. (1992). Correlation between pairing initiation sites, recombination nodules and meiotic recombination in Sordaria macrospora. *Genetics*, *132*(1), 135–148.